

Weak interaction axial form factors of the octet baryons in nuclear medium

G. Ramalho¹, K. Tsushima² and Myung-Ki Cheoun¹

¹*Department of Physics and OMEG Institute, Soongsil University,
Seoul 06978, Republic of Korea and*

²*Laboratório de Física Teórica e Computacional – LFTC,
Universidade Cidade de São Paulo, 01506-000, São Paulo, SP, Brazil*

(Dated: April 18, 2025)

We study the axial-vector and the induced pseudoscalar form factors associated with the weak transitions between the octet baryon members in nuclear medium, using a covariant constituent quark model. We extend previous calculations of the axial transition form factors from the vacuum (free space) to the nuclear medium (symmetric nuclear matter). The extension of the model to the nuclear medium takes into account the modifications of the properties of hadrons in the medium (masses and coupling constants), as determined by the quark-meson coupling model. The axial-vector (G_A) and the induced pseudoscalar (G_P) form factors are evaluated for different values of the nuclear density ρ in terms of the square transfer momentum $q^2 = -Q^2$. We conclude that, in general, the G_A and G_P form factors are reduced in the nuclear medium. The reduction is stronger for light baryons and high densities. The medium modifications are milder for the heavier octet baryons, particularly at large Q^2 . The calculations presented here can be used to estimate the cross sections of neutrino and antineutrino scattering with nucleus, and neutrino and antineutrino scattering with hyperons bound to a nucleus, as well as those in the cores of compact stars.

I. INTRODUCTION

In recent years a considerable effort has been made in the experimental and theoretical studies of the internal structure of hadrons, including the electromagnetic and weak structures of the nucleon and other baryons in the vacuum [1–11], and in nuclear matter, and dense nuclear medium [12–21]. The normal nuclear matter may be characterized by the saturation density $\rho_0 \simeq 0.15 \text{ fm}^{-3}$, and the energy per nucleon $\simeq -15.7 \text{ MeV}$. The structure of the hadrons is modified when immersed in the nuclear medium. Studies in vacuum are important to set a reference to study in nuclear matter. Studies in the nuclear medium are important for the understanding of environments with dense nuclear matter from the high-energy nucleus-nucleus collisions to the cores of compact stars (neutron stars and magnetars) [22–28]. At the moment, however, there are not many theoretical studies about the internal structure modifications of baryons in nuclear matter.

The present work highlights the study of the axial structure of baryons in nuclear matter. The main motivation is to develop a formalism that can be used to make predictions of physical properties of baryons at relatively high densities as well as moderate, and large Q^2 , based on the degrees of freedom manifest in the free space: valence quarks and meson cloud excitations of the baryon cores. Within the formalism one can estimate the modifications of the axial transition form factors due to the nuclear medium, by comparison with the corresponding functions in the free space [28, 29]. Deviations between the in-medium and in-vacuum form factors are a manifestation of the role of the medium on the internal

structure of the baryons. The possible effects were observed already in electromagnetic reactions [21, 30–32], although the interpretations of the observed modifications in connection with the European Muon Collaboration (EMC) effect [33] are still in debate [34, 35]. The calculations presented here can be used in the study of reactions of neutrinos/antineutrinos with nucleus and reactions of neutrinos/antineutrinos with hyperons in dense nuclear matter. The methods developed here for the octet baryons can be extended in the future to the other baryon systems, like decuplet baryons and transitions between octet baryons and decuplet baryons, as well as for densities larger than the normal nuclear matter.

Our starting point is the axial structure of the octet baryons in free space, in particular the G_A and G_P form factors for elastic transitions and semileptonic decays (like the $n \rightarrow p + e^- + \bar{\nu}_e$ beta decay) [4–7, 10].

Although there are not many recent developments from the experimental side, there has been a significant progress in lattice QCD simulations for weak axial-vector couplings and transition form factors of the nucleon [36–44], as well as for the axial-vector couplings of the octet baryons [45–47]. Lattice QCD simulations for pion mass values close to the physical limit reproduce accurately the experimental value of the nucleon axial-vector coupling, $g_A = G_A(0)$, but there are still discrepancies on the axial-vector form factors $G_A(Q^2)$ for finite Q^2 [36, 37].

The combined analysis of lattice simulations and experimental data for large Q^2 , with model calculations based on different frameworks, suggests that the octet baryon weak axial-vector form factors can be interpreted as the result of a dominant contribution associated with the valence quark and a component associated with the meson cloud dressing of the baryon cores [7, 48].

In a previous work we have calculated the weak axial transition form factors between the octet baryon members in the vacuum [7]. The model in the vacuum was derived from the framework of the covariant spectator quark model [7, 8, 49–51], developed in a first stage for the study of the electromagnetic structure of the baryons, including the nucleon and nucleon resonances [8, 52–57].

The model based on the SU(6) spin-flavor symmetry for the quark states has been applied in particular, in the study of the octet baryons, the decuplet baryons and transitions between the octet and decuplet baryons [9, 28, 29, 58–64]. The starting point is the representation of the quark weak axial structure in terms of quark axial form factors parametrized in a vector meson dominance form. The free parameters of the models are fixed by the study of the weak axial form factors (G_A and G_P) in the lattice QCD regime for the nucleon. Once the model is calibrated (quark form factors and radial wave functions), the calculations are extrapolated for the octet baryons in the physical regime. The contributions of the valence quarks are combined with a phenomenological SU(3) parametrization of the meson cloud contribution. The comparison between model estimates for the nucleon and the experimental data is used to estimate the magnitude of the contributions from the meson cloud effects.

The model for the vacuum is in the present work extended to the study of the octet baryon weak axial form factors in symmetric nuclear matter. The methodology used is based on the extension of a model developed previously in vacuum [7] to the nuclear medium. The extension uses the quark-meson coupling (QMC) model [23], to estimate the masses of the baryons and the mesons, as well as the baryon-meson couplings in nuclear medium. The QMC model extends the properties of the bag model [23, 65, 66] to the nuclear matter. The cloudy bag model has already been combined with the covariant spectator quark model in the study of the electromagnetic transitions between baryon states in vacuum [61–63]. In these works the correspondence between the quark effective electromagnetic structure in the two models is used to calculate the electromagnetic interaction with baryons in intermediate states. The valence quark component of the model in medium is obtained considering the natural generalization of the covariant spectator quark model based on the vector meson dominance parametrization of the quark current and radial wave functions expressed in terms of the mass of the baryons [28]. The extension of the meson cloud component is performed using an effective SU(3) baryon-meson parametrization [7] and taking into account the medium modifications of the baryon-meson couplings. The weak axial form factors are then calculated in nuclear medium for different values of the nuclear density ρ .

The first studies of the electromagnetic and axial structure of baryons were made using Skyrme and soliton models [67–81] and the QMC model [23–27]. Other studies of the axial structure of the nucleon and octet baryons based on different frameworks in vacuum can be found

in Refs. [82–97], while, studies of the electromagnetic and axial structure of the nucleon and octet baryons in medium can be found in Refs. [98–112].

This article is organized as follows: In the next section we define the currents and transition form factors associated with the weak transitions between the octet baryon states. In Sec. III we review the covariant spectator formalism for the octet baryon states and the weak axial interactions in the vacuum. The extension of the model to nuclear matter is discussed in Sec. IV. Numerical results for the weak axial form factors G_A and G_P in the nuclear medium are presented in Sec. V, and they are also compared with those in free space. In Sec. VI we exemplify how the model calculations can be used for the study of neutrino/antineutrino scattering with nucleus. The outlook and conclusions are given in Sec. VII.

II. WEAK INTERACTION AXIAL FORM FACTORS

A. Axial-vector current

The weak axial form factors (G_A and G_P) for the transitions between the octet baryon members B and B' can be represented as

$$J_5^\mu = \frac{1}{2} \bar{u}_{B'}(P_f) \left[G_A(Q^2) \gamma^\mu + G_P \frac{q^\mu}{2M_{BB'}} \right] \gamma_5 u_B(P_i), \quad (2.1)$$

where $u_{B'}$ and u_B are the corresponding Dirac spinors, and $M_{BB'}$ is the average mass of the final (mass $M_{B'}$) and initial (mass M_B) baryons $M_{BB'} = \frac{1}{2}(M_{B'} + M_B)$. The factor 1/2 in Eq. (2.1) is included to be consistent with the nucleon case [7]. The form factors G_A and G_P depend then on the indices B and B' . For simplicity, we omit those indices when possible.

The expression Eq. (2.1) is obtained after a proper projection in the flavor space. Those flavor operators can be represented in terms of the Gell-Mann matrices λ_i ($i = 1, \dots, 8$) [5] as discussed in Appendix A. For the present study the cases of interest are the operators $I_0 = \lambda_3$ (neutral transitions), I_\pm (increases/decreases the isospin projection) and V_\pm (decreases/increases the number of strange quarks).

The form factor G_P is suppressed in the neutrino-nucleon cross sections by a factor $(m_\ell/M_{BB'})^2$, where m_ℓ is the lepton mass, the counterpart of the neutrino (electron or muon) [101]. One expects then that the effect of G_P can be neglected in $\nu_e N$ and $\bar{\nu}_e N$ reactions. Nevertheless, in the present work, we calculate the function G_P for several reasons: (i) The theoretical effort is equivalent to the calculation of G_A , (ii) it may be necessary for calculations of $\nu_\mu N$ and $\bar{\nu}_\mu N$ reactions, and (iii) there is the chance that the function G_P may be relevant for other observables or physical processes to be proposed in a near future. (see e.g., Ref. [6]).

Transition	$G_A(0)$
$n \rightarrow p$	1.2723 ± 0.0023
$\Lambda \rightarrow p$	-0.879 ± 0.018
$\Sigma^- \rightarrow n$	0.340 ± 0.017
$\Xi^- \rightarrow \Lambda$	-0.306 ± 0.061
$\Xi^0 \rightarrow \Sigma^+$	1.22 ± 0.05

TABLE I. Experimental values for $G_A(0)$ [114].

B. Experimental status

We start with the case of the nucleon. The function G_A can be measured by neutrino scattering and pion electroproduction off nucleons. Both experiments suggest a dipole-type function dependence $G_A(Q^2) = G_A(0)/(1 + Q^2/M_A^2)^2$, where the value of M_A varies between 1.03 and 1.07 GeV depending on the method [4, 113].

To represent the experimental data in a general form we consider the interval between the two functions, $G_A^{\text{exp-}}$ and $G_A^{\text{exp+}}$, given by [7]

$$G_A^{\text{exp}\pm}(Q^2) = \frac{G_A^0(1 \pm \delta)}{\left(1 + \frac{Q^2}{M_{A\pm}^2}\right)^2}, \quad (2.2)$$

where $G_A^0 = 1.2723$ is the nucleon experimental value of $G_A(0)$ [114], $\delta = 0.03$ is a parameter that expresses the precision of the data, and $M_{A-} = 1.0$ GeV and $M_{A+} = 1.1$ GeV are, respectively, the lower and upper limits for M_A . The central value of the parametrization (2.2) can be approximated by the dipole function form with $M_A \simeq 1.05$ GeV. This value is almost identical to the recent analysis from antineutrino-proton scattering [101].

Most of the data analyses are restricted to the region $Q^2 < 1$ GeV² [4]. Recently the nucleon axial-vector G_A form factor was determined in the range $Q^2 = 2-4$ GeV² at CLAS/JLab [115]. The new data are consistent with the parametrization (2.2).

There are also nucleon data for G_P in the range $Q^2 = 0-0.2$ GeV² determined by muon capture [4] and from pion electroproduction data using the low-energy theorem [116].

Concerning the other members of the baryon octet, there are data for $G_A(0)$ determined by the semileptonic decays indicated in Table I. The possible transitions between the octet baryon members are discussed in the next section.

We discuss next, how the axial form factors can be estimated in the context of a quark model with meson cloud dressing of the valence quark core.

C. Theory

The theoretical calculation of the transition form factors within a quark model framework starts with the rep-

resentation of the physical baryon state in the form [7]

$$|B\rangle = \sqrt{Z_B} [|qqq\rangle + c_B |MC\rangle], \quad (2.3)$$

where $|qqq\rangle$ is the three-quark state and $c_B |MC\rangle$ represents the baryon-meson state associated with the meson cloud dressing. The coefficient c_B is determined by the normalization $Z_B(1 + c_B^2) = 1$, assuming that $|MC\rangle$ is normalized to unity.

In this representation $Z_B = \sqrt{Z_B}\sqrt{Z_B}$ measures the probability of finding the qqq state in the physical baryon state. Consequently, $1 - Z_B$ measures the probability of finding the dressed baryon (simultaneously the qqq plus meson cloud) component in the physical state.

In Eq. (2.3), we include only the first order, or "one meson in the air" correction for the meson cloud, associated with the baryon-meson states. In principle, we should also include corrections associated with baryon-meson-meson states. These corrections are, in general, small due to the suppression associated with the multiple meson excitations. One can exemplify this effect using the nucleon case as an example. The nucleon meson cloud is dominated by the $|N\pi\rangle$ with $N \equiv qqq$ component. Based on previous work [7], we can estimate the probability of the $|N\pi\rangle$ state as $1 - Z_N \approx 0.3$. The correction associated with the two pion plus $N = qqq$ state ($|N\pi\pi\rangle$) contribution is then attenuated by the factor $(1 - Z_N)^2 \approx 0.09$.

The decomposition (2.3) is model dependent since the contributions from the meson cloud cannot be disentangled in experiments. The model dependence is a consequence of the relation between the meson cloud contributions and the scale associated to the bare core [117-119]. In Sec. III B, we discuss how the model dependence can be reduced by the comparison with lattice QCD simulations with large pion masses [8, 52, 61].

III. MODEL FOR THE VACUUM

We discuss here the framework of the covariant spectator quark model used in the present work for the study of the electroweak structure of baryons in vacuum.

The covariant spectator quark model is a constituent quark model derived from the covariant spectator theory [8, 49, 120]. Within the framework, the baryons are described as three-constituent quark systems, where a quark is free to interact with electroweak fields in the impulse approximation. The electromagnetic interaction with the quarks is described in terms of quark electromagnetic and axial form factors, that simulate the structure associated with the gluon and quark-antiquark dressing of the quarks. The constituent quark form factors are parametrized using a vector meson dominance picture calibrated in the study of the electromagnetic structure of the nucleon and baryon decuplet [49, 50].

In the electroweak interaction with the baryon systems the probes act on the individual quarks in the relativistic impulse approximation. In the covariant spectator theory formalism [120] one can then integrate over

B	$ M_A\rangle$	$ M_S\rangle$
p	$\frac{1}{\sqrt{2}}(ud - du)u$	$\frac{1}{\sqrt{6}}[(ud + du)u - 2uud]$
n	$\frac{1}{\sqrt{2}}(ud - du)d$	$-\frac{1}{\sqrt{6}}[(ud + du)d - 2ddu]$
Λ^0	$\frac{1}{\sqrt{12}}[s(du - ud) - (dsu - usd) + 2(ud - du)s]$	$\frac{1}{2}[(dsu - usd) - s(ud - du)]$
Σ^+	$\frac{1}{\sqrt{2}}(us - su)u$	$\frac{1}{\sqrt{6}}[(us + su)u - 2uus]$
Σ^0	$\frac{1}{2}[(dsu + usd) - s(ud + du)]$	$\frac{1}{\sqrt{12}}[s(ud + du) + (dsu + usd) - 2(ud + du)s]$
Σ^-	$\frac{1}{\sqrt{2}}(ds - sd)d$	$\frac{1}{\sqrt{6}}[(sd + ds)d - 2dds]$
Ξ^0	$\frac{1}{\sqrt{2}}(us - su)s$	$-\frac{1}{\sqrt{6}}[(us + su)s - 2ssu]$
Ξ^-	$\frac{1}{\sqrt{2}}(ds - sd)s$	$-\frac{1}{\sqrt{6}}[(ds + sd)s - 2ssd]$

TABLE II. Representations of the flavor wave functions of the octet baryons.

the quark-pair degrees of freedom since they are spectators in the interaction, and reduce the system to a quark-diquark state, where the diquark can be represented as an on-mass-shell particle with effective mass m_D [49, 51]. The baryon wave functions are derived from spin-flavor-radial $SU(6) \otimes O(3)$ symmetry associated with the quark-diquark configurations. The radial wave functions are determined phenomenologically by experimental data, or lattice QCD results for some ground state systems [9, 28, 49, 50, 54, 55, 60]. In the model, the $SU(3)$ quark flavor symmetry-breaking effect is reflected at the level of the baryon radial wave functions considering different range parameters for the systems with zero, one and two strange quarks, as discussed next.

We can now summarize the results from Ref. [7] for the octet baryon axial form factors G_A and G_P in the vacuum.

We consider the decomposition of the axial-vector G_A and induced pseudoscalar G_P form factors, according to

$$G_A = G_A^B + G_A^{MC}, \quad (3.1)$$

$$G_P = G_P^B + G_P^{\text{pole}} + G_P^{MC}. \quad (3.2)$$

The pseudoscalar meson pole contribution to G_P can be defined as

$$G_P^{\text{pole}} = \frac{4M_{BB'}^2}{\mu^2 + Q^2} G_A^B, \quad (3.3)$$

where $\mu = m_\pi$ (pion mass) for $|\Delta I| = 1$ transitions and $\mu = m_K$ (kaon mass) for $|\Delta S| = 1$ transitions, as discussed in Ref. [7].

The explicit meaning of these bare (B) and meson cloud (MC) contributions are explained in the following sections.

A. Bare contribution

Our starting point is the covariant spectator quark model for the nucleon and octet baryons developed for the study of the electromagnetic structure of those systems [9, 49]. The main difference between the two works

is that in the study of the weak axial structure we consider, in addition to the dominant S -state, a P -state contribution to the octet baryon quark-diquark wave functions [7, 51]:

$$\Psi_B(P, k) = n_S \Psi_S(P, k) + n_P \Psi_P(P, k), \quad (3.4)$$

where P is the momentum of the baryon (mass M_B), n_P is the P -state admixture coefficient and $n_P = \sqrt{1 - n_S^2}$. The S - and P -state wave functions are defined as [7]

$$\Psi_S(P, k) = \frac{1}{\sqrt{2}} [\phi_S^0 |M_A\rangle + \phi_S^1 |M_S\rangle] \psi_S(P, k), \quad (3.5)$$

$$\Psi_P(P, k) = \tilde{k} \frac{1}{\sqrt{2}} [\phi_S^0 |M_A\rangle + \phi_S^1 |M_S\rangle] \psi_P(P, k), \quad (3.6)$$

where $\phi_S^{0,1}$ are the spin wave functions labeled by the diquark spin ($S = 0, 1$), $|M_{S,A}\rangle$ are the flavor states, symmetric (S) or antisymmetric (A) in the exchange of the flavors between the quarks 1 and 2, ψ_S and ψ_P are the radial wave functions and $\tilde{k} = k - \frac{P \cdot k}{M_B^2} P$. The flavor states $|M_{S,A}\rangle$ for the octet baryons are presented in Table II.

The operator \tilde{k} is included to generate a P -state wave function based on the structure of a S -state wave function [7, 51]. In our calculations, we consider the correlation between S - and P -state radial wave functions given by $\psi_P(P, k) = N_P \psi_S(P, k) / \sqrt{-\tilde{k}^2}$, where N_P is a normalization constant. In this case the P -state radial wave function is described by the same momentum range parameters as the S -state.

As discussed in Ref. [7] the inclusion of the P -state is very important for the description of the lattice QCD data for the nucleon and the consequent extension of the calibration from lattice to the physical regime.

For the study of the weak axial structure of the baryon we consider the quark axial current operator

$$j_{Aq}^\mu = \left(g_A^q(Q^2) \gamma^\mu + g_P^q(Q^2) \frac{q^\mu}{2M_N} \right) \gamma_5 \frac{\lambda_a}{2}, \quad (3.7)$$

where λ_a ($a = 1, \dots, 8$) are the Gell-Mann matrices and g_A^q and g_P^q are the quark axial-vector and induced pseudoscalar form factors, respectively. In Eq. (3.7) the flavor

operators λ_a act on the quark flavor states ($|M_{A,S}\rangle$) and the Lorentz operators on the baryon spin states. The explicit form of the matrices λ_a are presented in Appendix A. Notice in Eq. (3.7) the inclusion of the nucleon mass in the definition of the quark current. This property, used already in the definition of the electromagnetic current [49, 50] is fundamental for the extension of the model to the lattice QCD regime.

As discussed in Ref. [7], we consider the following parametrization for the quark form factors

$$g_A^q(Q^2) = \lambda + (1 - \lambda) \frac{m_\rho^2}{m_\rho^2 + Q^2} + c_- \frac{Q^2 M_h^2}{(M_h^2 + Q^2)^2}, \quad (3.8)$$

$$g_P^q(Q^2) = \alpha \frac{m_\rho^2}{m_\rho^2 + Q^2} + \beta \frac{M_h^2}{M_h^2 + Q^2}, \quad (3.9)$$

where m_ρ is the ρ meson mass and M_h represents a mass of an effective heavy meson that simulates the structure of all the high mass resonances. We consider $M_h = 2M_N$, where M_N is the nucleon mass. The parameters λ , c_- , α and β were determined in previous studies [7, 28].

In the covariant spectator quark model the radial wave functions of the baryon B are represented in terms of

$$\chi_B = \frac{(M_B - m_D)^2 - (P - k)^2}{M_B m_D}, \quad (3.10)$$

where M_B is the mass of the baryon.

The radial wave functions of the octet baryon S -states take the form

$$\psi_B(P, k) = \frac{N_B}{m_D(\beta_1 + \chi_B)(\beta_l + \chi_B)}, \quad (3.11)$$

where $l = 2$ (N), $l = 3$ (Λ and Σ) or $l = 4$ (Ξ). Numerically we use the parametrization from Ref. [28]. Notice that $\beta_2 > \beta_3 > \beta_4$ reproduce the natural size of the baryons, where systems with more strange quarks are more compact.

In the covariant spectator quark model the weak transition form factors are determined in the relativistic impulse approximation by the current [49–51]

$$(J_5^\mu)_{B'B} = 3 \sum_\Gamma \int_k \bar{\Psi}_{B'}(P_+, k) (j_{Aq}^\mu) \Psi_B(P_-, k), \quad (3.12)$$

where the index a in Eq. (3.7) is determined by the flavors associated with the transition $B \rightarrow B'$. The integration symbol represent the integration on the diquark on-shell momentum.

In the previous equation we consider the axial coupling with the single quark (label 3) when the spectator quarks have labels 1 and 2 [diquark (12)]. The remaining contributions associated with the diquarks (13) and (23) are identical due to the symmetry in the change of the quark labels. The final contribution can then be obtained considering the contribution of a single diquark state multiplied by the factor 3 [49, 51]. The final expression for

the transition current (3.12) based on a single quark operator (i.e. no exchange or interaction currents) is valid when we consider a phenomenological quark-diquark radial wave function with effective parameters determined by physical or lattice QCD data. A more detailed derivation of the relativistic impulse approximation within the covariant spectator quark model framework can be found in Ref. [51].

For the determination of the axial form factors we assume that the current (3.12) can be written in the form

$$(J_5^\mu)_{B'B} = \frac{1}{2} \bar{u}(P_+) \left[\tilde{G}_A^B(Q^2) \gamma^\mu + \tilde{G}_P^B(Q^2) \frac{q^\mu}{2M_{BB'}} \right] \gamma_5 u(P_-), \quad (3.13)$$

which defines the bare contributions \tilde{G}_A^B and \tilde{G}_P^B to the axial form factors. These functions do not include the effect of the normalization of the wave functions, which are discussed later.

With the form (3.11) chosen for the radial wave functions, including the factor $1/m_D$, the transition form factors are independent of the diquark mass [49, 50]. As mentioned already, the SU(3) symmetry breaking due to the mass of the strange quark is taken into account in the range parameters of the wave functions determined by the global fit to the octet baryon electromagnetic form factors [28].

The results obtained for the form factors for the wave functions (3.4) and current (3.7) are

$$\tilde{G}_A^B = g_A^q \mathcal{F} \left\{ \frac{3}{2} n_S^2 B_0 - 3n_{SP} \frac{\tau}{1 + \tau} B_1 + \frac{6}{5} n_P^2 [\tau B_2 - (1 + \tau) B_4] \right\}, \quad (3.14)$$

$$\tilde{G}_P^B = g_A^q \mathcal{F} \left\{ -3n_{SP} \frac{1}{1 + \tau} B_1 + \frac{3}{2} n_P^2 \left[\frac{B_5}{\tau} + 2(B_2 - B_4) \right] + \frac{M_{BB'}}{M} g_P^q \mathcal{F} \left\{ \frac{3}{2} n_S^2 B_0 - 3n_{SP} B_1 + \frac{3}{2} n_P^2 [\tau B_2 + B_3 - (2 + \tau) B_4] \right\} \right\}, \quad (3.15)$$

where $n_{SP} = n_S n_P$, $\tau = \frac{Q^2}{4M_{BB'}^2}$, and the functions B_i ($i = 0, \dots, 5$) are integrals that include the radial wave functions ψ_S and ψ_P of the initial and final states.

The factor \mathcal{F} take the form

$$\mathcal{F} = f_X^A - \frac{1}{3} f_X^S, \quad (3.16)$$

where the coefficients $f_X^{A,S}$ are determined by the projections of the flavor transition operators ($X = I_\pm$ or $X = V_\pm$) on the flavor states

$$f_X^A = B' \langle M_A | X | M_A \rangle_B, \quad (3.17)$$

$$f_X^S = B' \langle M_S | X | M_S \rangle_B. \quad (3.18)$$

		$B \rightarrow B'$	f_X^A	f_X^S	\mathcal{F}
$ \Delta I = 1$	(I_+)	$n \rightarrow p$	1	$-\frac{1}{3}$	$\frac{10}{9}$
	(I_{\mp})	$\Sigma^{\pm} \rightarrow \Lambda$	$\pm \frac{1}{\sqrt{6}}$	$\mp \frac{1}{\sqrt{6}}$	$\pm \frac{2\sqrt{2}}{3\sqrt{3}}$
	(I_+)	$\Sigma^- \rightarrow \Sigma^0$	$\frac{1}{\sqrt{2}}$	$\frac{1}{3\sqrt{2}}$	$\frac{4\sqrt{2}}{9}$
	(I_+)	$\Sigma^0 \rightarrow \Sigma^+$	$\frac{1}{\sqrt{2}}$	$\frac{1}{3\sqrt{2}}$	$\frac{4\sqrt{2}}{9}$
	(I_+)	$\Xi^- \rightarrow \Xi^0$	0	$\frac{2}{3}$	$-\frac{2}{9}$
$ \Delta S = 1$	(V_+)	$\Lambda \rightarrow p$	$-\frac{2}{\sqrt{6}}$	0	$-\sqrt{\frac{2}{3}}$
	(V_+)	$\Sigma^- \rightarrow n$	0	$-\frac{2}{3}$	$\frac{2}{9}$
	(V_+)	$\Sigma^0 \rightarrow p$	0	$-\frac{\sqrt{2}}{3}$	$\frac{\sqrt{2}}{9}$
	(V_+)	$\Xi^- \rightarrow \Lambda$	$-\frac{1}{\sqrt{6}}$	$-\frac{1}{\sqrt{6}}$	$-\frac{\sqrt{2}}{3\sqrt{3}}$
	(V_+)	$\Xi^- \rightarrow \Sigma^0$	$\frac{1}{\sqrt{2}}$	$-\frac{1}{3\sqrt{2}}$	$\frac{5\sqrt{2}}{9}$
	(V_+)	$\Xi^0 \rightarrow \Sigma^+$	1	$-\frac{1}{3}$	$\frac{10}{9}$
$\Delta I = 0,$	(I_0)	$N \rightarrow N$	τ_3	$-\frac{1}{3}\tau_3$	$\frac{10}{9}\tau_3$
$\Delta S = 0$	(I_0)	$\Sigma \rightarrow \Sigma$	I_{Σ}	$\frac{1}{3}I_{\Sigma}$	$\frac{8}{9}I_{\Sigma}$
	(I_0)	$\Xi \rightarrow \Xi$	0	$\frac{2}{3}\tau_3$	$-\frac{2}{9}\tau_3$

TABLE III. Coefficients $f_I^{S,A}$ and $f_V^{S,A}$ for the octet baryon transitions. The last three lines are associated with the neutral transitions. The operators act on the isospin states $p = \Xi^0 = (1\ 0)^T$ (T : transposition) and $n = \Xi^- = (0\ 1)^T$ for isospin 1/2 and $I_{\Sigma} = \text{diag}(1, 0, -1)$ act on the isospin 1 states (charge operator). In the last column we include the factor \mathcal{F} .

The flavor transition operators are discussed in Appendix A. The coefficients $f_X^{A,S}$ and the factor \mathcal{F} are presented in Table III.

In the previous equations \tilde{G}_A , \tilde{G}_P , g_A^q , g_P^q and B_i are functions of Q^2 . The explicit expressions for B_i ($i = 0, \dots, 5$) can be found in Ref. [7]. The normalization of the radial wave functions leads to $B_0(0) = 1$. The effect of the mass (M_N or $M_{BB'}$) on the transition form factors appears on the functions B_i . The dependence of the transition form factors on the mass of the baryons was studied in detail in Ref. [7], demonstrating the relevance of taking into account implicitly the effects of the SU(3) flavor-symmetry breaking.

The leading-order contributions for \tilde{G}_A^B and \tilde{G}_P^B comes from the S -state contribution. In the S -state limit ($n_P = n_{SP} = 0$) the form factors are proportional to $\frac{3}{2}\mathcal{F}$ and we recover nonrelativistic results. For the nucleon $\tilde{G}_A^B \simeq \frac{5}{3}g_A^q B_0$. Different SU(3) coefficients are obtained for the other transitions.

In Table III, the transitions $|\Delta I| = 1$ correspond to $d \rightarrow u$ transition, except for the $\Sigma^+ \rightarrow \Lambda$ ($u \rightarrow d$ transition). From the table, we can conclude that the $\Sigma^+ \rightarrow \Lambda$ and $\Sigma^- \rightarrow \Lambda$ transition form factors differ by a sign, and that the $\Sigma^0 \rightarrow \Sigma^+$ and $\Sigma^- \rightarrow \Sigma^+$ transition form factors are identical. One can then conclude that in the case $|\Delta I| = 1$ there are only four cases of interest.

For the study of the Q^2 dependence of the form factors at large Q^2 it is convenient to determine the asymptotic form of the different components of the axial form factors. At large Q^2 we expect that the bare form factors follow:

$$G_A^B \propto \frac{1}{Q^4}, \quad G_P^B \propto \frac{1}{Q^6}. \quad (3.19)$$

These results are the consequence of the asymptotic form from the functions B_i and that $g_A^q \propto 1$ and $g_P^q \propto 1/Q^2$. From the expressions in Ref. [7] one can conclude that $B_0, B_1 \propto 1/Q^4$ and that $B_i \propto 1/Q^6$ for $i = 2, 3, 4, 5$.

B. Meson cloud contribution

We consider now the effect of the meson cloud. Following Ref. [7], we consider a phenomenological description of the meson cloud effects. The use of a phenomenological description was motivated by the fact that the magnitude of the meson cloud contributions is expected to be smaller than the valence quark contributions [7, 9, 28], and by simplicity.

When the baryon wave function has contributions from valence quarks and from the meson cloud we can consider the following decomposition

$$G_A(Q^2) = \sqrt{Z_{B'}Z_B} \left[\tilde{G}_A^B(Q^2) + \tilde{G}_A^{\text{MC}}(Q^2) \right], \quad (3.20)$$

where Z_B represents the normalization factor determined in the study of the baryon B electromagnetic factors [28]. The bare contribution is associated with the short-range interactions, and the meson cloud contribution is associated with the long-range interactions.

From the comparison with Eqs. (3.1) and (3.2) we can write $G_A^B = \sqrt{Z_{B'}Z_B}\tilde{G}_A^B$ and $G_A^{\text{MC}} = \sqrt{Z_{B'}Z_B}\tilde{G}_A^{\text{MC}}$. In the transition $n \rightarrow p$, we can replace $\sqrt{Z_{B'}Z_B} \rightarrow Z_N$.

As mentioned already, the decomposition from Eq. (3.20) into a bare and meson cloud contributions is model dependent [3, 121]. This model dependence is a consequence of the ambiguities on the calibration

of the background and in the identification of the bare states [117–119, 121, 122]. The impact of the model dependence can be reduced by matching the valence quark contributions of our model with the results from lattice QCD simulations for large pion masses, as explained next. Although quenched and unquenched lattice QCD simulations include some meson cloud effects, those effects are reduced for larger pion masses [121, 123].

The meson cloud contribution to G_P is determined by pole contribution associated with G_A^{MC}

$$G_P^{\text{MC}}(Q^2) = \sqrt{Z_{B'}Z_B} \frac{4M_{BB'}^2}{\mu^2 + Q^2} \tilde{G}_A^{\text{MC}}(Q^2), \quad (3.21)$$

where $\mu = m_\pi$ (pion mass) for $|\Delta I| = 1$ transitions and $\mu = m_K$ (kaon mass) for $|\Delta S| = 1$ transitions, as discussed in Ref. [7].

To simplify the terminology, we call the tilde quantities (\tilde{G}_A^{B} , \tilde{G}_P^{B} , \tilde{G}_A^{MC} , $\tilde{G}_P^{\text{pole}}$ and \tilde{G}_A^{MC} , bare, MC or pole) as relative contributions to the form factors, and the relations corrected by the wave function normalization factors as the effective contributions to the form factors. Notice that the final result requires the factor $\sqrt{Z_{B'}Z_B}$, while the bare contributions are naturally independent of these factors. At large Q^2 the meson cloud contribution is suppressed and $G_A \simeq \sqrt{Z_{B'}Z_B} \tilde{G}_A^{\text{B}}$. In the present work, we assume that the dominant contribution is the pion cloud and use the relations from Ref. [28] to determine Z_B .

The normalization constant Z_B is determined by the study of the octet baryon electromagnetic form factors [9, 28], and can be represented as

$$Z_B = \frac{1}{1 + 3a_B b_1}, \quad (3.22)$$

where $b_1 = 0.121$ and $a_N = 1$, $a_\Lambda = 0.48$, $a_\Sigma = 0.59$ and $a_\Xi = 0.04$. The values for a_B are the result of the SU(3) structure of the pion-baryon interaction. The coefficient for Σ include the intermediate couplings with Σ and Λ in an effective way.

We consider here the calibration derived in the study of the axial-vector form factors. More specifically Z_N was determined by the comparison of $Z_N \tilde{G}_A^{\text{B}}$ with the experimental parametrization of G_A for $Q^2 > 1 \text{ GeV}^2$ (large Q^2 region) [7].

In the representation (3.22) the explicit dependence of the pion cloud contributions on the coupling constants $g_{\pi BB'}$ is transferred to the factor b_1 since the coefficients a_B are normalized by the result for the nucleon. Since in the electromagnetic interaction with the pion cloud in leading order includes two pion-baryon-baryon vertices (processes similar to Fig. 1), associated with the coupling constants $g_{\pi BB'}$, and that in an SU(3) meson-baryon interaction the coupling constants are proportional to $g_{\pi NN}$, we can write

$$b_1 \propto g_{\pi NN}^2. \quad (3.23)$$

We can now discuss the function \tilde{G}_A^{MC} which determines the meson cloud contribution to the form factors

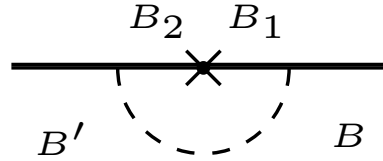


FIG. 1. Diagram associated with the meson cloud interaction in leading order.

G_A . For \tilde{G}_A^{MC} , we consider an effective parametrization based on an SU(3) meson-baryon coupling, with two independent functions F' and D' of Q^2 [5, 7]. We use primes to emphasize the difference to the standard SU(3) meson-baryon model, where the functions parametrize the combination of valence and meson cloud contributions. The value of the functions for $Q^2 = 0$ can be determined by the results for $G_A(0)$ for different known transitions ($n \rightarrow p$, $\Lambda \rightarrow p$, $\Sigma^- \rightarrow n$, $\Xi^- \rightarrow \Lambda$ and $\Xi^0 \rightarrow \Sigma^+$). The explicit values are

$$F_0 \equiv F'(0) = 0.1775, \quad D_0 \equiv D'(0) = 0.4284. \quad (3.24)$$

For convenience we define also $H_0 = F_0 + D_0$.

In the extension from the nucleon to the octet baryon cases we replace F' and D' by functions of Q^2 , according to the Q^2 dependence observed for the meson cloud contribution to the $n \rightarrow p$ transition, as described next.

We emphasize that we consider here a *modified version*, where, only the meson cloud contributions are described by a meson-baryon SU(3) symmetry model. The bare contributions are determined by our approximated SU(6) quark model, where the breaking is included at the level of the radial wave functions with parameters depending on the number of strange quarks, and by the values of the baryon masses.

The meson cloud contribution for the nucleon axial-vector form factor is determined by the fit to the nucleon data based on the results for G_A estimated by the lattice QCD data

$$\tilde{G}_{A,N}^{\text{MC}}(Q^2) = \frac{G_A^{\text{MC0}}}{\left(1 + \frac{Q^2}{\Lambda^2}\right)^4}, \quad (3.25)$$

where $G_A^{\text{MC0}} = 0.6059$ and $\Lambda = 1.05 \text{ GeV}$. In the notation of Table IV, $G_A^{\text{MC0}} = H_0$. In Ref. [7], we demonstrated the advantage of using a SU(3) meson-baryon parametrization to describe the meson cloud component of the model.

The generalization of the meson cloud to an arbitrary $B \rightarrow B'$ transition follows the form

$$\tilde{G}_A^{\text{MC}}(Q^2) = \eta_{BB'} \tilde{G}_{A,N}^{\text{MC}}(Q^2), \quad (3.26)$$

where $\tilde{G}_{A,N}^{\text{MC}}$ represents the parametrization of the nucleon's meson cloud contribution given by Eq. (3.25) and

	Process	\tilde{G}_A^{MC}	$\eta_{BB'}$
$ \Delta I = 1$	$n \rightarrow p$	$F' + D'$	$\frac{F_0 + D_0}{H_0}$
	$\Sigma^\pm \rightarrow \Lambda$	$\pm \sqrt{\frac{2}{3}} D'$	$\pm \sqrt{\frac{2}{3}} \frac{D_0}{H_0}$
	$\Sigma^- \rightarrow \Sigma^0$	$\sqrt{2} F'$	$\sqrt{2} \frac{F_0}{H_0}$
	$\Sigma^0 \rightarrow \Sigma^+$	$\sqrt{2} F'$	$\sqrt{2} \frac{F_0}{H_0}$
	$\Xi^- \rightarrow \Xi^0$	$F' - D'$	$\frac{F_0 - D_0}{H_0}$
$ \Delta S = 1$	$\Lambda \rightarrow p$	$-\sqrt{\frac{3}{2}} (F' + \frac{1}{3} D')$	$-\sqrt{\frac{3}{2}} \frac{F_0 + D_0/3}{H_0}$
	$\Sigma^- \rightarrow n$	$-F' + D'$	$-\frac{F_0 - D_0}{H_0}$
	$\Sigma^0 \rightarrow p$	$-\frac{1}{\sqrt{2}} (F' - D')$	$-\frac{1}{\sqrt{2}} \frac{F_0 - D_0}{H_0}$
	$\Xi^- \rightarrow \Lambda$	$-\sqrt{\frac{3}{2}} (F' - \frac{1}{3} D')$	$-\sqrt{\frac{3}{2}} \frac{F_0 - D_0/3}{H_0}$
	$\Xi^- \rightarrow \Sigma^0$	$\frac{1}{\sqrt{2}} (F' + D')$	$\frac{1}{\sqrt{2}} \frac{F_0 + D_0}{H_0}$
	$\Xi^0 \rightarrow \Sigma^+$	$F' + D'$	$\frac{F_0 + D_0}{H_0}$
$\Delta I = 0,$	$N \rightarrow N$	$(F' + D')\tau_3$	$\frac{F_0 + D_0}{H_0} \tau_3$
$\Delta S = 0$	$\Sigma \rightarrow \Sigma$	$2F' I_\Sigma$	$2 \frac{F_0}{H_0} I_\Sigma$
	$\Xi \rightarrow \Xi$	$(F' - D')\tau_3$	$\frac{F_0 - D_0}{H_0} \tau_3$

TABLE IV. Octet baryon axial-vector form factors $G_A(Q^2)$, expressed in terms of F' and D' of SU(3) scheme [5, 45, 46]. F_0 and D_0 are defined by Eq. (3.24) and $H_0 = F_0 + D_0$. The last rows refer to the neutral currents. The contributions to Λ and Σ^0 are zero [7].

$\eta_{BB'}$ is the coefficient associated with the SU(3) symmetry displayed in the last column in Table IV. Notice that the coefficient $\eta_{BB'}$ is a constant defined by the values of F_0 and D_0 and the Q^2 dependence comes exclusively from the function $\tilde{G}_{A,N}^{\text{MC}}$.

The effective meson cloud contribution to the axial-vector form factors is obtained when we take into account the normalization factors

$$G_A^{\text{MC}}(Q^2) = \sqrt{Z_{B'} Z_B} \tilde{G}_A^{\text{MC}}(Q^2). \quad (3.27)$$

In Table IV we represent some factors $\eta_{BB'}$ by using the factor $(F_0 + D_0)/H_0$ when we could have used unity. This representation is intentional in order to prepare the generalization for a case where the meson-baryon coupling may change, as discussed in the next section (extension to the nuclear medium). In that case we consider that the functions \tilde{G}_A^{MC} change with the (squared) coupling constants. This can be done by assuming that F_0 and D_0 include the dependence on the coupling constants, while H_0 is constant determined numerically and independent of the coupling constants.

Like the meson cloud contributions, the bare contributions are broken by the normalization associated with the baryon wave functions (factors $\sqrt{Z_B}$). In these conditions the meson cloud contributions for G_A for the transitions $n \rightarrow p$ and $\Xi^0 \rightarrow \Sigma^+$, determined by $F' + D'$, are not the same since the suppression associated with the factors $\sqrt{Z_B}$ is stronger for the nucleon (smaller $\sqrt{Z_B}$).

In the present work we consider a modification of the parametrization from Ref. [7], in order to correct small numerical errors in the calculation of Z_Ξ and Z_Σ . We use this opportunity to calibrate the parametrization for F_0 and D_0 since the previous estimates of the Ξ decays

were slightly overestimated. The new parameters are displayed in Eq. (3.24). Compared with Ref. [7] the corrections are very small (less than 0.5%), but we consider the new values for consistency. The main difference between the calculations is due to the factor Z_Ξ , underestimated about 10%. The numerical results for the axial-vector form factors in vacuum are presented and discussed in Sec. V A.

C. Combination of bare and meson cloud

Our model for the octet baryon axial form factors is then based on Eqs. (3.1), (3.2), (3.3), (3.14), (3.15), (3.21) and (3.26) with the proper normalizations.

The formalism described in the present section for bare and meson cloud contribution implies that there is a proportionality between the transition form factors for $\Sigma^- \rightarrow n$ and $\Sigma^0 \rightarrow p$ (factor $1/\sqrt{2}$) and also between $\Xi^- \rightarrow \Sigma^0$ and $\Xi^0 \rightarrow \Sigma^+$ (also a factor $1/\sqrt{2}$). The result can be inferred from the comparison between the coefficients for the bare contribution (Table III) and meson cloud contributions (Table IV). This result also implies that when we compare ratios between form factors we obtain the same result for $\Sigma^- \rightarrow n$ and $\Sigma^0 \rightarrow p$, as well as for $\Xi^- \rightarrow \Sigma^0$ and $\Xi^0 \rightarrow \Sigma^+$.

We can now discuss the asymptotic form of the different components of the axial form factors (3.1) and (3.2). Based on Eqs. (3.19) and (3.26), one has

$$G_A^{\text{B}} \propto \frac{1}{Q^4}, \quad G_A^{\text{MC}} \propto \frac{1}{Q^8}. \quad (3.28)$$

The corresponding expressions for G_P , based on

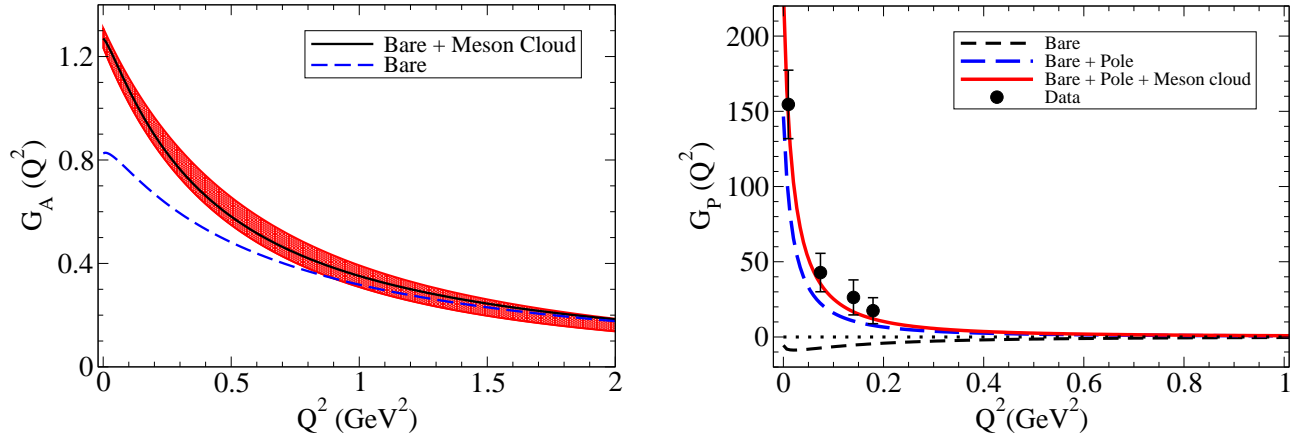


FIG. 2. Model results for the nucleon form factors G_A and G_P according to the calibration discussed in the text. **At the left:** we compare the G_A total and bare results with the parametrization of the data (red band) and the estimate of the bare contribution (blue dashed line) extrapolated from lattice [7, 38]. **At the right:** we present the results for G_P , decomposed into bare contribution, (bare + pole) and (bare + pole + meson cloud). The G_P data are from Refs. [4, 116].

Eqs. (3.3), (3.19) and (3.27) are

$$G_P^B \propto \frac{1}{Q^6}, \quad G_P^{\text{pole}} \propto \frac{1}{Q^6}, \quad G_P^{\text{MC}} \propto \frac{1}{Q^{10}}. \quad (3.29)$$

The results of the calibration of the model for the nucleon system are presented in Fig. 2. In the following, we present the results from the extension for the octet baryons in the vacuum, and the extension of those results to the nuclear medium.

For the extension of the formalism to the nuclear medium it is convenient to relate the effective coefficients F' and D' used in Eqs. (3.26) and (3.27) to the explicit meson cloud mechanisms and the meson-baryon couplings. From the analysis of the meson cloud diagrams depicted in Fig. 1, one can conclude that the meson cloud contribution is proportional to $g_{MBB_1}g_{MB_1B'}$ where M is the dressing meson (π , K , ...) and B_1 is an intermediate baryon state (octet or decuplet). Since, in the effective SU(3) meson-baryon interactions we can write all $g_{MBB'}$ in terms of a coefficient times $g_{\pi NN}$, we conclude that

$$\tilde{G}_A^{\text{MC}} \propto g_{\pi NN}^2. \quad (3.30)$$

The results for the other octet baryon members are presented in Sec. V, where we will discuss also the results for the nuclear medium.

IV. EXTENSION OF THE MODEL TO SYMMETRIC NUCLEAR MEDIUM

We discuss now the extension of the model for the vacuum described in the previous section to symmetric nuclear matter. The extension is based on the modification

of the properties of the hadrons and the meson-baryon coupling constants to the nuclear matter. These properties can be estimated by the QMC model applied to the symmetric nuclear matter [23, 24].

The *standard* QMC model which we use is based on the MIT bag model, to be able to describe the symmetric nuclear matter reasonably well by using the σ and ω mean fields self-consistently. The self-consistent exchange of the Lorentz-scalar-isoscalar σ and Lorentz-vector-isoscalar ω mean fields among the light quarks in nucleons provides a good description of the symmetric nuclear matter, with the incompressibility value of about 300 MeV (within the extracted empirical range), without introducing complicated nonlinear higher-order meson interactions. Based on this rather simple treatment with very less number of parameters, the QMC model has been applied successfully for many nuclear phenomena (see e.g., Refs. [23, 24]). The in-medium effective masses of hadrons are controlled by the values of the self-consistently obtained σ mean field. The coupling constants in medium are estimated using the Goldberger-Treiman relation and the medium values of the baryon masses, baryon axial-couplings and pion decay constant f_π in medium.

In the extension of our model to nuclear matter, we consider the values of the hadron masses (baryons and mesons) m_h from the vacuum to the medium m_h^* , the vector potentials, as well as the modifications of the coupling constants $g_{MBB'}$ in vacuum to $g_{MBB'}^*$ in medium. The consequence of this extension is that the bare contributions to the axial form factors are modified, since we replace m_ρ , m_ϕ and $M_h = 2M_N$, respectively, by m_ρ^* , m_ϕ^* and $M_h^* = 2M_N^*$ in the quark axial current and the radial wave functions of the baryon B are modified by replacing the baryon mass M_B by the effective baryon

ρ/ρ_0	M_N^*	m_ρ^*	$g_{\pi NN}^*/g_{\pi NN}$	g_A^{N*}/g_A^N	$G_A^N(0)$	n_P
0	0.9390	0.7545	1.000	1.0000	1.125	-0.5067
0.5	0.8313	0.7061	0.921	0.9404	1.058	-0.5371
1.0	0.7545	0.6537	0.899	0.8920	1.003	-0.5610

TABLE V. Model parameters used in the extension to the nuclear medium (nucleon case). The last columns include the ratio g_A^{N*}/g_A^N used to fix n_P for $\rho > 0$.

mass in medium M_B^* . As for the meson cloud contributions, they change as a consequence of the modification of the coupling $g_{MBB'}$ to $g_{MBB'}^*$.

In addition to the bare contributions (\tilde{G}_A^B replaced by \tilde{G}_A^{B*}), the effect of the nuclear medium acts in two levels: on the meson cloud contribution (\tilde{G}_A^{MC} replaced by \tilde{G}_A^{MC*}) and on the wave function normalization factors Z_B and $Z_{B'}$ (global modification of $\sqrt{Z_B Z_{B'}}$ to $\sqrt{Z_B^* Z_{B'}^*}$).

We discuss the modifications on the function \tilde{G}_A^{MC} first. From the discussion from Eq. (3.26) relative to the meson cloud contribution to a generic $B \rightarrow B'$ transition, we conclude that \tilde{G}_A^{MC} include linear combinations of F' and D' , which are proportional to the product of two coupling constants $g_{\pi BB'}^2$, since these include diagrams with two pion-baryon couplings (see Fig. 1). The combination of coupling constants can be expressed in terms of $g_{\pi NN}^2$, as discussed already. The conclusion is then that $\tilde{G}_A^{MC} \propto g_{\pi NN}^2$ and we can write

$$\tilde{G}_A^{MC*} = \left(\frac{g_{\pi NN}^*}{g_{\pi NN}} \right)^2 \tilde{G}_A^{MC}. \quad (4.1)$$

In the extension to the nuclear medium we assume, for simplicity, that medium effects associated with the meson cloud contributions are taken into account using the modified coupling constants and normalization factors. Thus, in medium $\tilde{G}_{A,N}^{MC}$ is determined by Eq. (3.25) where the cutoff Λ value is determined by nucleon data in vacuum.

We discuss now the impact of the nuclear medium on the wave function normalization factors, due to the modification of the meson-baryon couplings. The discussion is related to the discussion of the factor b_1 in Eq. (3.22). Since as already discussed, the effect of the coupling constants affects only b_1 and the effect is quadratic, we can write

$$b_1^* = \left(\frac{g_{\pi NN}^*}{g_{\pi NN}} \right)^2 b_1. \quad (4.2)$$

The normalization factors are then modified by

$$Z_B^* = \frac{1}{1 + 3a_B b_1^*}, \quad (4.3)$$

where the variables a_B keep the values in vacuum.

All the discussions about the medium effects of \tilde{G}_A^{B*} and \tilde{G}_A^{MC*} , can be extended to \tilde{G}_P^{B*} , $\tilde{G}_P^{\text{pole}*}$ and \tilde{G}_P^{MC*} . We just need to keep in mind that, since pole and meson cloud contributions for G_P (3.3) and (3.21) depend on the meson mass (m_π or m_K), those masses are replaced by the meson masses in medium m_π^* or m_K^* . In the case of the pion, however, based on Refs. [17–20], we consider no pion mass modification in nuclear matter ($m_\pi^* = m_\pi$).

The axial-vector form factors of baryon octet in vacuum were already calculated in Ref. [7]. We consider now the extension to the nuclear medium. An important property observed in the nuclear medium is the suppression of the axial-vector form factors due to the enhancement of the P -state component, in general associated with the lower component of the quark Dirac spinors. In the present case the simplest way to include the P -state effect is to modify the value of n_P . In the absence of a solid, established reference, we adjust the value of n_P in order to reproduce the suppression estimated by the bag model from Ref. [66]. Since our bare estimate for $G_A^B(0)$ for the nucleon is similar to the Bag Model g_A^N , we use the in-medium to free space bare axial-vector coupling ratio g_A^{N*}/g_A^N to fix the amount of P -state admixture (coefficient n_P). Notice that the determination of n_P by the values of g_A^{N*}/g_A^N is not an additional constraint of the model. It is a necessary condition associated with the consistency with the QMC model. The QMC model uses the input of the bag model for g_A^{N*} [66] and this result is used in the calculation of coupling constants $g_{MB_1 B_2}^*$ [28]. When we include the effect of the meson cloud for the nucleon on the functions G_A^* we modify the values of $G_A(0)$ and $G_A^*(0)$, and, consequently, the ratio $G_A^*(0)/G_A(0)$ deviates from the g_A^{N*}/g_A^N .

The reduction of the axial coupling g_A^N in the nuclear medium is also observed in calculations based on the soliton model [69, 71, 75].

The determination of the value of n_P is based on the relation [7]

$$\tilde{G}_A^B(0) = \frac{15 - 19n_P^2}{9} g_A^q(0), \quad (4.4)$$

where $g_A^q(0) = 1$.

In Table V, we present the parameters used in the medium calculations to the axial-vector and induced pseudoscalar form factor for the nucleon (densities $0.5\rho_0$ and ρ_0). The coupling constant $g_{\pi NN}^*$ in medium is calculated based on the Goldberger–Treiman relation, the values of f_π^* , the axial-vector coupling g_A^{N*} and the nucleon masses M_N^* [23, 28, 124, 125]. The parameters necessary for the calculations of the other transitions between the octet baryons are presented in the next section. The values of f_π^* in medium are based on Ref. [125], and are limited to values of ρ below $2.5\rho_0$. The value of n_P is determined by the value of g_A^{N*} estimated by the ratio included in the table.

ρ/ρ_0	M_N^*	M_Λ^*	M_Σ^*	M_Ξ^*	m_K^*	m_ρ^*	m_ϕ^*	$g_{\pi NN}^*/g_{\pi NN}$	n_P
0	0.9390	1.1160	1.1920	1.3180	0.4937	0.7545	1.0195	1.000	-0.507
0.5	0.8313	1.0439	1.1214	1.2822	0.4573	0.7061	1.0191	0.921	-0.536
1.0	0.7545	0.9927	1.0704	1.2567	0.4305	0.6537	1.0189	0.899	-0.560

TABLE VI. Model parameters used in the extension to the nuclear medium (baryon octet case). The discussion about the values of n_P are in the previous sections. The kaon mass is used in the calculation of the G_P pole term in the $|\Delta S| = 1$ transitions. For $m_\pi^* \simeq m_\pi$ we use $m_\pi = 0.138$ GeV [17–20].

V. NUMERICAL RESULTS

Results for G_A

In this section we present our numerical results for the octet baryon axial form factors G_A and G_P in vacuum and in medium. In the calculations we use the parameters from Table VI.

As discussed already, the axial transitions between octet baryon members correspond to six $|\Delta I| = 1$ transitions (four independent) and six $|\Delta S| = 1$ transitions. To simplify the analysis and the discussion of the results, we consider here only typical cases, for the $|\Delta I| = 1$ and $|\Delta S| = 1$ channels, associated with different octet baryon masses. The comparison of all channels is presented in Appendixes B and C.

We start with the discussion of the results for the vacuum and some remarks about the calibration of our model in vacuum (Sec. V A). Next we discuss the results in the nuclear medium (Sec. V B). We display the vacuum and in-medium results side by side in order to better observe the modifications due to the nuclear medium (Figs. 3, 4, 5 and 6).

We use the ratio between the form factors in medium and vacuum for a clear visualization of the medium modifications (Sec. V C). Deviations from unity (one) are the signature of medium effects. We study also the slope of the form factors near $Q^2 = 0$.

We summarize the results for G_A and G_P in medium in Sec. V D. We finish the section with a general discussion of our results, the limitations of the model, and the possible improvements (Sec. V E).

A. Axial form factors in vacuum

Using the formalism given in Sec. III, we calculate the form factors G_A and G_P in vacuum. These calculations are the extension of the parametrization for the nucleon (Fig. 2) to the octet baryons. This extension is based on our analysis of the nucleon lattice and physical data, combining the bare contributions with an effective parametrization of the meson cloud. The meson cloud component is calibrated by the nucleon physical data and for the octet baryon $G_A(0)$ physical data.

Some examples of the $B' \rightarrow B$ octet baryon axial-vector form factors G_A are presented on the left side in Figs. 3 ($|\Delta I| = 1$) and 4 ($|\Delta S| = 1$). The results for all transitions are presented in Appendix B (Figs. B1, B2 and B3). The contributions from the quark core are represented by the dash lines and the contributions from the meson cloud by the dash-dotted lines. The final results correspond to the solid lines. In the cases where the final result G_A is negative, we represent the function $-G_A$, for an easier comparison with the other reactions. In the figures we include also the available data for $G_A(0)$.

From these figures and from Figs. B1, B2 and B3, we can conclude that we can have different relative magnitudes for the form factor, for the bare contribution and for the meson cloud contribution. Most transitions are dominated by the bare contributions but some transitions have significant relative meson cloud contributions ($\Xi^- \rightarrow \Xi^0$, $\Sigma^- \rightarrow n$, $\Sigma^0 \rightarrow p$ and $\Xi^0 \rightarrow \Sigma^+$). Transitions with a large magnitude ($|G_A(0)| \gtrsim 1$) can have about 33% of meson cloud contributions (transitions $n \rightarrow p$, $\Lambda \rightarrow p$, $\Xi^- \rightarrow \Sigma^0$ and $\Xi^0 \rightarrow \Sigma^+$).

In comparison with previous work [7] we correct here the normalization of the Ξ baryons, relatively to the previous work, as discussed already in Sec. III. The main difference to the previous calculations are then the results for $\Xi^- \rightarrow \Lambda$ and $\Xi^0 \rightarrow \Sigma^+$, which are modified by the value of Z_Ξ . As a consequence, both, the bare and the meson cloud contributions are enhanced. With the present parametrization the description of $\Xi^- \rightarrow \Lambda$ transition is improved, while the numerical result for $\Xi^0 \rightarrow \Sigma^+$ overestimates the data.

Since the estimates follow approximate SU(6) and SU(3) symmetries, and the results for $\Xi^0 \rightarrow \Sigma^+$ are expected to be similar to the results for $n \rightarrow p$, we may question the quality of the SU(3) description for the meson cloud component. We note, however, that these results are a consequence of the normalization of the Ξ states, based on the studies of the electromagnetic structure of the octet baryons, which assume the dominance of the pion cloud for the meson cloud. This leads to a stronger suppression in the nucleon system ($Z_N \simeq 0.73$) than in the Ξ systems ($Z_\Xi \simeq 0.98$). The inclusion of the kaon cloud for the systems Λ , Σ and Ξ (expected to be more significant) imply a correction of the denominator in Eq. (3.22) and a reduction of the factor Z_B for the

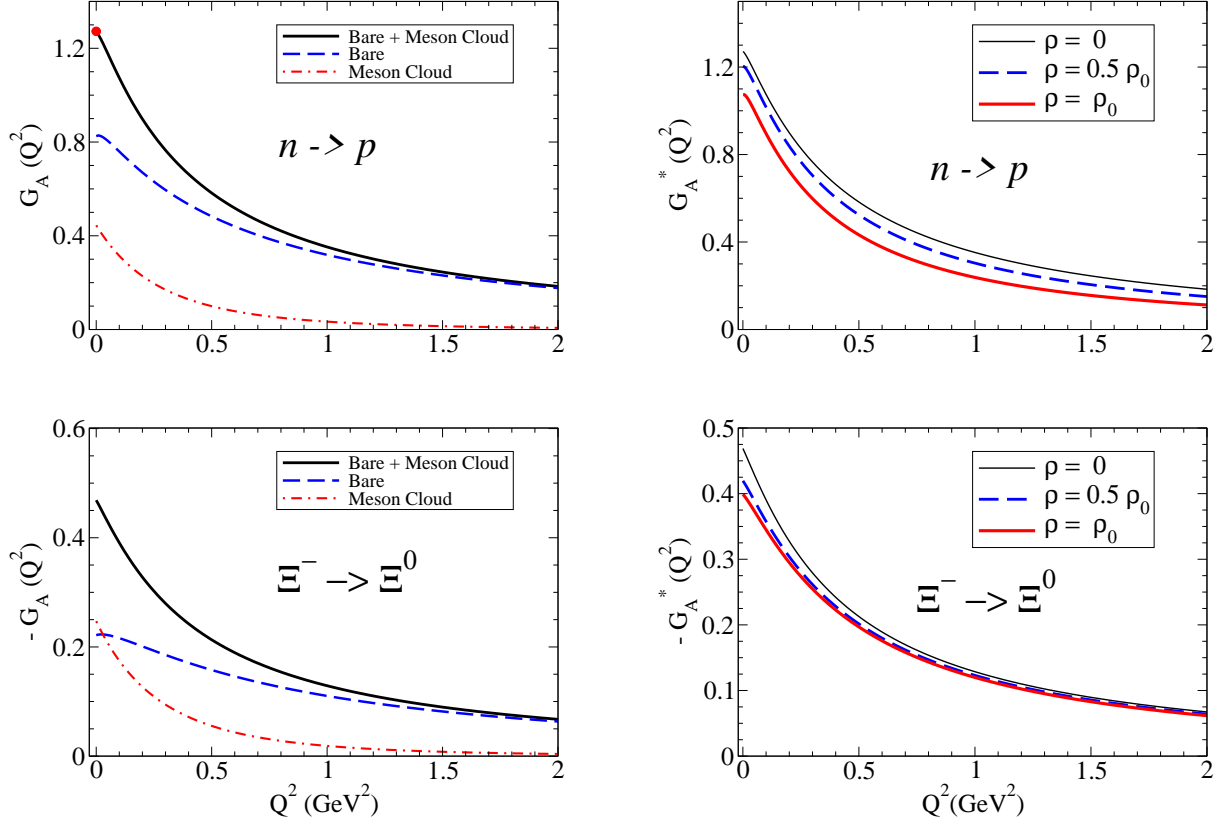


FIG. 3. Axial-vector form factor G_A for $|\Delta I| = 1$ transitions. **Left panel:** results in vacuum (bare, meson cloud and total). **Right panel:** total results for the medium $\rho = 0.5\rho_0$ and ρ_0 compared with vacuum ($\rho = 0$). The results for the $\Sigma^+ \rightarrow \Lambda$ and $\Sigma^0 \rightarrow \Sigma^+$ transitions are presented in Appendix B, Fig. B1.

systems with one or two strange quarks. As a consequence the estimates for the Ξ axial form factors would be reduced, improving the description of the data.

Results for G_P

Some examples of our predictions for G_P are on the left side of Fig. 5 for $|\Delta I| = 1$, and on the left side of Fig. 6 for $|\Delta S| = 1$. The results for G_P for all transitions are presented in Appendix C (Figs. C1, C2 and C3). As for the function G_A , in the cases where the final result G_P is negative, we represent the function $-G_P$. In the figures, we discriminate the result for the bare contribution, the combination of the bare and pseudoscalar meson pole contribution, and the sum of all the contributions (Bare + Pole + Meson Cloud). We adjust the upper limits of Q^2 in order to discriminate the different contributions at low Q^2 according to the falloff of the form factors.

In the calculations for $|\Delta I| = 1$ (Figs. 5 and C1) it is clear the impact of the factor $1/(m_\pi^2 + Q^2)$ in the Bare + Pole result and in the final result. The strong reduction with Q^2 is a consequence of the small magnitude of m_π . In the case of the nucleon, the combination of

the bare contribution and the meson cloud contribution is decisive for the good agreement of the model with the physical form factor data (see Fig. 2 and Sec. III). In the remaining cases our calculations are pure predictions.

The results for $|\Delta S| = 1$ (Figs. 6, C2 and C3) show a slower falloff for the form factor G_P than for $|\Delta I| = 1$, as expected from the kaon pole contribution associated with the factor $1/(m_K^2 + Q^2)$. The magnitude of G_P decreases slower with Q^2 than for $|\Delta I| = 1$ as a consequence of the kaon mass of the pole. The differences of magnitudes near $Q^2 = 0$ in comparison with $|\Delta I| = 1$ are mainly the consequence of the amplification of the meson mass.

Another important point is the relative magnitude of the terms. The bare and pole terms have, in the case $|\Delta S| = 1$, similar magnitudes, and there is a partial cancellation between the pole terms and the bare terms, which have opposite signs for all transitions. Notice that, since the pole and meson cloud contributions have the same sign for the transitions under discussion, one can also say that there is a partial cancellation between bare and meson cloud contributions at low Q^2 . The consequence of these effects is that the form factors G_P for $|\Delta S| = 1$ are about one order of magnitude smaller than the form factors G_P for $|\Delta I| = 1$. In a few cases

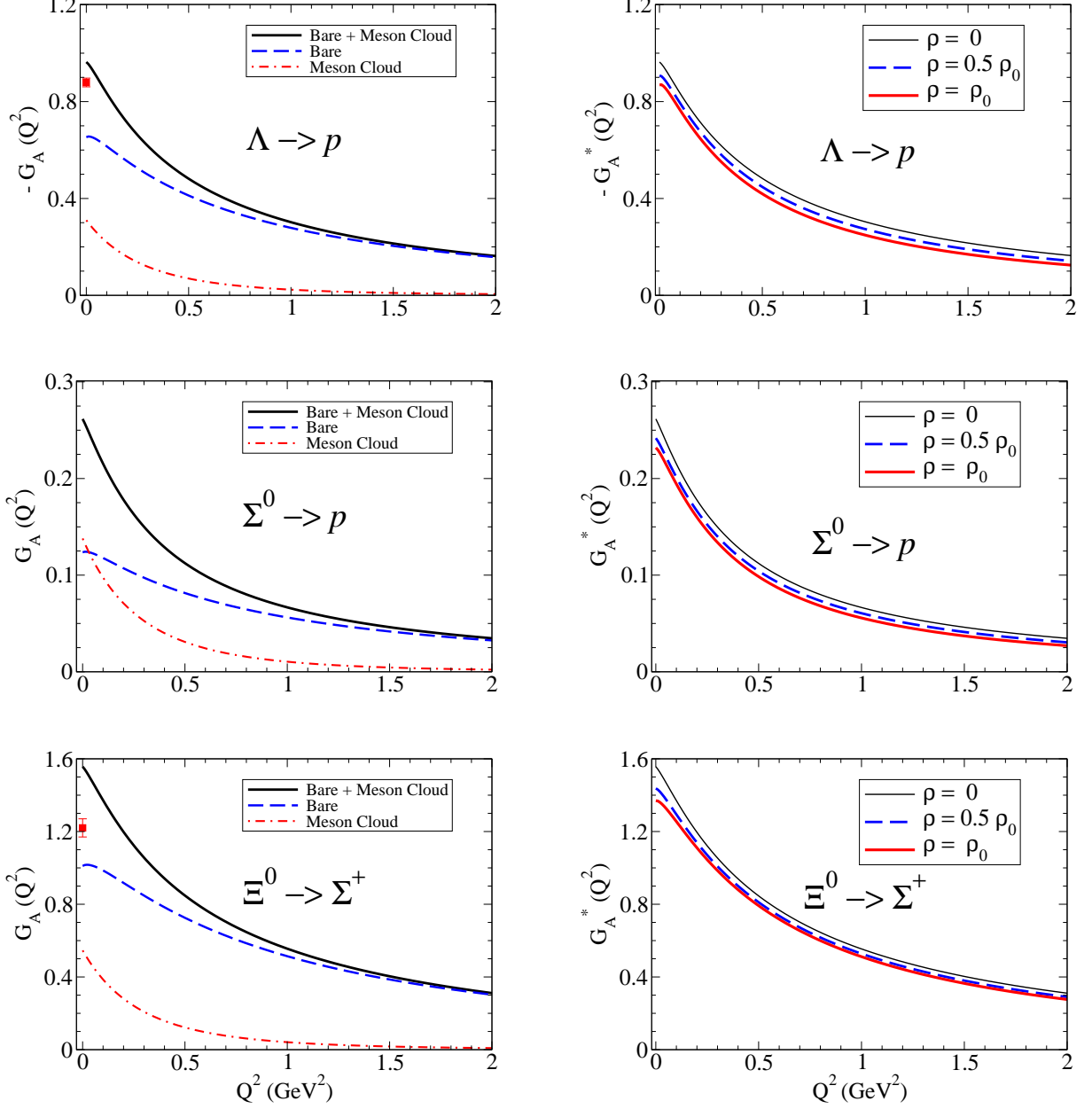


FIG. 4. Axial-vector form factor G_A for $|\Delta S| = 1$ transitions. **Left panel:** results in vacuum (bare, meson cloud and total). **Right panel:** total results for the medium $\rho = 0.5\rho_0$ and ρ_0 compared with vacuum ($\rho = 0$). The results for the $\Sigma^- \rightarrow n$ transition are presented in Appendix B, Fig. B2. The results for $\Xi^- \rightarrow \Lambda$ and $\Xi^- \rightarrow \Sigma^0$ transitions are presented in Appendix B, Fig. B3.

($\Xi^- \rightarrow \Lambda$, $\Xi^- \rightarrow \Sigma^0$ and $\Xi^0 \rightarrow \Sigma^+$) the bare contribution has a magnitude comparable with the meson cloud contribution at low Q^2 .

For future discussion, notice that, near the upper limit of Q^2 one can observe the convergence of the full result (solid line) and the Bare + Pole contribution (dashed line). This result means that in the region where the bare contribution is reduced (close to the horizontal zero line) the meson cloud contributions become also negligible. Recall that for large Q^2 , we expect $G_P^{\text{MC}} \propto 1/Q^{10}$. Notice

also that, although, G_P^{B} and G_P^{pole} are expected to have similar asymptotic behaviors ($\propto 1/Q^6$), numerically G_P^{B} falls down much faster, since $G_P \simeq G_P^{\text{B}} + G_P^{\text{pole}} \simeq G_P^{\text{pole}}$ for large Q^2 . The small magnitude of G_P^{B} at large Q^2 is a consequence of the model calibration of the G_P lattice QCD data for the nucleon.

Our last remark about G_P is the enhancement of G_P near $Q^2 = 0$ as a consequence of the low- Q^2 turning point of the function G_P^{B} . The effect appears also for

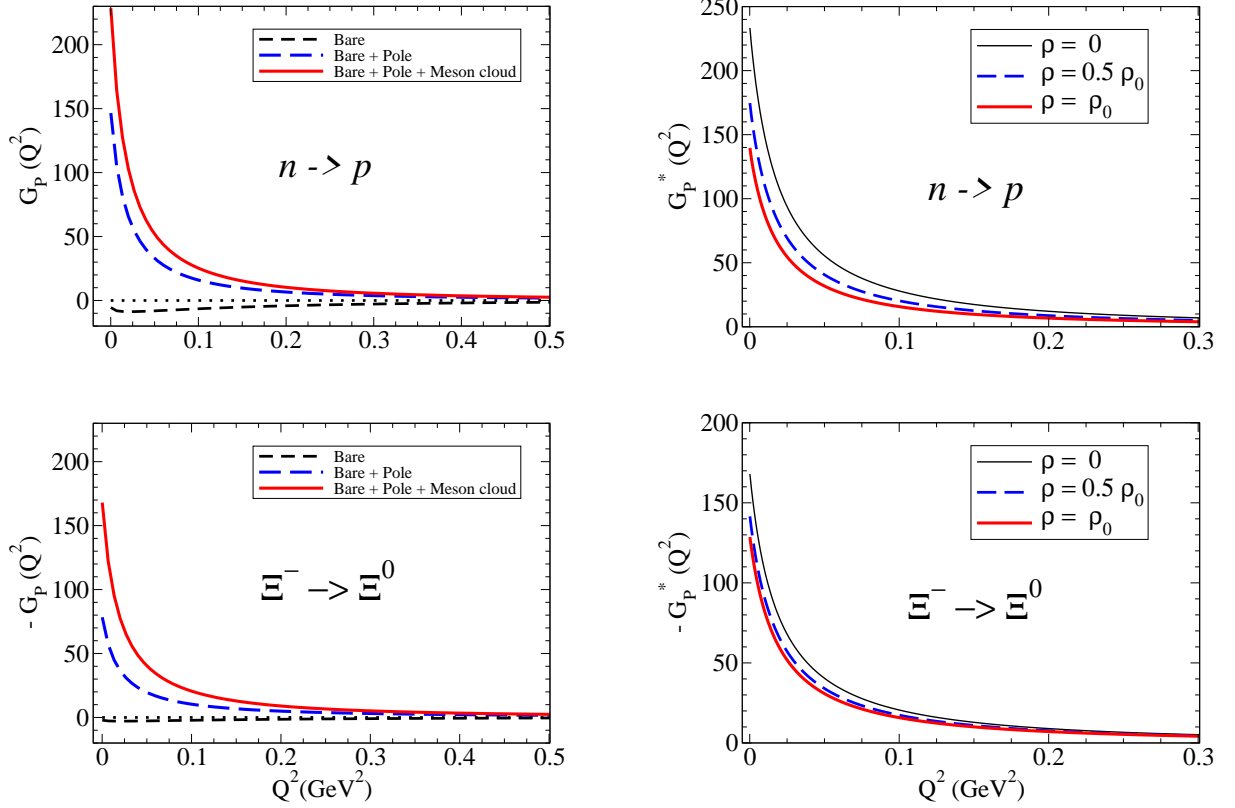


FIG. 5. Induced pseudoscalar form factor G_P for $|\Delta I| = 1$ transitions. **Left panel:** results for bare, bare plus meson cloud and total. **Right panel:** total results for the medium $\rho = 0.5\rho_0$ and ρ_0 compared with vacuum ($\rho = 0$). The results for the $\Sigma^+ \rightarrow \Lambda$ and $\Sigma^0 \rightarrow \Sigma^+$ transitions are presented in Appendix C, Fig. C1.

$|\Delta I| = 1$ (Figs. 5 and C1), but it is overshadowed by the magnitude of the pole and meson cloud terms. It can be observed more clearly in the figures for $|\Delta S| = 1$ (Figs. 6, C2 and C3). This behavior is a consequence of the method used to calibrate the model: an unconstrained fit to the lattice QCD data for the nucleon. The lattice datasets used in the calibration include no G_P data below $Q^2 = 0.15 \text{ GeV}^2$ [38]. Therefore, it is possible that G_P^B may be poorly constrained, affecting consequently the accuracy of the description of G_P near $Q^2 = 0$.

In the present study, we use the calibration from Ref. [7] as a first approximation. The results are, in principle, more accurate for the $|\Delta I| = 1$ sector, less sensitive to the magnitude of the function G_P^B . Future improvements of the present scheme are discussed in Sec. V E.

B. Axial form factors in medium

Some examples of our extension of the model to the octet baryons in the nuclear medium are presented on the right side of Figs. 3 ($|\Delta I| = 1$) and 4 ($|\Delta S| = 1$) for G_A , and on the right side of Figs. 5 ($|\Delta I| = 1$) and 6 ($|\Delta S| = 1$) for G_P . The results for all transitions are

presented in Appendix B (Figs. B1, B2 and B3) for G_A , and Appendix C (Figs. C1, C2 and C3) for G_P .

For the nuclear medium, for simplicity, we present only the final results for the densities $\rho = 0.5\rho_0$ and $\rho = \rho_0$, in comparisons with the result in vacuum ($\rho = 0$), omitting the decomposition of the bare and meson cloud contributions.

For the discussion of the results in medium it is important to look to the ratios G_A^*/G_A presented on the left side of Figs. 7 and 8 and the ratios G_P^*/G_P presented on the left side of Figs. 9 and 10. The ratios for all transitions are presented in Appendix B (Figs. B4 and B5) for G_A , and in Appendix C (Figs. C4 and C5) for G_P . In this respect, we recall the discussion in Sec. III C, according to which the ratios for $\Sigma^0 \rightarrow p$ are the same as the ratios for $\Sigma^- \rightarrow n$. The same property is verified for the transitions $\Xi^0 \rightarrow \Sigma^+$ and $\Xi^- \rightarrow \Sigma^0$.

1. Results for G_A^*

From the results for the form factor G_A in medium: right side of Figs. 3, 4, B1, B2 and B3 for the function G_A^* , and left side of Figs. 7, 8, B4 and B5 for the function

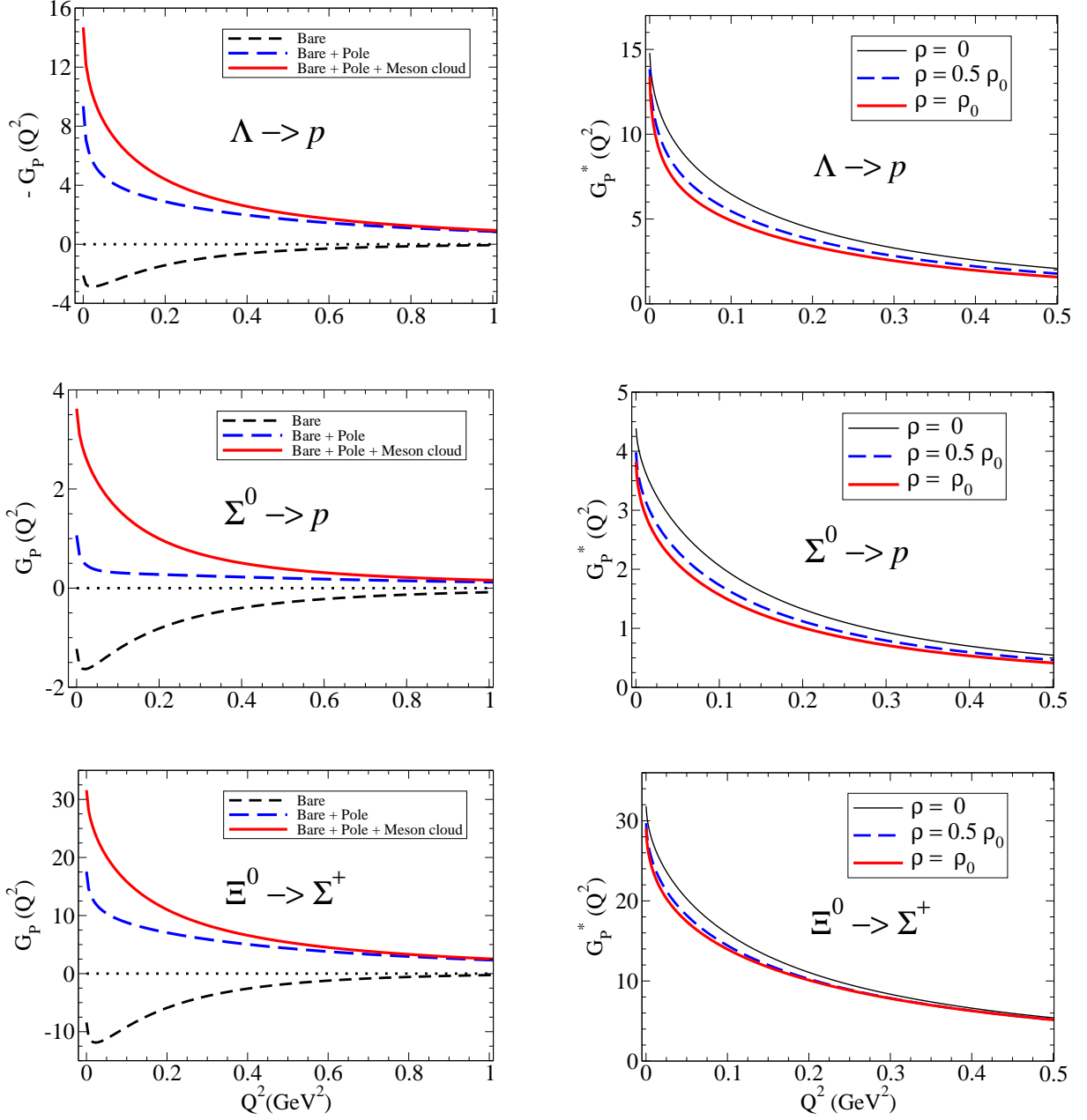


FIG. 6. Induced pseudoscalar form factor G_P for $|\Delta S| = 1$ transitions. **Left panel:** results for bare, bare plus meson cloud and total. **Right panel:** total results for the medium $\rho = 0.5\rho_0$ and ρ_0 compared with vacuum ($\rho = 0$). The results for the $\Sigma^- \rightarrow n$ transition are presented in Appendix C, Fig. C2. The results for $\Xi^- \rightarrow \Lambda$ and $\Xi^- \rightarrow \Sigma^0$ transitions are presented in Appendix C, Fig. C3.

G_A^*/G_A , we conclude that, in general, the axial-vector form factor G_A is reduced in the nuclear medium, or symmetric nuclear matter (suppression of G_A in medium). The conclusion is valid for $|\Delta I| = 1$ and $|\Delta S| = 1$.

The quenching of G_A for the octet baryon is mainly a consequence of the effect discussed already in the case of the nucleon (see Sec. IV). The enhancement of the P -state components in medium leads to reduction of the functions compared to vacuum.

In the present case these results are a consequence of

the suppression in medium of both the meson cloud and bare contributions. The suppression of the meson cloud contribution is more effective at low Q^2 , while the suppression of the bare contributions is more effective at large Q^2 . The magnitude of the suppression can be better observed using the function G_A^*/G_A in terms of Q^2 (left side of Figs. 7 and B4 for $|\Delta I| = 1$, and left side of Figs. 8 and B5 for $|\Delta S| = 1$). The suppression is stronger for lighter baryons and larger densities.

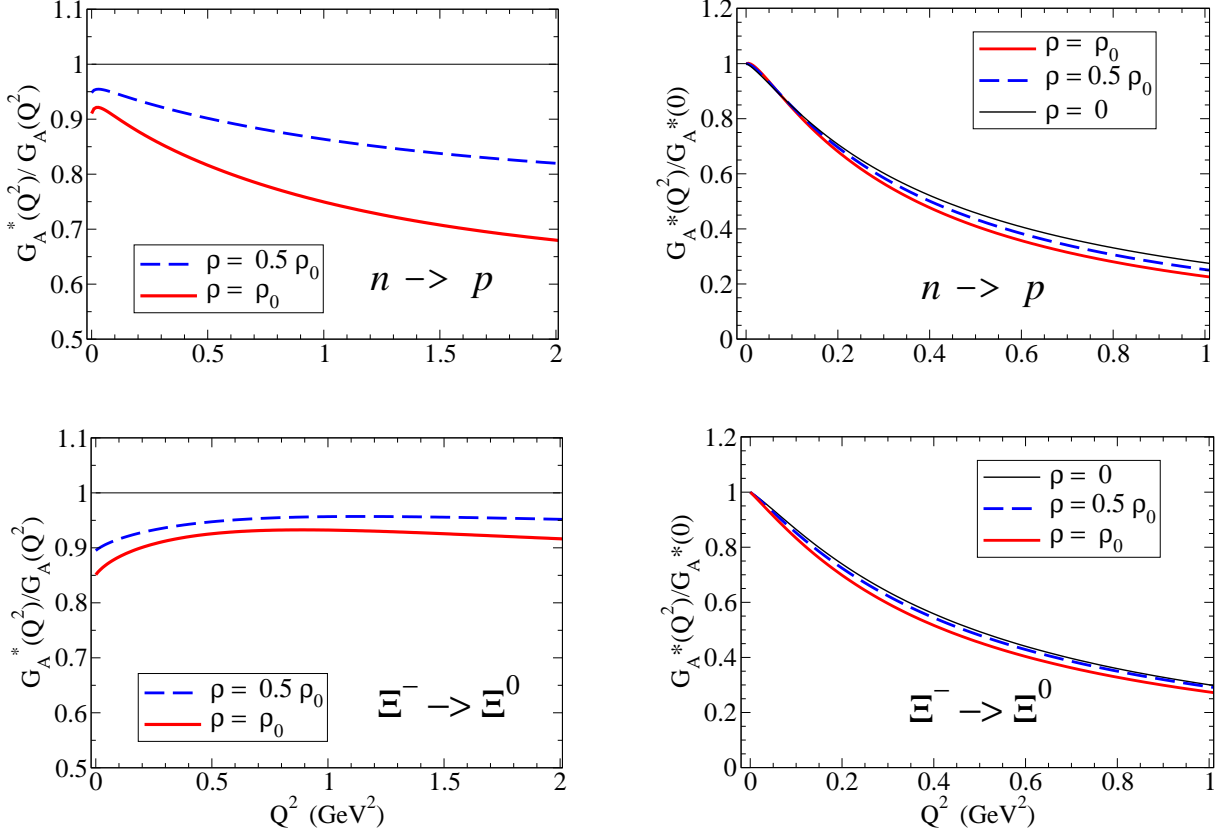


FIG. 7. Axial-vector form factor G_A for $|\Delta I| = 1$ transitions. Ratios G_A^*/G_A and $G_A^*(Q^2)/G_A^*(0)$. The results for the $\Sigma^+ \rightarrow \Lambda$ and $\Sigma^0 \rightarrow \Sigma^+$ transitions are presented in Appendix B, Fig. B4.

From the observation of Figs. 7, 8, B4 and B5, we can classify the ratios G_A^*/G_A using the shape and the magnitude of the suppression in the order:

- $n \rightarrow p$,
- $\Lambda \rightarrow p, \Sigma^+ \rightarrow p/\Sigma^- \rightarrow n$,
- $\Sigma^+ \rightarrow \Lambda, \Sigma^0 \rightarrow \Sigma^+, \Xi^- \rightarrow \Lambda, \Xi^- \rightarrow \Sigma^0/\Xi^0 \rightarrow \Sigma^+$,
- $\Xi^- \rightarrow \Xi^0$.

The range of variation discussed next is relative to the interval $Q^2 = 0-2 \text{ GeV}^2$.

The first reaction ($n \rightarrow p$) includes no transitions between the strange and light quarks, and, thus, it is the reaction with stronger suppression in medium. The effect increases with Q^2 . For $\rho/\rho_0 = 0.5$ one has a reduction of about 5–18%. For $\rho/\rho_0 = 1.0$ the reduction varies from 8–32%.

The second type includes the $\Lambda \rightarrow p$ transition, that is similar to the $n \rightarrow p$ transition, but with a weaker reduction of the ratio G_A^*/G_A . The $\Sigma^+ \rightarrow p/\Sigma^- \rightarrow n$ ratio has a similar shape.

The third class of transitions ($\Sigma \rightarrow \Lambda, \Sigma, \Xi \rightarrow \Lambda, \Sigma$) includes systems composed by a strange quark in the final state and have smaller and slower reductions with Q^2 .

The last case ($\Xi^- \rightarrow \Xi^0$) is a transition between baryons with two strange quarks and reveals a significant suppression at low Q^2 (meson cloud contributions significantly reduced in medium) and only a mild dependence on Q^2 , for $Q^2 > 1 \text{ GeV}^2$.

Our estimates for G_A^*/G_A for the nucleon can be compared with the calculations of the bag model [25, 26, 66]. The main difference between our calculations and the bag model calculations is that the latter does not include the effects of the meson cloud dressing. Apart from small differences at low Q^2 , the calculations differ on the shape of the ratio. The bag model ratio estimates decrease till the region $Q^2 = 0.5-1 \text{ GeV}^2$, and start to increase after that. After a certain value of Q^2 , one has an enhancement of G_A^* . This is due to the Lorentz contraction effect that is taken into account for the "bag shape" in Ref. [66], and, thus, for larger Q^2 the effect starts to appear stronger. Or, this is due to the finite size effect of the nucleon bag which is subject to the Lorentz contraction. The present calculations in contrast, suggest that the medium suppression keeps increasing for large Q^2 although with a reduced rate.

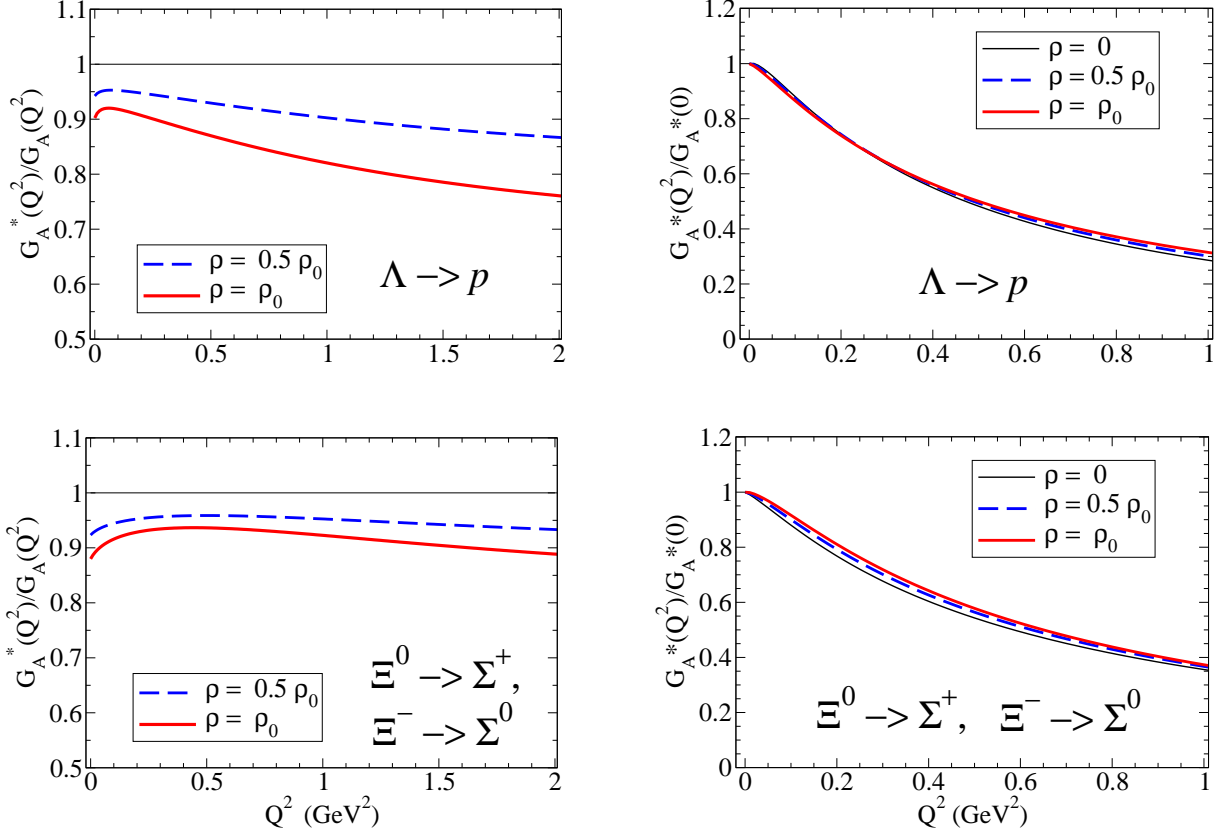


FIG. 8. Axial-vector form factor G_A for $|\Delta S| = 1$ transitions. Ratios G_A^*/G_A and $G_A^*(Q^2)/G_A^*(0)$. The results for the $\Sigma^- \rightarrow n$, $\Sigma^0 \rightarrow p$ and $\Xi^- \rightarrow \Lambda$ transition are presented in Appendix B, Fig. B5. The ratios are the same for $\Sigma^- \rightarrow n$ and $\Sigma^0 \rightarrow p$. The ratios are the same for $\Xi^- \rightarrow \Sigma^0$ and $\Xi^0 \rightarrow \Sigma^+$.

2. Results for G_P^*

Examples of our calculations for the induced pseudoscalar form factor G_P in the nuclear medium are presented on the right side of Fig. 5 for $|\Delta I| = 1$ and Fig. 6 for $|\Delta S| = 1$. The results for all transitions are presented in Appendix C (Figs. C1, C2 and C3). Examples of ratios G_P^*/G_P are presented on the left side of Figs. 9 for $|\Delta I| = 1$ and 10 for $|\Delta S| = 1$. The comparison of the ratios for all transitions is presented in Appendix C (Figs. C4 and C5). The range of Q^2 is adjusted to each case in order to better visualize the shape of the functions.

On the right side of Figs. 5, 6, C1, C2 and C3, we can still observe the enhancement of G_P near $Q^2 = 0$ as in vacuum, for both $|\Delta I| = 1$ and $|\Delta S| = 1$. Since, as mentioned already, the G_P estimates at $Q^2 = 0$ may be inaccurate, we avoid definitive conclusions about the point $Q^2 = 0$, and for the ratios G_P^*/G_P in Figs. 9, 10, C4 and C5, we display only the region $Q^2 > 0.012 \text{ GeV}^2$.

In general, one can observe an overall suppression of the form factors G_P^* for both cases ($|\Delta I| = 1$ and $|\Delta S| = 1$) compared with the vacuum, particularly at low Q^2 . The suppression increases with the density. The

suppression at low Q^2 is diluted when Q^2 increases. In some cases, there are apparent overlaps of the different calculations ($\rho = 0, 0.5\rho_0$ and ρ_0), particularly for heavy baryons. See the last two lines on the right side of Fig. C1 and all lines on the right side of Fig. C3. The apparent overlaps are the consequence of the reduced scale in Q^2 and the thickness of the lines.

The analysis of the suppression effect in medium on G_P is simplified when we look at the ratios G_P^*/G_P that are presented on the left side of Figs. 9 and C4 for $|\Delta I| = 1$ and on the left side of Figs. 10 and C5 for $|\Delta S| = 1$.

In some cases ($\Sigma^+ \rightarrow \Lambda$, $\Sigma^0 \rightarrow \Sigma^+$, $\Xi^- \rightarrow \Lambda$ and $\Xi^- \rightarrow \Sigma^+$) we have more significant reductions of G_P^*/G_P at low Q^2 due to the more effective reduction of the meson cloud component, as discussed already for G_A^* (recall that $G_P^* \propto G_A^*$). At large Q^2 , we can expect for sufficient large values of Q^2 the dominance of the pole term (proportional to G_A^{B*}). This effect can be observed in the figures for the vacuum (left side of Figs. C1, C2 and C3) in the upper limit of Q^2 .

We start the discussion with the $|\Delta I| = 1$ transitions. For the transitions $|\Delta I| = 1$, on the left side of Figs. 9 and C4, the significant reduction of the ratio G_P^*/G_P can be understood as a consequence of the dominance of the pole and meson cloud terms, a sum proportional to

$G_A^* = G_A^{B*} + G_A^{MC*}$. In that case, $G_P^* \propto (M_{BB'}^*)^2 G_A^*$, since in the present model m_π has the same value for the vacuum and medium (m_π is almost insensitive to the medium modifications [17–20]).

In these conditions, we can conclude that

$$\frac{G_P^*}{G_P} \simeq \left(\frac{M_B^* + M_{B'}^*}{M_B + M_{B'}} \right)^2 \frac{G_A^*}{G_A}. \quad (5.1)$$

The result $G_P^*/G_P < 1$ is then naturally explained by the mass reduction in medium ($\frac{M_B^* + M_{B'}^*}{M_B + M_{B'}} < 1$) and by the reduction of G_A in medium ($G_A^*/G_A < 1$) discussed already. The suppression is more effective due to the power 2 in the mass ratio. One can then expect a triple suppression of the ratio G_P^*/G_P in medium for $|\Delta I| = 1$. The impact of the suppression is smaller for heavy baryons (mass ratio and G_A^*/G_A are reduced more weakly), and lower densities ρ . Note, in this respect, that the reduction of G_P^*/G_P is very mild for the $\Xi^- \rightarrow \Xi^0$ near the upper limit of Q^2 .

We consider now the $|\Delta S| = 1$ transitions. In this case, the pole and the meson cloud term include the factor $\frac{(M_B^* + M_{B'}^*)^2}{m_K^{*2} + Q^2}$. At low Q^2 the effect of mass reduction of the kaon cancels in part the effect of the reduction of the baryon masses in medium (factor $\frac{(M_B^* + M_{B'}^*)^2}{(M_B + M_{B'})^2}$), since $\frac{m_K^2}{m_K^{*2}} > 1$. Thus, at low Q^2 , the ratio is dominated by the reduction of the meson cloud contribution (more significant reduction at low Q^2). For large Q^2 , the effect of the kaon mass modification $m_K \rightarrow m_K^*$ is included in the factor $1 + \frac{m_K^2 - m_K^{*2}}{m_K^{*2} + Q^2}$ and decreases quickly to the unit. The consequence is that ratio G_P^*/G_P can be described by Eq. (5.1), with G_A^* replaced by G_A^{B*} (dominance of the pole term at large Q^2). The conclusion is then that at large Q^2 , we can expect a stronger suppression for light baryons (more significant baryon mass effect and reduction of G_A^{B*}/G_A^B) and almost no medium effects for heavy baryons ($G_P^*/G_P \approx 1$).

The final conclusion is then that $G_P^*/G_P < 1$ if the mass reduction effect is significant (light baryons, large densities). For heavy baryons, the mass reduction is less effective, and we can observe the convergence of the calculation ($G_P^*/G_P \approx 1$) for relatively small values of Q^2 (see transitions $\Xi^- \rightarrow \Lambda$, $\Xi^- \rightarrow \Sigma^0$ and $\Xi^0 \rightarrow \Sigma^+$).

C. Axial form factors in medium – Falloffs with Q^2

To finish the discussion about the form factors G_A and G_P in medium we analyze the dependence of the form factors on Q^2 . This information is important when we discuss the slope of the form factors near $Q^2 = 0$, at large Q^2 , or parametrize the form factors (vacuum or medium) in terms of simple dipole forms.

Notice that we do not discuss now the variation G_A^* relative to G_A in terms of Q^2 (the same for G_P^* and G_P), but that we are now interested in the variation of the form

factors relative to the result at $Q^2 = 0$. The ratios discussed in the previous section give us information about the amount (percentage) of variation from the vacuum to the medium, but tell us nothing about the relative falloff of the form factors.

We look now at the functions $G_A^*(Q^2)/G_A^*(0)$ and $G_P^*(Q^2)/G_P^*(0)$. In the limit $Q^2 = 0$ the slope of the ratio gives information about the derivatives of the functions at $Q^2 = 0$. Taking G_A as an example, one has for small Q^2 : $G_A(Q^2) - G_A(0) = -\frac{1}{6} \langle r_A^2 \rangle Q^2 G_A(0)$, where the axial-vector square radius is $\langle r_A^2 \rangle = -\frac{6}{G_A(0)} \frac{dG_A}{dQ^2}(0)$. A similar form can be used for G_P .

The ratios for finite Q^2 measure the variation of the falloff with Q^2 and can be used to observe variations from simple dipole forms.

1. Axial-vector form factor G_A^*

Examples of calculations of $G_A^*(Q^2)/G_A^*(0)$ are presented on the right side of Figs. 7 and 8, for $|\Delta I| = 1$ and $|\Delta S| = 1$, respectively. The results for all transitions are presented in Appendix B (Figs. B4 and B5).

The results can be divided into three main cases in terms of the dependence on ρ : (i) $n \rightarrow p$ and $\Lambda \rightarrow p$ transitions: differences for large Q^2 ; (ii) $\Sigma^- \rightarrow n$ transition: almost no dependence; (iii) remaining cases: differences at low and large Q^2 . Even in the last case, the dependence on ρ is not strong (variation of a few percent). The main conclusion is then that the effect of the medium is more significant in the magnitude of G_A^* , discussed in the previous section.

As mentioned already, the slope of $G_A^*(Q^2)/G_A^*(0)$ is related to the axial-vector square radius $\langle r_A^2 \rangle$ in the limit $Q^2 = 0$. The results displayed on Figs. 7, 8, B4, and B5 suggest, however, that the slope is smaller than that we can expect from a typical dipole form (2.2) with $M_A \simeq 1.05$ GeV: $\langle r_A^2 \rangle = \frac{12}{M_A^2} \simeq 0.42$ fm² for the $n \rightarrow p$ transition. The axial-vector square radius obtained for the vacuum is of the order of 0.1 fm² for the $n \rightarrow p$, $\Sigma^0 \rightarrow \Sigma^+$ transitions; 0.16 fm² for $\Xi^- \rightarrow \Sigma^0$ and $\Xi^0 \rightarrow \Sigma^+$ transitions; 0.2 fm² for the $\Sigma^+ \rightarrow \Lambda$ and about 0.35 fm² for the $\Xi^- \rightarrow \Xi^0$, $\Lambda \rightarrow p$, $\Sigma^- \rightarrow n$ and $\Sigma^0 \rightarrow p$. The $\Xi^- \rightarrow \Lambda$ transition is more atypical and has a negative axial-vector square radius (as can be inferred from the figure). These results are a consequence of the smooth dependence of the function G_A near $Q^2 = 0$, that can be linked with P -state contributions to the transition form factors. This topic is discussed in Sec. V E. The conclusion is then that near $Q^2 = 0$, at the scale of $Q^2 = 0.01$ GeV² the axial-vector form factor G_A has a slower falloff than suggested by a dipole parametrization of G_A with a typical cutoff $M_A \simeq 1.05$ GeV, for the $n \rightarrow p$ transition (0.13 fm² to be compared with the *experimental* estimate 0.42 fm²).

The present results suggest then that $\langle r_A^2 \rangle$ may decrease slightly in medium, contrary to what we naively

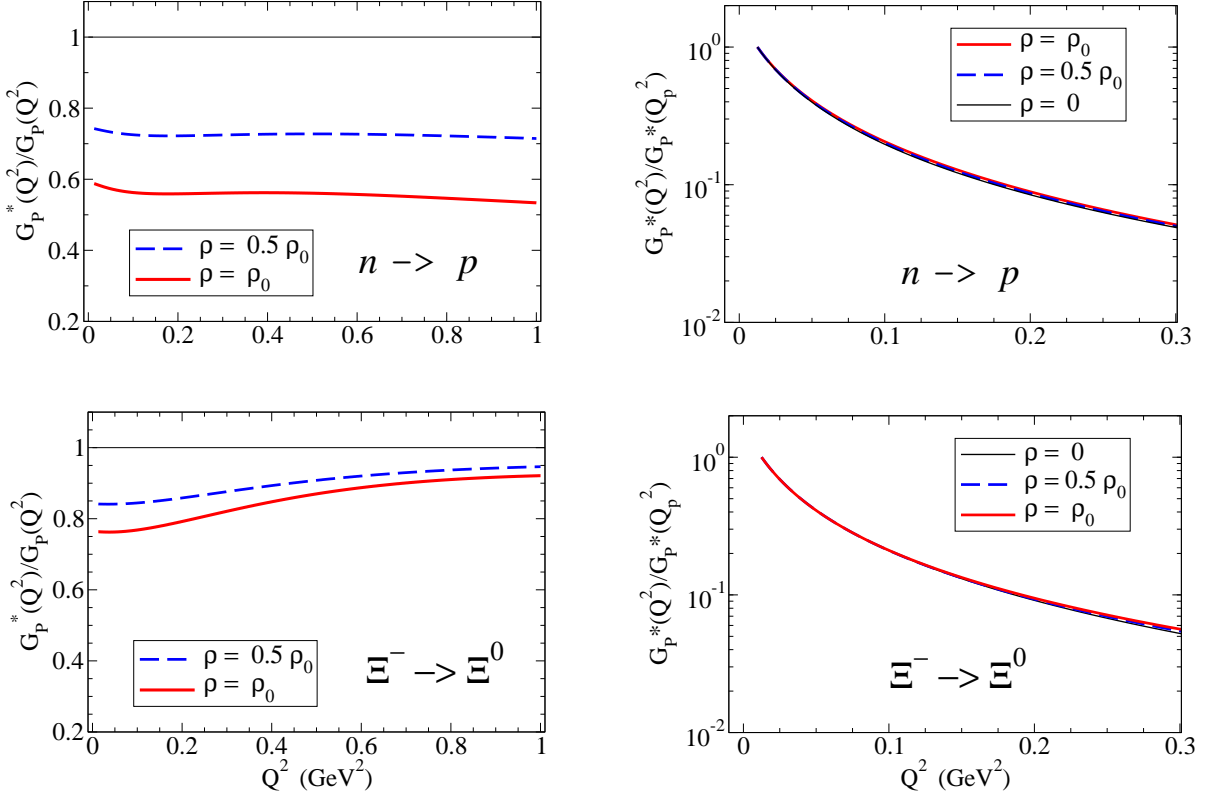


FIG. 9. Induced pseudoscalar form factor G_P for $|\Delta I| = 1$ transitions. Ratios G_P^*/G_P and $G_P^*(Q^2)/G_P^*(Q_p^2)$. The results for the $\Sigma^+ \rightarrow \Lambda$ and $\Sigma^0 \rightarrow \Sigma^+$ transitions are presented in Appendix C, Fig. C4.

observe, for instance by the calculations of the corresponding electromagnetic form factors, namely, charge radii of the octet baryons increase in medium [21, 27–29]. In contrast, the calculations of $\langle r_A^2 \rangle$ from Refs. [126, 127] suggest that we may expect a small enhancement in medium.

We notice, however, that the slow falloff of G_A near $Q^2 = 0$ is a local effect, and when we extend the analysis to the range $Q^2 = 0.1$ GeV², our model calculation for G_A compares well with the dipole parametrization discussed above. Only for $Q^2 > 1.2$ GeV², do we observe significant differences from the dipole parametrization. Our model has a falloff slower than the dipole parametrization.

The conclusion of this section is that (i) the falloff does not vary significantly with the density ρ , (ii) our calculations for G_A can be approximated globally by a dipole parametrization in the region $Q^2 = 0$ –1.2 GeV²; (iii) above $Q^2 = 1.2$ GeV², we expect G_A to have a falloff slower than a dipole parametrization with $M_A \simeq 1.05$ GeV.

2. Induced pseudoscalar form factor G_P^*

The study of the falloff of G_P^* must be taken with care due to the very rapidly changing function near $Q^2 = 0$, dis-

cussed in the previous sections. We make then a more qualitative analysis based on a ratio to a value of Q^2 in a range where the falloffs of G_P are more well defined. We consider then the value $Q_p^2 = 0.012$ GeV² (still a small value, large enough to avoid the turning effect of the function G_P^B). Examples of calculations of $G_P^*(Q^2)/G_P^*(Q_p^2)$ are presented on the right side of Fig. 9 for $|\Delta I| = 1$, and on the right side of Figs. 10 for $|\Delta S| = 1$. The calculations for all transitions are presented in Appendix C (see Figs. C4 and C5).

The difference between the calculations for different ρ for the case $|\Delta I| = 1$ (right side of Figs. 9 and C4) are difficult to observe, so we use a logarithmic scale. The similarity of the calculations is a consequence of the fact that the mass of the pion is unmodified by the medium and the factor $1/(m_\pi^2 + Q^2)$. From the figures, one can conclude that, apart from the value of the function G_P near $Q^2 = 0$, the cases $\rho/\rho_0 = 0, 0.5$ and 1 are indistinguishable at low Q^2 ($Q^2 < 0.1$ GeV²). The ratio can then be interpreted as an universal function. The corollary of this result is that at low Q^2 , we can determine the function $G_P^*(Q^2)$ correcting the function in vacuum $G_P(Q^2)$ by $G_P^*(Q_p^2)/G_P(Q_p^2)$.

An additional conclusion can be obtained when we represent all ratios $G_P^*(Q^2)/G_P^*(Q_p^2)$ in one figure. All lines are almost indistinguishable below $Q^2 = 0.1$ GeV². This

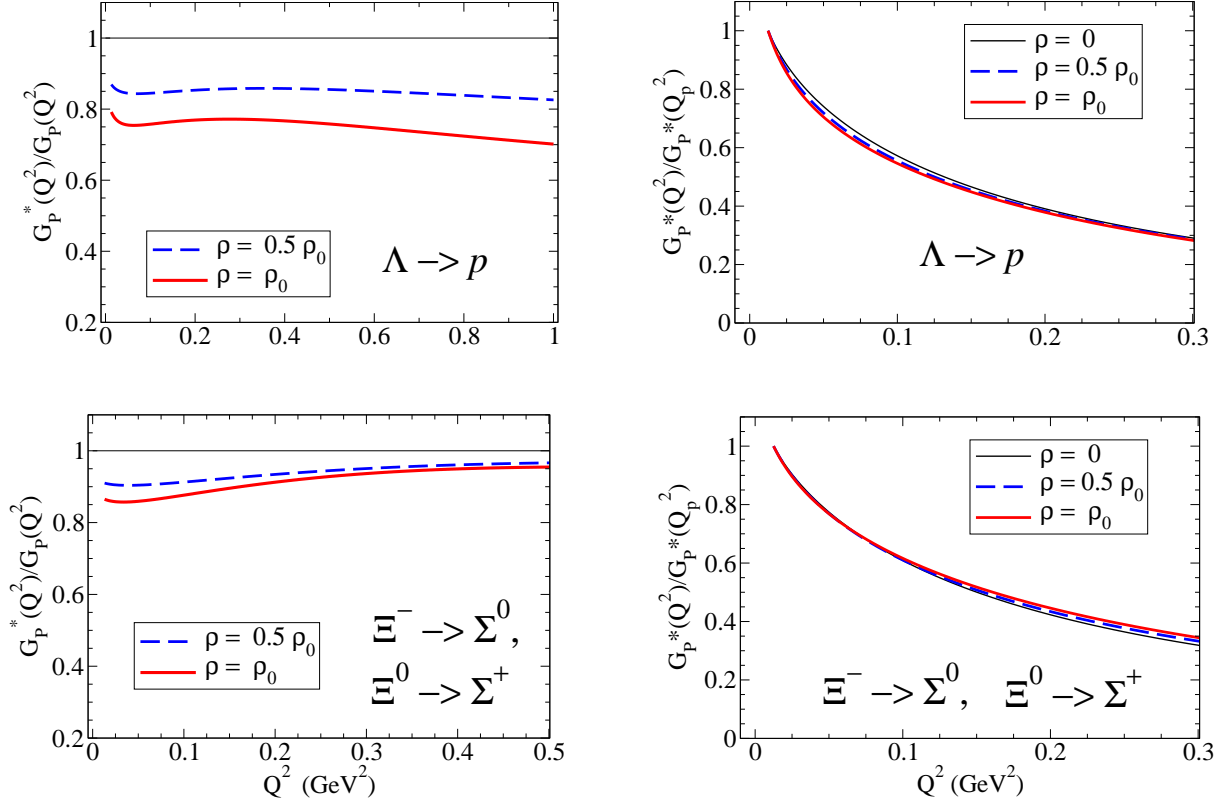


FIG. 10. Induced pseudoscalar form factor G_P for $|\Delta S| = 1$ transitions. Ratios G_P^*/G_P and $G_P^*(Q^2)/G_P^*(Q_p^2)$. The results for the $\Sigma^- \rightarrow n$, $\Sigma^0 \rightarrow p$ and $\Xi^- \rightarrow \Lambda$ transition are presented in Appendix C, Fig. C5. The ratios are the same for $\Xi^- \rightarrow \Sigma^0$ and $\Xi^0 \rightarrow \Sigma^+$.

result means that, in that range $G_P^*(Q^2)/G_P^*(Q_p^2)$ is a universal function (flavor independent) that can be estimated using the results for the nucleon.

The results for $|\Delta S| = 1$ (right side of Figs. 10 and C5), now in a linear scale, show a different behavior from $|\Delta I| = 1$ cases, as a consequence of the factors $1/(m_K^{*2} + Q^2)$. There are two typical cases, divided into light baryons (Λ and Σ decays) and into heavy baryons (Ξ decays). In the first case, for the $\Lambda \rightarrow p$ and $\Sigma^- \rightarrow n/\Sigma^0 \rightarrow p$ transitions, the ratios are almost the same near $Q^2 = Q_p^2$ but differ in the range $Q^2 \simeq 0.02$ – 0.2 GeV^2 , till the lines converge again. In that region the ratios are smaller for larger densities. In the second case, for the $\Xi^- \rightarrow \Lambda$ and $\Xi^- \rightarrow \Sigma^0$ transitions the ratios are the same below $Q^2 = 0.5$ GeV^2 , and differ after that point (larger ratio for larger densities). Differently from the case $|\Delta I| = 1$, the different transitions are characterized by similar but different slopes for $G_P^*(Q^2)/G_P(Q_p^2)$ at low Q^2 .

The overall conclusion is that the functions $G_P^*(Q^2)/G_P(Q_p^2)$ have a very sharp variation at low Q^2 , as a consequence of the significant effect of the pole terms associated with the pion and the kaon. In the case of $|\Delta I| = 1$, we may expect that the ratio $G_P^*(Q^2)/G_P(Q_p^2)$ is the same for all transitions at low Q^2 .

The description of the function G_P^* can be improved in the future, once stronger constraints are included in the determination of the component G_P^B , and on the axial form factors, in general.

D. Summary of the results in medium

We can summarize now the numerical results for the weak interaction axial form factors, for the $|\Delta I| = 1$ and $|\Delta S| = 1$ transitions.

*Axial-vector form factor G_A^**

From the discussion in Sec. VB1, we conclude that the axial-vector form factors are suppressed (quenched) in medium, since $G_A^*/G_A < 1$ for the densities $\rho = 0.5\rho_0$ and ρ_0 . This suppression is a consequence of a reduction of the meson cloud contribution, more significant at low Q^2 , and the bare contribution, more significant at large Q^2 .

The suppression is stronger for light baryons (like in the $n \rightarrow p$ and $\Lambda \rightarrow p$ transitions) than for heavy baryons (like in the $\Xi^- \rightarrow \Xi^0$, $\Xi^0 \rightarrow \Sigma^+$ and $\Xi^- \rightarrow \Sigma^0$ transitions) and increases with the density. At low Q^2 , there

is, in general, a stronger suppression of G_A due to the suppression of the meson cloud contribution. In the case of light baryons, one can have a substantial suppression for intermediate Q^2 (about 30% for $n \rightarrow p$ and 25% for $\Lambda \rightarrow p$ for $Q^2 = 2 \text{ GeV}^2$ and $\rho = \rho_0$). In the case of the heavy baryons one has milder suppressions. For the transitions $\Xi^- \rightarrow \Xi^0$, $\Xi^0 \rightarrow \Sigma^+$ and $\Xi^- \rightarrow \Sigma^0$ one can observe a suppression of 8%–12% at $\rho = \rho_0$, with a weak Q^2 dependence for the ratio G_A^*/G_A . For the intermediate mass cases (transitions $\Sigma^+ \rightarrow \Lambda$, $\Sigma^0 \rightarrow \Sigma^+$, $\Sigma^- \rightarrow n$, $\Sigma^0 \rightarrow p$ and $\Xi^- \rightarrow \Lambda$) we observe intermediate suppressions.

Except for a slightly stronger suppression on the $|\Delta I| = 1$ transitions, there are no significant differences in the magnitudes of G_A^*/G_A between the $|\Delta I| = 1$ and $|\Delta S| = 1$ transitions.

Induced pseudoscalar form factor G_P^*

We summarize now the results from Sec. VB2 for the induced pseudoscalar form factor in medium. In general, one observes also a reduction of the ratio G_P^*/G_P in the nuclear medium. In the present case, however, we need to distinguish between the results for the $|\Delta I| = 1$ and $|\Delta S| = 1$ transitions. The magnitude of the suppression increases with the density.

The difference between the $|\Delta I| = 1$ and $|\Delta S| = 1$ transitions is due to the dependence of the pole and meson cloud terms on the mass of the pion ($|\Delta I| = 1$) or the mass of the kaon ($|\Delta S| = 1$). As a consequence, G_P has larger magnitudes near $Q^2 = 0$ for the $|\Delta I| = 1$ transitions than for the $|\Delta S| = 1$ transitions (the results for $|\Delta I| = 1$ are about 10 times larger than the results for $|\Delta S| = 1$). Another difference between the $|\Delta I| = 1$ and $|\Delta S| = 1$ transitions is that G_P displays a much slower falloff with Q^2 for $|\Delta S| = 1$, due to the factor $1/(m_K^{*2} + Q^2)$ on the pole and meson cloud terms (the in-medium kaon mass is still larger than the pion mass).

In the case of $|\Delta I| = 1$, the dominant term is the pole term. In these conditions, one can expect that $G_P^*/G_P \propto (M_{BB'}^*/M_{BB'})^2(G_A^*/G_A)$. The consequence of this relation is that G_P is suppressed in the nuclear medium and that the magnitude of the suppression is determined by the reduction of the masses, by the factor $(M_{BB'}^*/M_{BB'})^2$ and by the reduction of the G_A^* in medium (factor G_A^*/G_A). The combination of the two effects is then a strong suppression for decays of light baryons and a not so strong suppression for decays of heavy baryons (smaller suppression factors).

As for the $|\Delta S| = 1$ transitions, one observes also a reduction of G_P in medium but with different trends for low and intermediate/large Q^2 . At low Q^2 , the magnitude of G_P^*/G_P is smaller than the $|\Delta I| = 1$ transitions, because in this case the reduced mass of the kaon tends to increase the magnitude of G_P in-medium [$G_P^*/G_P \propto (m_K/m_K^*)^2$], canceling partially the reduction due to the baryon masses and G_A^*/G_A . For larger values of Q^2 ,

however, the variation of m_K^* became irrelevant and we recover the relation $G_P^*/G_P \propto (M_{BB'}^*/M_{BB'})^2(G_A^*/G_A)$ (valid for $|\Delta I| = 1$). As a consequence, there is a significant suppression for light baryons and a very small suppression for heavy baryons (with almost no dependence on Q^2 at large Q^2).

In both cases ($|\Delta I| = 1$ and $|\Delta S| = 1$), the suppression on G_P is stronger at low Q^2 , due to the effect of the meson cloud (stronger suppression of G_A in medium).

Combining the cases $|\Delta I| = 1$ and $|\Delta S| = 1$ one can have at intermediate Q^2 ($Q^2 \approx 1 \text{ GeV}^2$) and $\rho = \rho_0$, reductions of about 30–40% for light baryons ($n \rightarrow p$, $\Lambda \rightarrow p$, $\Sigma^- \rightarrow n$ and $\Sigma^0 \rightarrow p$) and about 5%–10% for heavy baryons ($\Xi^- \rightarrow \Xi^0$, $\Xi^- \rightarrow \Sigma^0$ and $\Xi^0 \rightarrow \Sigma^+$). For intermediate mass baryons ($\Sigma^+ \rightarrow \Lambda$, $\Sigma^0 \rightarrow \Sigma^+$, $\Sigma^- \rightarrow n$, $\Sigma^0 \rightarrow p$ and $\Xi^- \rightarrow \Lambda$) one has intermediate reductions (15%–20%).

E. Discussion

The results of the previous sections for G_A and G_P , in vacuum and in the medium, are a natural consequence of the formalism proposed and discussed in Secs. III and IV. As a consequence, the properties of the functions G_A and G_P are the by-product of the assumptions and methods used. We discuss here the virtues and the limitations of the present calculations.

Some of the results for G_A and G_P mentioned in the previous sections are the outcome of the methodology used to determine the free parameters of the model to the lattice QCD data for the nucleon [7, 38]. The calibration based on the lattice QCD data has been limited by the lack of data between $Q^2 = 0$ and $Q^2 = 0.15 \text{ GeV}^2$. This lack of data has consequences on the determination of the n_P and on the quark form factor g_P^q , and may affect the accuracy of the calibration of the functions G_A and G_P at low Q^2 .

We first comment on the results for G_A . As mentioned already, the weak axial-vector form factor is very smooth near $Q^2 = 0$. This property was already present in the model for the vacuum [7], but was not so clearly observed due to the competition between the bare contribution and the meson cloud contribution with a sharp shape $\propto 1/(1 + Q^2/M_A^2)^4$. The smooth shape of the bare contribution can be seen in the bare contribution in Fig. 2 for the nucleon, and it is a consequence of P -wave contributions. Since the P -state mixture was determined by a fit to lattice and physical data in a range $Q^2 = 0\text{--}3 \text{ GeV}^2$ (equal weight for all Q^2 points), no special constraint was included in the fit to the data near $Q^2 = 0$. This is the main reason why the square axial radius deviates from the estimate based on a dipole function. In medium, the function G_A has become softer when $|n_P|$ increases. The present results for G_A are then mainly a consequence of the determination of the parameters of the model based on the lattice QCD simulations, where the low- Q^2 region is not well represented, due to the gap of 0.3 or 0.4 GeV^2

between the lattice QCD data points [38]. The properties of the function G_A for the nucleon are extended to the octet baryon case.

Also related to the previous topic are the results for G_P at low Q^2 . Contrarily to the functions G_A , there are no lattice QCD data for $Q^2 = 0$ (as there are no lattice QCD data for the Pauli form factor F_2). Since the function $g_P^q(Q^2)$, defined in Eq. (3.9), contributes only to the bare contribution in the induced pseudoscalar form factor G_P [see Eq. (3.15)], the free parameters of $g_P^q(Q^2)$ are determined exclusively by the fit to the G_P lattice QCD data. In these conditions, the calibration of the function g_P^q is the result of the data above the minimum value for Q^2 ($Q^2 > 0.15 \text{ GeV}^2$) which may significantly affect the result for G_P near $Q^2 = 0$, since that is the point where the global function G_P is expected to have its maximum. More recent data with a wide range in Q^2 , or independent estimates of $G_P(0)$ may help to improve the calibration of G_P^B for $|\Delta I| = 1$ and $|\Delta S| = 1$. In the alternative, a fitting procedure with some theoretical constraints to the function G_P at low Q^2 may also be used in future studies.

To finish the discussion about the present calculations we comment on possible improvements in the model. As mentioned already, the formalism was applied first to the calculation of the electromagnetic form factors in the nuclear medium using the simplest form for the octet baryon wave functions, restricted to an S -state component [28, 29]. In a previous work [7], we concluded, however, that for the study of the axial form factors in addition to the S -state, it was also necessary a P -state component. The contributions of the meson cloud effects, the octet baryon wave functions, assumed to be dominated by the pion cloud effects, were determined phenomenologically by the electromagnetic form factor data. In the study of the axial structure, we have considered the formalism derived from the electromagnetic structure, with different proportion of the pion cloud contribution (different pion-nucleon self-energy parameter b_1). In the future, we should consider a global parametrization, where the electromagnetic and axial structure form factors of the octet baryons are calculated using the same wave functions, and the same proportion of the meson cloud in the normalization of the baryon states.

The parametrization of the meson cloud contributions at the level of the electromagnetic structure can also be improved with the inclusion of terms associated with the kaon cloud for the Λ , Σ and Ξ systems. The inclusion of the new terms will be sufficient to improve the description of the Σ and Ξ weak decay data, because it reduces the value of $\sqrt{Z_B}$ and, consequently, the magnitude of the G_A (see Sec. V A).

In the future, we may also consider a less phenomenological and more physical motivated description of the meson cloud contribution for the axial form factors, instead of the simplified SU(3) baryon-meson interaction (functions F' and D'). That can be done considering a microscopic connection between the covariant

spectator quark model and the bag model relating the electromagnetic-baryon and meson-baryon couplings of the two frameworks as in Refs. [61, 62].

The methodology discussed in the present work combined with the models developed for the decuplet baryon and the octet baryon to decuplet baryon transitions [50, 60–63] can be used to extend the model calculations to the study of the electromagnetic and axial structure of decuplet baryons and the octet baryon to decuplet baryon transitions in nuclear matter.

VI. NUMERICAL RESULTS FOR NEUTRINO-NUCLEUS CROSS SECTIONS

In the present section, we exemplify how the weak axial form factors calculated in the previous section, can be used to calculate neutrino-nucleus and antineutrino-nucleus cross sections considering the interaction of a neutrino or antineutrino with nucleons immersed in a nuclear matter with density ρ . In addition to the form factor G_A we need also to know the electric (G_E) and magnetic (G_M) form factors in medium. In that case we consider the model from Ref. [28] also derived within the covariant spectator quark model formalism.

The interactions with neutrinos/antineutrinos can be divided in neutral current (NC) and charged current (CC) reactions where leptons (e, μ) can be found in the final state. Here we use M to represent the nucleon mass in vacuum or in medium. For convenience, we analyze the reaction at the Lab frame, where the nucleon (momentum p) is at rest and the neutrino/antineutrino (momentum k) has an energy E_ν , and the transfer momentum to the nucleon is q . In these conditions, the transition cross sections can be expressed in terms of the invariants Q^2 , $y = \frac{p \cdot q}{p \cdot k} = \frac{Q^2}{2ME_\nu}$, the energy E_ν , and the nucleon electromagnetic and axial form factors, as described below.

The single-differential cross section for NC reactions ($\nu N \rightarrow \nu N$ and $\bar{\nu} N \rightarrow \bar{\nu} N$) takes the form [26, 128, 129]

$$\begin{aligned} \left(\frac{d\sigma}{dQ^2} \right)_{\nu(\bar{\nu})}^{\text{NC}} &= \frac{G_F^2}{2\pi} \left[\frac{1}{2} y^2 (G_M^{\text{NC}})^2 \right. \\ &+ \left(1 - y - \frac{M}{2E_\nu} y \right) \frac{(G_E^{\text{NC}})^2 + \frac{E_\nu}{2M} y (G_M^{\text{NC}})^2}{1 + \frac{E_\nu}{2M} y} \\ &+ \left(\frac{1}{2} y^2 + 1 - y + \frac{M}{2E_\nu} y \right) (G_A^{\text{NC}})^2 \\ &\mp 2y \left(1 - \frac{1}{2} y \right) G_M^{\text{NC}} G_A^{\text{NC}} \left. \right], \end{aligned} \quad (6.1)$$

where $G_F = 1.664 \times 10^{-5} \text{ GeV}^{-2}$ is the Fermi constant, and G_ℓ^{NC} ($\ell = E, M$) and G_A^{NC} are the NC form factors, as defined next. The upper sign in the last term corresponds to the reactions with neutrinos and the lower sign the reaction with antineutrinos.

The NC form factors take the form ($\ell = E, M$)

$$G_\ell^{\text{NC}} = \begin{cases} \frac{t}{2}G_\ell^p - \frac{1}{2}G_\ell^n & p \text{ target} \\ \frac{t}{2}G_\ell^n - \frac{1}{2}G_\ell^p & n \text{ target} \end{cases}, \quad (6.2)$$

with $t = 1 - 4 \sin^2 \theta_w \simeq 0.076$, (θ_w is the weak mixing or Weinberg angle) and

$$G_A^{\text{NC}} = \begin{cases} -\frac{1}{2}G_A^{np} & p \text{ target} \\ \frac{1}{2}G_A^{np} & n \text{ target} \end{cases}. \quad (6.3)$$

The function G_A^{np} is the nucleon axial-vector form factor (associated with the $n \rightarrow p$ decay) discussed in the previous sections.

The single-differential cross sections for the CC reactions ($\nu_e n \rightarrow e^- p$ and $\bar{\nu}_e p \rightarrow e^+ n$) can be also written in a similar form (assuming that the electron mass can be neglected) [25, 128, 129]

$$\begin{aligned} \left(\frac{d\sigma}{dQ^2}\right)_{\nu(\bar{\nu})}^{\text{CC}} &= \frac{G_F^2}{2\pi} \left[\frac{1}{2}y^2 (G_M^{\text{CC}})^2 \right. \\ &+ \left(1 - y - \frac{M}{2E_\nu}y\right) \frac{(G_E^{\text{CC}})^2 + \frac{E_\nu}{2M}y (G_M^{\text{CC}})^2}{1 + \frac{E_\nu}{2M}y} \\ &+ \left(\frac{1}{2}y^2 + 1 - y + \frac{M}{2E_\nu}y\right) (G_A^{\text{CC}})^2 \\ &\left. \mp 2y \left(1 - \frac{1}{2}y\right) G_M^{\text{CC}} G_A^{\text{CC}} \right], \quad (6.4) \end{aligned}$$

where ($\ell = E, M$)

$$G_\ell^{\text{CC}} = G_\ell^p - G_\ell^n, \quad (6.5)$$

and

$$G_A^{\text{CC}} = -G_A^{np}. \quad (6.6)$$

Again, the signs in the last term, respectively, correspond to the reactions with neutrinos (upper sign) or antineutrinos (lower sign).

The previous relations use the magnetic form factors G_M in natural units: $G_M = F_1 + F_2$, where F_1 , F_2 are the Dirac and Pauli form factors respectively.

In this analysis, we neglect for simplicity the strange quark contributions for the electromagnetic form factors (G_E^s , G_M^s) and axial form factors (G_A^s) [25, 26, 129]. For a discussion about the effect of the strange quark see Refs. [12, 128].

The previous expressions are valid for the vacuum using M as the nucleon mass in free space, and for a nuclear medium replacing the nucleon mass by M_N^* and the form factors (G_ℓ and G_A) by the in-medium form factors (G_ℓ^* and G_A^*). In the nuclear medium the value of y is also corrected to

$$y = \frac{Q^2}{2M'E_\nu}, \quad (6.7)$$

where $M' = M_N^* + V$ and V is a vector potential term associated with the nucleon-medium interaction. Numerically one has $V = 0.0627$ GeV for $\rho = 0.5\rho_0$ and $V = 0.1253$ GeV for $\rho = \rho_0$. The last correction is a consequence of the modification of the nucleon energy at rest in medium, where the nucleon momentum takes the form $p = (M', \mathbf{0})$ [23]. The transfer momentum q is then modified in medium¹ leading to the result (6.7).

The expressions for NC reactions can be generalized from electrons for muons (ν_e to ν_μ). The generalization of the CC reactions from electrons to muons is only approximated due to the (large) mass of the muon.

The transitions mentioned above can be divided into the following categories:

- NC transitions (proton target):
 $\nu p \rightarrow \nu p$ and $\bar{\nu} p \rightarrow \bar{\nu} p$,
- NC transitions (neutron target):
 $\nu n \rightarrow \nu n$ and $\bar{\nu} n \rightarrow \bar{\nu} n$,
- CC transitions:
 $\nu n \rightarrow e^- p$ and $\bar{\nu} p \rightarrow e^+ n$.

The magnitudes of the cross sections for these three cases are a consequence of the magnitude of the form factors G_ℓ and G_A . We start by looking for the form factors for the three kinds of transitions.

A. Form factors for NC and CC reactions

The form factors for NC transitions are defined by Eqs. (6.2) and (6.3) for proton and neutron targets, and are presented at the top (proton) and central (neutron) panels in Fig. 11, respectively. The form factors for the CC transitions are defined by Eqs. (6.5) and (6.6) and are presented at the bottom panel in Fig. 11.

The results from Fig. 11 exhibit a reduction of the magnitude in the form factors (absolute values) in the nuclear medium. The reduction increases with the density ρ (the form factors are quenched in medium). These results are a consequence of the combination of proton and neutron form factors. As discussed in Refs. [28, 29] proton and neutron form factors are modified differently in the nuclear medium. The exceptions to the suppression are the results of the electric and the magnetic form factors at $Q^2 = 0$. The suppression of G_A in medium was already discussed in Sec. IV.

At $Q^2 = 0$ the electric form factor is unmodified by the medium because the electric charge does not change in medium. As for the magnetic form factor at $Q^2 = 0$, the invariance of $G_M^{\text{NC}}(0)$ is only approximated, and it is a consequence of the general dominance of the valence

¹ The transfer momentum takes the form $q = (\omega, \mathbf{q})$, where $\omega = \frac{Q^2}{2M'}$ and $|\mathbf{q}|^2 = Q^2 \left(1 + \frac{Q^2}{4M'^2}\right)$.

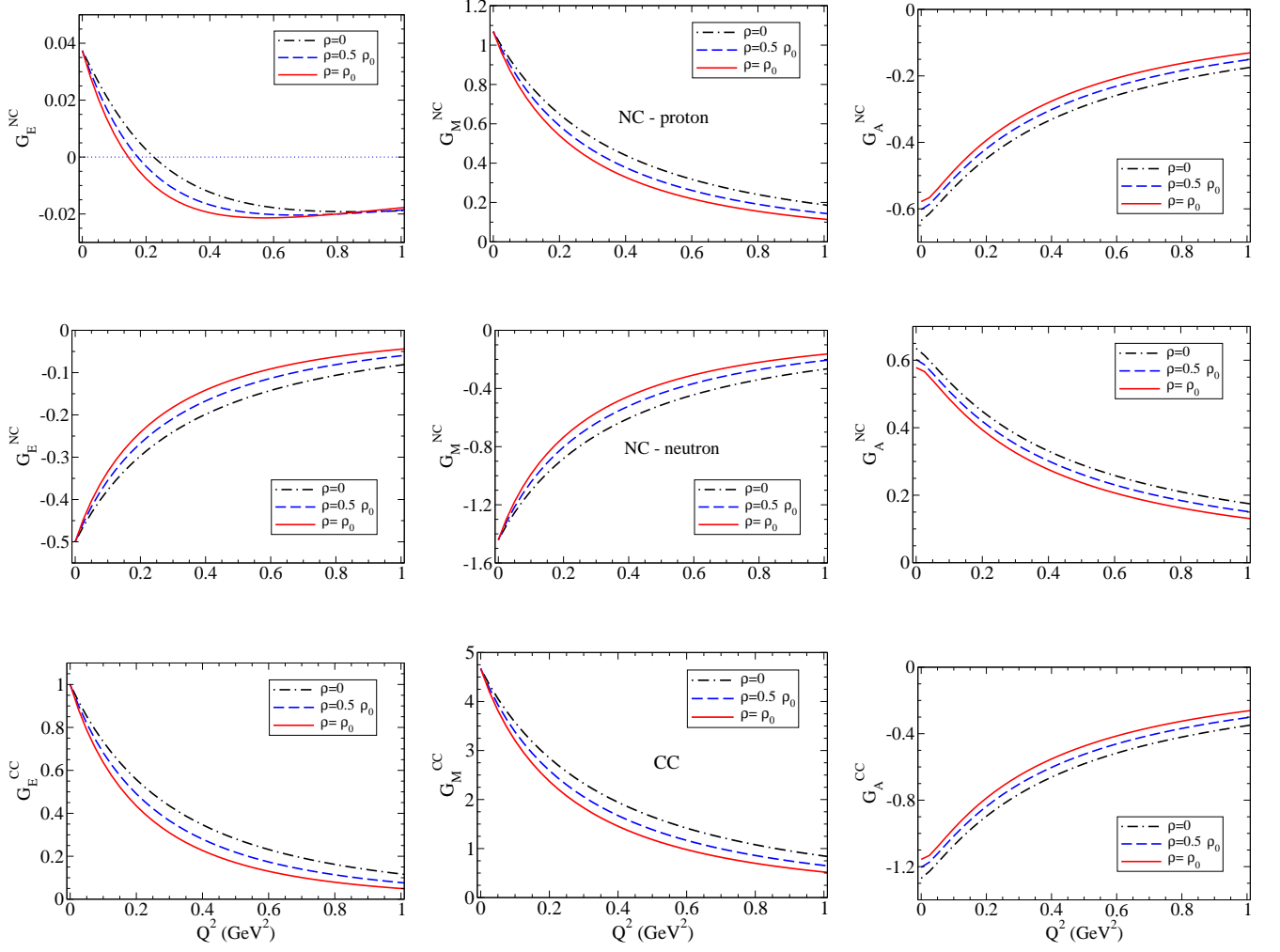


FIG. 11. Electric, magnetic and axial form factor associated with different reactions. **At the top:** NC reactions with proton targets. **At the center:** NC reactions with neutron targets. **At the bottom:** CC reactions.

quark contributions in the nuclear medium [28]. [The quark anomalous magnetic moments in natural units are not modified in medium.]

The medium effect on the magnetic form factors has a different trend when expressed in terms of the nuclear magneton in vacuum [units $e/(2M_N)$], instead of the natural units, as discussed in Ref. [28]. In the first case the nucleon magnetic form factors in medium are corrected by the factor $\frac{M_N}{M_N^*}$ [28]. The consequence of this conversion is that since $G_M^{\text{NC}}(0)$ in natural units is almost independent of the medium, $G_M^{\text{NC}}(0)$ is enhanced when expressed in units $e/(2M_N)$.

For the cases under discussion, the functions $G_M^{\text{NC}}(Q^2)$ and $G_M^{\text{CC}}(Q^2)$ from Fig. 11 (combinations of proton and neutron form factors), we can conclude that the amplification due to the factor $\frac{M_N}{M_N^*}$ dominates over the suppression of $G_M^{\text{NC}}(Q^2)$ in natural units. In conclusion, $G_M(Q^2)$ is enhanced in medium at low Q^2 , when we use units $e/(2M_N)$. When expressed in natural units, $G_M^{\text{NC}}(Q^2)$ and $G_M^{\text{CC}}(Q^2)$ are suppressed in medium.

The results from Fig. 11 show that the function G_E^{NC} is very small for proton targets, as a consequence of the small magnitude of $1 - 4 \sin^2 \theta_w$. For the discussion, we also notice that the magnitude of the form factors G_E and G_A for CC reactions are about 2 times the magnitudes for NC reactions with neutron targets. This effect has an impact on the magnitude of the neutrino-nucleon cross sections, as discussed later.

It is worth mentioning that the single-differential cross sections in terms of Q^2 and the neutrino energy E_ν are not directly measured. The comparison between the theoretical expressions and experimental data for $\frac{d\sigma}{dQ^2}$ in terms of Q^2 requires the knowledge of the neutrino/antineutrino energy spectrum, since measurements are made for defined ranges of neutrino/antineutrino energies [128, 130]. In most cases, measurements include the scattering of electron and muon neutrinos [128, 130–132].

B. Kinematics

In the calculation of the single-differential cross sections one needs to take into account the kinematic relations between the neutrino energy E_ν and Q^2 . As before we consider the Lab frame (initial nucleon at rest).

The squared momentum transfer Q^2 for the neutrino-nucleon scattering with a neutrino energy E_ν and an angle of θ_l between the outgoing and incoming neutrino is [133]

$$Q^2 = \frac{2E_\nu^2(1 - \cos\theta_l)}{1 + \frac{E_\nu}{M}(1 - \cos\theta_l)}, \quad (6.8)$$

neglecting the neutrino mass. The same analysis is valid for antineutrino reactions. From the previous relation we can conclude that the range of values of Q^2 according to the possible values of $u = \cos\theta_l$: $-1 \leq u \leq 1$ is in the interval

$$0 \leq Q^2 \leq \frac{4ME_\nu^2}{M + 2E_\nu}. \quad (6.9)$$

The same conclusion is obtained when the analysis is made at the center of mass of the neutrino-nucleon system [134].

The upper limit (Q_{\max}^2) defines the maximum value of Q^2 that can be obtained for the neutrino energy E_ν . One can then conclude that for $E_\nu = 5$ MeV one has $Q_{\max}^2 \simeq 10^{-4}$ GeV², for $E_\nu = 20$ MeV, one has $Q_{\max}^2 \simeq 1.5 \times 10^{-3}$ GeV², and for $E_\nu = 100$ MeV, one has $Q_{\max}^2 \simeq 0.035$ GeV². Higher values can be obtained for Q_{\max}^2 when we consider the scattering of muon neutrinos/antineutrinos ($\nu_\mu/\bar{\nu}_\mu$) instead of electron neutrinos/antineutrinos ($\nu_e/\bar{\nu}_e$) [135]. In these estimates we use the nucleon mass for the density $\rho = 0.5\rho_0$ as an example.

The relation $E_\nu - Q_{\max}^2$ explains why the last term of the NC and CC single-differential cross sections (6.1) and (6.4) does not change sign when the sign of $G_M^{\text{NC}}G_A^{\text{NC}}$ and $G_M^{\text{CC}}G_A^{\text{CC}}$ is preserved. The conditions (6.9) are equivalent to $0 \leq y < 1$. [In that range, the factor $1 - \frac{1}{2}y$ is always positive, or zero (when $Q^2 = 0$).]

The expressions mentioned above can be used also to determine the value of the neutrino energy E_ν necessary to obtain a given value Q_{\max}^2 :

$$E_\nu = M \left[\sqrt{\tau_m + \tau_m^2} + \tau_m \right], \quad (6.10)$$

where $\tau_m = \frac{Q_{\max}^2}{4M^2}$.

We conclude then that we need $E_\nu = 100$ MeV to reach $Q_{\max}^2 = 0.035$ GeV², and $E_\nu = 0.88$ GeV to reach $Q_{\max}^2 = 1$ GeV². Again, we use the values of the nucleon mass for $\rho = 0.5\rho_0$.

C. Cross sections for NC reactions

The NC transitions for proton and neutron targets are presented in Figs. 12 and 13, respectively, for the den-

sities $\rho = 0, 0.5\rho_0$ and ρ_0 . In the upper panels we represent the $\nu N \rightarrow \nu N$ transitions and in the central panels the $\bar{\nu} N \rightarrow \bar{\nu} N$ transitions. The vertical lines represent the upper limit of Q^2 associated with the neutrino energies $E_\nu = 5, 20$ and 100 MeV. The results for the different energies can be inferred from the upper limit for Q^2 .

The first conclusion from the observations of the figures is that the single-differential cross sections are reduced in medium (quenched effect) and that the suppression is more significant for higher densities. These results are a consequence of the suppression of the form factors G_ℓ^{NC} and G_A^{NC} in medium, discussed earlier. The difference of magnitudes between proton and neutron reactions is a consequence of the magnitude of the form factors [see Fig. 11].

The second conclusion is that there is a dominance of the cross sections for neutrinos (upper panel) over the cross sections for antineutrinos (center panel). The dominance of the reactions with neutrinos over the antineutrinos is a general property of the νN and $\bar{\nu} N$ reactions. The result is a consequence of the last term in Eq. (6.1), where neutrino contributions (sign $-$) are positive, because $G_M^{\text{NC}}G_A^{\text{NC}} < 0$, while the contributions for the antineutrino (sign $+$) are negative.

For a better visualization of this effect, we compare at the bottom panel in Figs. 12 and 13 the results for $\nu N \rightarrow \nu N$ the $\bar{\nu} N \rightarrow \bar{\nu} N$ for a fixed density ($\rho = 0.5\rho_0$). Similar results are obtained for $\rho = 0$ and $\rho = \rho_0$.

In the limit $Q^2 = 0$ the neutrino and antineutrino cross sections have the same value because the last terms of Eqs. (6.1) and (6.4) vanishes. The magnitudes of the cross sections are larger for $E_\nu = 20$ MeV. The variation of the antineutrino cross sections with Q^2 for larger values of E_ν : almost constant for proton targets and a soft reduction with neutron targets is a consequence of the dependence of G_M^{NC} with Q^2 . The variation of the antineutrino cross sections with Q^2 : almost constant for proton targets and the reduction with neutron targets is a consequence of the dependence of G_M^{NC} with Q^2 . The product $G_M^{\text{NC}}G_A^{\text{NC}}$ is negative for protons and neutrons but the magnitude is larger for the case of the neutrons, because $|G_M^{\text{NC}}|$ is larger for neutron targets ($|G_A^{\text{NC}}|$ is the same for both cases). As a consequence, the antineutrino single-differential cross section is reduced for the neutron target when Q^2 increases.

D. Cross sections for CC reactions

The single-differential cross sections for the CC reactions $\nu n \rightarrow e^- p$ and $\bar{\nu} p \rightarrow e^+ n$ are presented in Fig. 14 for the densities $\rho = 0, 0.5\rho_0$ and ρ_0 . We consider the range of Q^2 associated to the neutrino energies $E_\nu = 5, 20$ and 100 MeV. As before, the results for the different energies can be inferred from the upper limit lines for Q^2 .

As for the NC transitions, we conclude that the cross sections are reduced in medium (quenched effect). Also for NC transitions one can observe the dominance of the

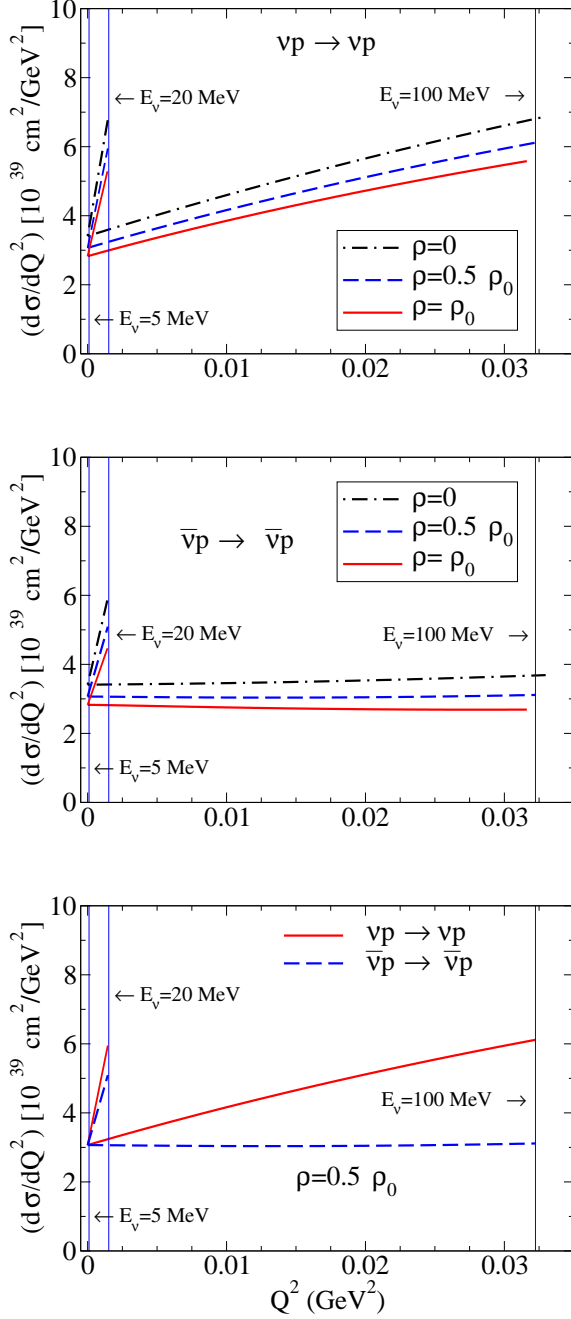


FIG. 12. Single-differential cross sections for NC reactions with proton targets for the densities $\rho = 0, 0.5\rho_0, \rho_0$. Neutrino energies: $E_\nu = 5, 20$ and 100 MeV. **At the top:** Neutrino-proton scattering $\nu p \rightarrow \nu p$. **At the center:** Antineutrino-proton scattering $\bar{\nu} p \rightarrow \bar{\nu} p$. **At the bottom:** Comparison between $\nu p \rightarrow \nu p$ and $\bar{\nu} p \rightarrow \bar{\nu} p$ transitions. $\rho = 0.5\rho_0$.

neutrino cross sections over the antineutrino cross sections.

In comparison with the NC transitions we can notice that the scale of the single-differential cross sections increases by a factor of about 4. This result is a consequence of the relations between the form factors G_E and

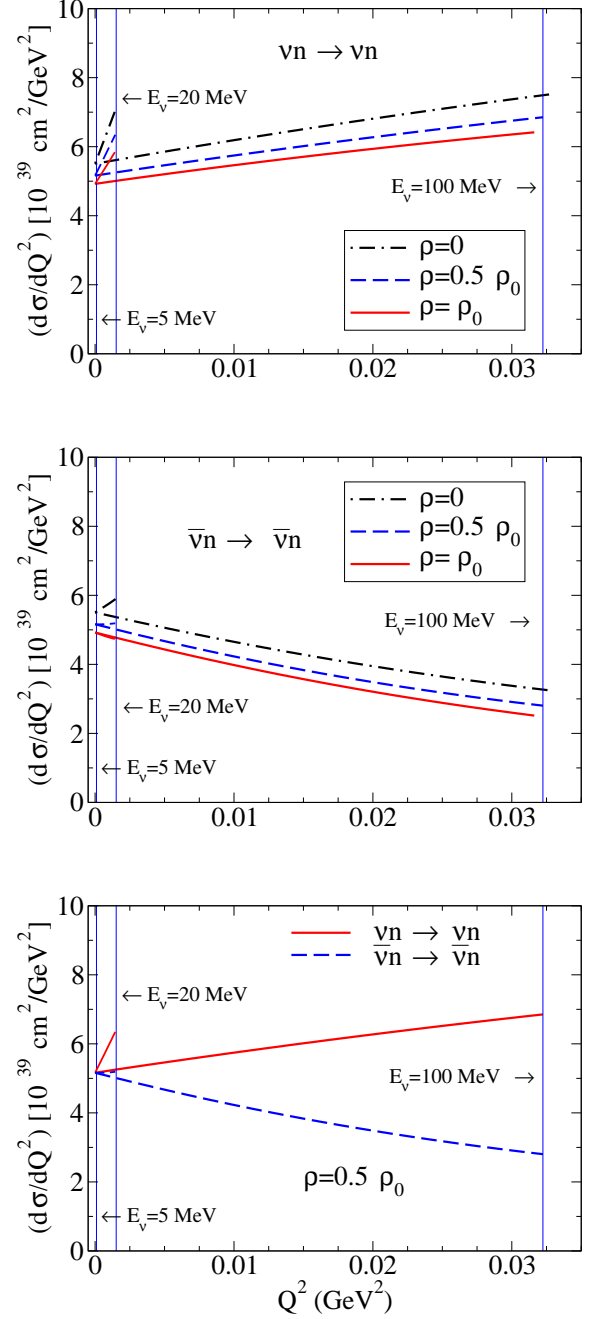


FIG. 13. Single-differential cross sections for NC reactions with neutron targets for the densities $\rho = 0, 0.5\rho_0, \rho_0$. Neutrino energies: $E_\nu = 5, 20$ and 100 MeV. **At the top:** Neutrino-neutron scattering $\nu n \rightarrow \nu n$. **At the center:** Antineutrino-neutron scattering $\bar{\nu} n \rightarrow \bar{\nu} n$. **At the bottom:** Comparison between $\nu n \rightarrow \nu n$ and $\bar{\nu} n \rightarrow \bar{\nu} n$ transitions. $\rho = 0.5\rho_0$.

G_A for NC reactions with neutron targets and CC reactions, discussed previously. The form factors for CC reactions are about 2 times larger. The effect of G_M in the cross sections is reduced by the multiplication with y .

The relation between the $\nu n \rightarrow e^- p$ and $\bar{\nu} p \rightarrow e^+ n$ cross sections confirm the role of the neu-

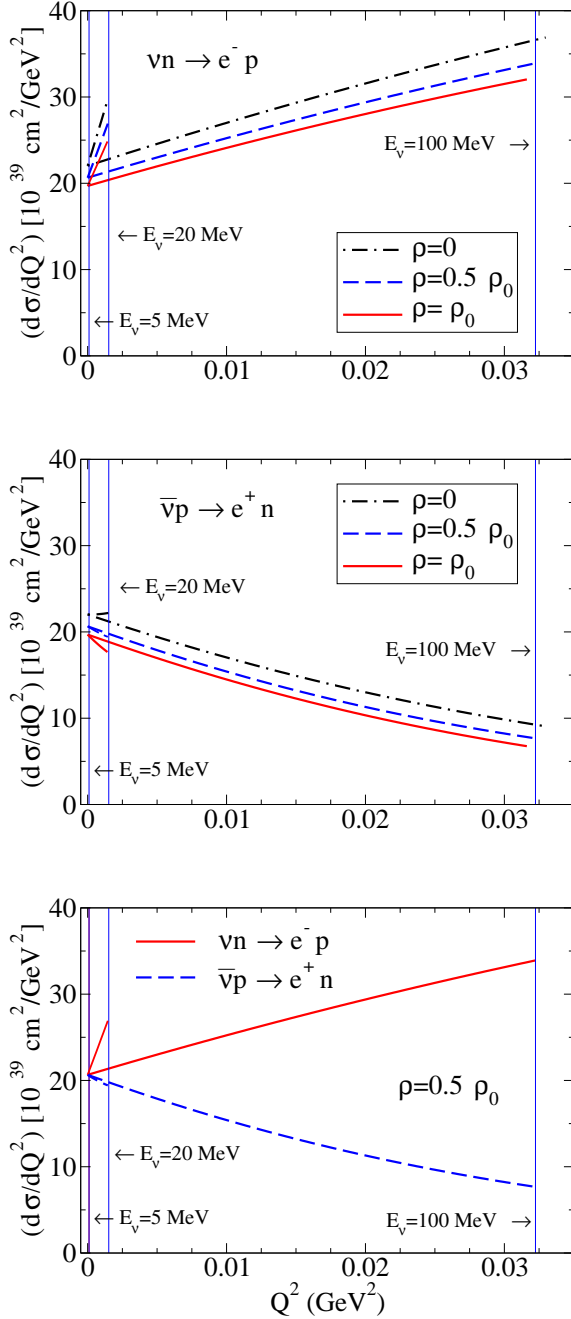


FIG. 14. Single-differential cross sections for CC reactions for the densities $\rho = 0, 0.5\rho_0, \rho_0$. Neutrino energies: $E_\nu = 5, 20$ and 100 MeV. **At the top:** $\nu n \rightarrow e^- p$ scattering. **At the center:** $\bar{\nu} p \rightarrow e^+ n$ scattering. **At the bottom:** Comparison between $\nu n \rightarrow e^- p$ and $\bar{\nu} p \rightarrow e^+ n$ single-differential cross sections. $\rho = 0.5\rho_0$.

trino/antineutrino reactions already discussed for $\nu N \rightarrow \nu N$ reactions (to be compared with $\nu n \rightarrow e^- p$) and $\bar{\nu} N \rightarrow \bar{\nu} N$ reactions (to be compared with $\bar{\nu} p \rightarrow e^+ n$).

E. Summary

In the present section, we exemplify how to use the calculations of the electromagnetic and axial-vector form factors in medium to calculate the single-differential cross sections of NC and CC reactions in medium. In general the cross sections are reduced in medium. The magnitude of the calculations depends on the incident particle (neutrino or antineutrino). The calculation of the $\frac{d\sigma}{dQ^2}$ in terms of Q^2 requires the knowledge of the neutrino/antineutrino energy E_ν distribution.

The present calculations are consistent with the dominance of the neutrino cross sections over the antineutrino single-differential cross sections. The effect was observed on the BNL experiments [128, 130], where the averaged neutrino over the antineutrino single-differential cross sections for muon neutrinos ($\nu_\mu p \rightarrow \nu_\mu p$ vs $\bar{\nu}_\mu p \rightarrow \bar{\nu}_\mu p$) are determined. The main difference to the present calculations is on the lepton family (muon neutrinos instead of electron neutrinos) and the energy range of neutrinos ($E_\nu \simeq 1$ GeV, instead of $E_\nu \simeq 0.1$ GeV).

VII. OUTLOOK AND CONCLUSIONS

The literature about the electromagnetic and axial structure of baryons in the nuclear medium is scarce, except for the case of the nucleon. This work is one more relevant contribution to the field. We present a systematic study of the axial form factors of the octet baryons in terms of the square transfer momentum ($q^2 = -Q^2$) and the density of the nuclear medium. We extend here previous studies in the free space for octet baryons immersed in a nuclear medium. The calculations presented can be used in the future studies of interactions between the octet baryons with neutrinos or antineutrinos in the nuclear medium, at low, intermediate and large Q^2 . We expect the present study to stimulate future works on the subject and promote a debate between the different formalisms used in the studies of the reactions in the nuclear medium.

Our calculations are based on the covariant spectator quark model, which takes into account the valence quark effects and the meson cloud dressing effects on the electroweak interactions with baryon systems. The model has been used successfully in studies of the electromagnetic and axial structure of several baryon systems including resonances of the nucleon in free space. The extension of the model to the nuclear medium takes into account the modifications of the properties of mesons and baryons (masses and coupling constants) in the medium determined by the quark-meson coupling model.

The valence quark component of the model uses a vector meson dominance parametrization of the quark current and the SU(6) flavor-spin symmetry to determine the radial wave functions of the baryon systems. The free parameters of the model were determined in the previous studies of the octet baryon systems in lattice QCD and

in the free space. The meson cloud dressing is estimated phenomenologically using the SU(3) baryon-meson model and the physical information of the octet baryon axial couplings.

We use the formalism to calculate the weak axial-vector G_A and induced pseudoscalar G_P form factor associated with the $B' \rightarrow B$ transitions between the octet baryon members, for different nuclear densities, including the vacuum ($\rho = 0$), and the normal nuclear matter density ($\rho = \rho_0 \simeq 0.15 \text{ fm}^{-3}$). The formalism can be used for other values of ρ including $\rho > \rho_0$.

Our calculations in the nuclear medium suggest that the weak axial-vector form factor G_A is suppressed in the nuclear medium. The suppression is stronger for light baryons and high densities. The effect increases, in general, with Q^2 . In the case of the $n \rightarrow p$ transition about 30% for the nuclear density for $Q^2 = 2 \text{ GeV}^2$.

As for the induced pseudoscalar form factor G_P , because it is an observable that is hard to measure even in the vacuum, we have made more qualitative estimates. Our calculations suggest that G_P is significantly suppressed in medium. In the case of $|\Delta I| = 1$ transitions (only u and d quarks are involved) the suppression is more significant for light baryons and for transitions with significant suppression in G_A . In the case of $|\Delta S| = 1$ transitions (a strange quark transition is involved), one can have significant suppression at low Q^2 in general. At large Q^2 the suppression can be relevant for light baryons and very mild for heavy baryons (especially for Ξ).

To exemplify how the present calculations can be used we calculate the single-differential cross sections of the neutrino and antineutrino interactions with a nucleon immersed in symmetric nuclear matter with densities $\rho = 0, 0.5\rho_0$ and ρ_0 . In the future, we will consider the application of the formalism for interactions of neutrinos or antineutrinos with specific nuclei.

The present formalism can be extended in the future to the study of the electromagnetic and axial structure of the decuplet baryons and for the octet baryon to decuplet baryon transitions.

ACKNOWLEDGMENTS

G. R. thanks H. Parada for useful discussions. G. R. was supported by the Basic Science Research Program funded by the Republic of Korea Ministry of Education (Grant No. NRF-2021R1A6A1A03043957). K.T. was supported by Conselho Nacional de Desenvolvimento Científico e Tecnológico (CNPq, Brazil), Processes No. 313063/2018-4, No. 426150/2018-0 and No. 3014199/2022-2, and FAPESP Processes No. 2019/00763-0 and No. 2023/07313-6, and his work was also part of the projects, Instituto Nacional de Ciência e Tecnologia - Nuclear Physics and Applications (INCT-FNA), Brazil, Process No. 464898/2014-5. The work of M. -K. C. is supported by the National

Research Foundation of Korea (Grants Nos. NRF-2021R1A6A1A03043957 and NRF-2020R1A2C3006177).

Appendix A: Gell-Mann matrices

To complement the discussion of the main text we present here the explicit form of the Gell-Mann matrices [5]

$$\begin{aligned} \lambda_1 &= \begin{pmatrix} 0 & 1 & 0 \\ 1 & 0 & 0 \\ 0 & 0 & 0 \end{pmatrix}, \lambda_2 = \begin{pmatrix} 0 & -i & 0 \\ i & 0 & 0 \\ 0 & 0 & 0 \end{pmatrix}, \lambda_3 = \begin{pmatrix} 1 & 0 & 0 \\ 0 & -1 & 0 \\ 0 & 0 & 0 \end{pmatrix}, \\ \lambda_4 &= \begin{pmatrix} 0 & 0 & 1 \\ 0 & 0 & 0 \\ 1 & 0 & 0 \end{pmatrix}, \lambda_5 = \begin{pmatrix} 0 & 0 & -i \\ 0 & 0 & 0 \\ i & 0 & 0 \end{pmatrix}, \\ \lambda_6 &= \begin{pmatrix} 0 & 0 & 0 \\ 0 & 0 & 1 \\ 0 & 1 & 0 \end{pmatrix}, \lambda_7 = \begin{pmatrix} 0 & 0 & 0 \\ 0 & 0 & -i \\ 0 & i & 0 \end{pmatrix}, \lambda_8 = \frac{1}{\sqrt{3}} \begin{pmatrix} 1 & 0 & 0 \\ 0 & 1 & 0 \\ 0 & 0 & -2 \end{pmatrix}. \end{aligned} \quad (\text{A1})$$

For completeness we can also define $\lambda_0 = \text{diag}(1, 1, 1)$.

In the first line λ_i ($i = 1, 2, 3$) are the SU(3) generalization of the Pauli matrices τ_i ($i = 1, 2, 3$). In the second line the matrices λ_4 and λ_5 mix the quarks u and s . In the last line the matrices λ_6 and λ_7 mix d and s . The matrix λ_8 acts on all flavors (u , d and s).

The neutral transitions ($\Delta I = 0$ and $\Delta S = 0$) are associated with the operator

$$I_0 = \lambda_3. \quad (\text{A2})$$

The transitions that increase/decrease the isospin ($\Delta I = \pm 1$) are defined by

$$I_{\pm} = \frac{1}{2}(\lambda_1 \pm i\lambda_2). \quad (\text{A3})$$

The transitions associated with $s \rightleftharpoons u$ ($\Delta S = \pm 1$) are represented by the operator

$$V_{\pm} = \frac{1}{2}(\lambda_4 \pm i\lambda_5). \quad (\text{A4})$$

For the discussion of the quark electromagnetic current, it is convenient to define

$$\lambda_s = \begin{pmatrix} 0 & 0 & 0 \\ 0 & 0 & 0 \\ 0 & 0 & -2 \end{pmatrix}, \quad (\text{A5})$$

which can also be written as

$$\lambda_s = \sqrt{3}\lambda_8 - \tau_0, \quad (\text{A6})$$

where $\tau_0 = \text{diag}(1, 1, 0)$ is the SU(3) generalization of the SU(2) unitary matrix.

-
- [1] I. G. Aznauryan *et al.*, *Int. J. Mod. Phys. E* **22**, 1330015 (2013) [arXiv:1212.4891 [nucl-th]].
- [2] I. G. Aznauryan and V. D. Burkert, *Prog. Part. Nucl. Phys.* **67**, 1 (2012) [arXiv:1109.1720 [hep-ph]].
- [3] G. Ramalho and M. T. Peña, *Prog. Part. Nucl. Phys.* **136**, 104097 (2024) [arXiv:2306.13900 [hep-ph]].
- [4] V. Bernard, L. Elouadrhiri and U. G. Meissner, *J. Phys. G* **28**, R1 (2002) [hep-ph/0107088].
- [5] J. M. Gaillard and G. Sauvage, *Ann. Rev. Nucl. Part. Sci.* **34**, 351 (1984).
- [6] T. Gorringer and H. W. Fearing, *Rev. Mod. Phys.* **76**, 31 (2004) [nucl-th/0206039].
- [7] G. Ramalho and K. Tsushima, *Phys. Rev. D* **94**, 014001 (2016) [arXiv:1512.01167 [hep-ph]].
- [8] G. Ramalho, *Few Body Syst.* **59**, 92 (2018) [arXiv:1801.01476 [hep-ph]].
- [9] G. Ramalho and K. Tsushima, *Phys. Rev. D* **84**, 054014 (2011) [arXiv:1107.1791 [hep-ph]].
- [10] M. Sajjad Athar, A. Fatima and S. K. Singh, *Prog. Part. Nucl. Phys.* **129**, 104019 (2023) [arXiv:2206.13792 [hep-ph]].
- [11] J. A. Formaggio and G. P. Zeller, *Rev. Mod. Phys.* **84**, 1307 (2012) [arXiv:1305.7513 [hep-ex]].
- [12] S. F. Pate, V. Papavassiliou, J. P. Schaub, D. P. Trujillo, M. V. Ivanov, M. B. Barbaro and C. Giusti, *Contribution to the Vector and Axial Form Factors of the Nucleon*, [arXiv:2402.10854 [hep-ph]].
- [13] J. Gonzalez-Rosa, G. D. Megias, J. A. Caballero and M. B. Barbaro, *Phys. Rev. D* **105**, 093009 (2022) [arXiv:2203.12308 [nucl-th]].
- [14] A. M. Ankowski, A. Ashkenazi, S. Bacca, J. L. Barrow, M. Betancourt, A. Bodek, M. E. Christy, L. D. S. Dytman, A. Friedland and O. Hen, *et al.* *J. Phys. G* **50**, 120501 (2023) [arXiv:2203.06853 [hep-ex]].
- [15] J. M. Franco-Patino, R. González-Jiménez, S. Dolan, M. B. Barbaro, J. A. Caballero, G. D. Megias and J. M. Udias, *Phys. Rev. D* **106**, 113005 (2022) [arXiv:2207.02086 [nucl-th]].
- [16] L. A. Ruso, A. M. Ankowski, S. Bacca, A. B. Balantekin, J. Carlson, S. Gardiner, R. González-Jiménez, R. Gupta, T. J. Hobbs and M. Hoferichter, *et al.* [arXiv:2203.09030 [hep-ph]].
- [17] R. S. Hayano and T. Hatsuda, *Rev. Mod. Phys.* **82**, 2949 (2010).
- [18] P. Kienle and T. Yamazaki, *Prog. Part. Nucl. Phys.* **52**, 85 (2004).
- [19] U. G. Meissner, J. A. Oller and A. Wirzba, *Annals Phys.* **297**, 27 (2002).
- [20] U. Vogl and W. Weise, *Prog. Part. Nucl. Phys.* **27**, 195 (1991).
- [21] W. K. Brooks, S. Strauch, K. Tsushima, *J. Phys. Conf. Ser.* **299**, 012011 (2011).
- [22] T. Miyatsu, M. K. Cheoun and K. Saito, *Astrophys. J.* **813**, 2, 135 (2015) [arXiv:1506.05552 [nucl-th]].
- [23] K. Saito, K. Tsushima and A. W. Thomas, *Prog. Part. Nucl. Phys.* **58**, 1 (2007).
- [24] K. Tsushima, *PTEP* **2022**, 043D02 (2022) [arXiv:2008.03724 [hep-ph]].
- [25] M. K. Cheoun, K. Choi, K. S. Kim, K. Saito, T. Kajino, K. Tsushima and T. Maruyama, *Phys. Lett. B* **723**, 464 (2013) [arXiv:1302.5770 [nucl-th]].
- [26] M. K. Cheoun, K. S. Choi, K. S. Kim, K. Saito, T. Kajino, K. Tsushima and T. Maruyama, *Phys. Rev. C* **87**, 065502 (2013) [arXiv:1303.5920 [nucl-th]].
- [27] D. H. Lu, A. W. Thomas, K. Tsushima, A. G. Williams and K. Saito, *Phys. Lett. B* **417**, 217 (1998); D. H. Lu, K. Tsushima, A. W. Thomas, A. G. Williams and K. Saito, *Phys. Lett. B* **441**, 27 (1998); D. H. Lu, K. Tsushima, A. W. Thomas, A. G. Williams and K. Saito, *Phys. Rev. C* **60**, 068201 (1999).
- [28] G. Ramalho, K. Tsushima and A. W. Thomas, *J. Phys. G* **40**, 015102 (2013) [arXiv:1206.2207 [hep-ph]].
- [29] G. Ramalho, J. P. B. C. de Melo and K. Tsushima, *Phys. Rev. D* **100**, 014030 (2019) [arXiv:1902.08844 [hep-ph]].
- [30] S. Dieterich, P. Bartsch, D. Baumann, J. Bermuth, K. Bohinc, R. Bohm, D. Bosnar, S. Derber *et al.*, *Phys. Lett. B* **500**, 47 (2001)
- [31] M. Paolone, S. P. Malace, S. Strauch, I. Albayrak, J. Arrington, B. L. Berman, E. J. Brash, B. Briscoe *et al.*, *Phys. Rev. Lett.* **105**, 072001 (2010).
- [32] S. Strauch *et al.* [Jefferson Lab E93-049 Collaboration], *Phys. Rev. Lett.* **91**, 052301 (2003).
- [33] J. J. Aubert *et al.* [European Muon], *Phys. Lett. B* **123**, 275 (1983).
- [34] W. Xing, X. G. Wang and A. W. Thomas, *Phys. Lett. B* **846**, 138195 (2023) [arXiv:2305.13666 [hep-ph]].
- [35] D. N. Kim, O. Hen, G. A. Miller, E. Piasetzky, M. Strikman and L. Weinstein, [arXiv:2404.15442 [nucl-th]].
- [36] A. S. Meyer, A. Walker-Loud and C. Wilkinson, *Ann. Rev. Nucl. Part. Sci.* **72**, 205 (2022) [arXiv:2201.01839 [hep-lat]].
- [37] C. C. Chang, A. N. Nicholson, E. Rinaldi, E. Berkowitz, N. Garron, D. A. Brantley, H. Monge-Camacho, C. J. Monahan, C. Bouchard and M. A. Clark, *et al.* *Nature* **558**, 91 (2018) [arXiv:1805.12130 [hep-lat]].
- [38] C. Alexandrou *et al.* [ETM Collaboration], *Phys. Rev. D* **83**, 045010 (2011) [arXiv:1012.0857 [hep-lat]]; C. Alexandrou, M. Constantinou, S. Dinter, V. Drach, K. Jansen, C. Kallidonis and G. Koutsou, *Phys. Rev. D* **88**, 014509 (2013) [arXiv:1303.5979 [hep-lat]].
- [39] C. Alexandrou *et al.* [Extended Twisted Mass], *Phys. Rev. D* **109**, 034503 (2024) [arXiv:2309.05774 [hep-lat]].
- [40] R. Gupta, Y. C. Jang, H. W. Lin, B. Yoon and T. Bhattacharya, *Phys. Rev. D* **96**, 114503 (2017) [arXiv:1705.06834 [hep-lat]]; Y. C. Jang, R. Gupta, B. Yoon and T. Bhattacharya, *Phys. Rev. Lett.* **124**, 072002 (2020) [arXiv:1905.06470 [hep-lat]]; Y. C. Jang *et al.* [Precision Neutron Decay Matrix Elements (PNDME)], *Phys. Rev. D* **109**, 014503 (2024) [arXiv:2305.11330 [hep-lat]].
- [41] D. Djukanovic, G. von Hippel, J. Koponen, H. B. Meyer, K. Ottnad, T. Schulz and H. Wittig, *Phys. Rev. D* **106**, 074503 (2022) [arXiv:2207.03440 [hep-lat]].
- [42] A. Abdel-Rehim, C. Alexandrou, M. Constantinou, P. Dimopoulos, R. Frezzotti, K. Hadjiyiannakou, K. Jansen, C. Kallidonis, B. Kostrzewa and G. Koutsou, *et al.* *Phys. Rev. D* **92**, 114513 (2015) [erratum: *Phys. Rev. D* **93**, 039904 (2016)] [arXiv:1507.04936 [hep-lat]].
- [43] N. Hasan, J. Green, S. Meinel, M. Engelhardt, S. Krieg, J. Negele, A. Pochinsky and S. Syritsyn, *Phys. Rev. D* **99**, 114505 (2019) [arXiv:1903.06487 [hep-lat]].

- [44] O. Tomalak, R. Gupta and T. Bhattacharya, Phys. Rev. D **108**, 074514 (2023) [arXiv:2307.14920 [hep-lat]].
- [45] H. W. Lin and K. Orginos, Phys. Rev. D **79**, 034507 (2009) [arXiv:0712.1214 [hep-lat]]; A. Savanur and H. W. Lin, Phys. Rev. D **102**, 014501 (2020) [arXiv:1901.00018 [hep-lat]].
- [46] G. Erkol, M. Oka and T. T. Takahashi, Phys. Lett. B **686**, 36 (2010) [arXiv:0911.2447 [hep-lat]]; G. Erkol and A. Ozpineci, Phys. Rev. D **83**, 114022 (2011) [arXiv:1105.1637 [hep-ph]].
- [47] G. S. Bali *et al.* [RQCD], Phys. Rev. D **108**, 034512 (2023) [arXiv:2305.04717 [hep-lat]].
- [48] G. Ramalho, Phys. Rev. D **97**, 073002 (2018) [arXiv:1707.07206 [hep-ph]].
- [49] F. Gross, G. Ramalho and M. T. Peña, Phys. Rev. C **77**, 015202 (2008) [arXiv:nucl-th/0606029 [nucl-th]].
- [50] G. Ramalho, K. Tsushima and F. Gross, Phys. Rev. D **80**, 033004 (2009) [arXiv:0907.1060 [hep-ph]].
- [51] F. Gross, G. Ramalho and M. T. Peña, Phys. Rev. D **85**, 093005 (2012) [arXiv:1201.6336 [hep-ph]].
- [52] G. Ramalho, M. T. Peña and F. Gross, Phys. Rev. D **78**, 114017 (2008) [arXiv:0810.4126 [hep-ph]]; G. Ramalho, M. T. Peña and F. Gross, Phys. Rev. D **81**, 113011 (2010) [arXiv:1002.4170 [hep-ph]]; G. Ramalho, Phys. Rev. D **94**, 114001 (2016) [arXiv:1606.03042 [hep-ph]]; G. Ramalho, Eur. Phys. J. A **54**, 75 (2018) [arXiv:1709.07412 [hep-ph]].
- [53] G. Ramalho, M. T. Peña, J. Weil, H. van Hees and U. Mosel, Phys. Rev. D **93**, 033004 (2016) [arXiv:1512.03764 [hep-ph]]; G. Ramalho and M. T. Peña, Phys. Rev. D **85**, 113014 (2012) [arXiv:1205.2575 [hep-ph]].
- [54] G. Ramalho and M. T. Peña, J. Phys. G **36**, 115011 (2009) [arXiv:0812.0187 [hep-ph]]; G. Ramalho and M. T. Peña, Phys. Rev. D **80**, 013008 (2009) [arXiv:0901.4310 [hep-ph]].
- [55] G. Ramalho and K. Tsushima, Phys. Rev. D **89**, 073010 (2014) [arXiv:1402.3234 [hep-ph]].
- [56] G. Ramalho, Phys. Rev. D **95**, 054008 (2017) [arXiv:1612.09555 [hep-ph]]; G. Ramalho and M. T. Peña, Phys. Rev. D **101**, 114008 (2020) [arXiv:2003.04850 [hep-ph]].
- [57] G. Ramalho and M. T. Peña, Phys. Rev. D **95**, 014003 (2017) [arXiv:1610.08788 [nucl-th]]; G. Ramalho and M. T. Peña, Phys. Rev. D **89**, 094016 (2014) [arXiv:1309.0730 [hep-ph]]; G. Ramalho, Phys. Rev. D **90**, 033010 (2014) [arXiv:1407.0649 [hep-ph]].
- [58] G. Ramalho and K. Tsushima, Phys. Rev. D **86**, 114030 (2012) [arXiv:1210.7465 [hep-ph]].
- [59] G. Ramalho and M. T. Peña, Phys. Rev. D **83**, 054011 (2011) [arXiv:1012.2168 [hep-ph]].
- [60] G. Ramalho and K. Tsushima, Phys. Rev. D **87**, 093011 (2013) [arXiv:1302.6889 [hep-ph]].
- [61] G. Ramalho and K. Tsushima, Phys. Rev. D **88**, 053002 (2013) [arXiv:1307.6840 [hep-ph]].
- [62] G. Ramalho and K. Tsushima, Phys. Rev. D **108**, 074019 (2023) [arXiv:2308.04773 [hep-ph]].
- [63] G. Ramalho, Phys. Rev. D **102**, 054016 (2020) [arXiv:2002.07280 [hep-ph]].
- [64] G. Ramalho, M. T. Peña and K. Tsushima, Phys. Rev. D **101**, 014014 (2020) [arXiv:1908.04864 [hep-ph]]; G. Ramalho, Phys. Rev. D **103**, 074018 (2021) [arXiv:2012.11710 [hep-ph]]; G. Ramalho, M. T. Peña, K. Tsushima and M. K. Cheoun, Phys. Lett. B **858**, 139060 (2024) [arXiv:2407.21397 [hep-ph]].
- [65] A. W. Thomas, Adv. Nucl. Phys. **13**, 1 (1984); S. Theberge and A. W. Thomas, Nucl. Phys. A **393**, 252 (1983).
- [66] D. H. Lu, A. W. Thomas and K. Tsushima, [arXiv:nucl-th/0112001 [nucl-th]].
- [67] T. H. R. Skyrme, Proc. Roy. Soc. Lond. A **260**, 127 (1961)
- [68] G. S. Adkins, C. R. Nappi and E. Witten, Nucl. Phys. B **228**, 552 (1983).
- [69] E. M. Nyman and D. O. Riska, Phys. Lett. B **199**, 5 (1987).
- [70] U. G. Meissner, N. Kaiser and W. Weise, Nucl. Phys. A **466**, 685 (1987).
- [71] U. G. Meissner, Phys. Lett. B **220**, 1 (1989).
- [72] P. Alberto, E. Ruiz Arriola, M. Fiolhais, F. Grummer, J. N. Urbano and K. Goeke, Phys. Lett. B **208**, 75 (1988).
- [73] F. Meier and H. Walliser, Phys. Rept. **289**, 383 (1997) [arXiv:hep-ph/9602359 [hep-ph]].
- [74] C. V. Christov, A. Z. Gorski, K. Goeke and P. V. Pobylitsa, Nucl. Phys. A **592**, 513 (1995) [arXiv:hep-ph/9507256 [hep-ph]].
- [75] A. Rakhimov, M. M. Musakhanov, F. C. Khanna and U. T. Yakhshiev, Phys. Rev. C **58**, 1738 (1998) [arXiv:nucl-th/9609049 [nucl-th]].
- [76] U. T. Yakhshiev, U. G. Meissner and A. Wirzba, Eur. Phys. J. A **16**, 569 (2003) [nucl-th/0211055].
- [77] U. Yakhshiev, PTEP **2014**, 123D03 (2014)
- [78] J. R. Smith and G. A. Miller, Phys. Rev. C **70**, 065205 (2004) [nucl-th/0407093].
- [79] T. Ledwig, J. Martin Camalich, L. S. Geng and M. J. Vicente Vacas, Phys. Rev. D **90**, 054502 (2014) [arXiv:1405.5456 [hep-ph]].
- [80] A. Silva, H. C. Kim, D. Urbano and K. Goeke, Phys. Rev. D **72**, 094011 (2005) [arXiv:hep-ph/0509281 [hep-ph]].
- [81] G. S. Yang and H. C. Kim, Phys. Rev. C **92**, 035206 (2015) [arXiv:1504.04453 [hep-ph]].
- [82] K. Kubodera, Y. Kohyama, K. Oikawa and C. W. Kim, Nucl. Phys. A **439**, 695 (1985); Y. Kohyama, K. Oikawa, K. Tsushima and K. Kubodera, Phys. Lett. B **186**, 255 (1987); K. Tsushima, T. Yamaguchi, Y. Kohyama and K. Kubodera, Nucl. Phys. A **489**, 557 (1988); K. Tsushima, T. Yamaguchi, M. Takizawa, Y. Kohyama and K. Kubodera, Phys. Lett. B **205**, 128 (1988); T. Yamaguchi, K. Tsushima, Y. Kohyama and K. Kubodera, Nucl. Phys. A **500**, 429 (1989).
- [83] X. Y. Liu, A. Limphirat, K. Xu, Z. Zhao, K. Khosonthongkee and Y. Yan, Phys. Rev. D **107**, 074006 (2023) [arXiv:2209.00808 [hep-ph]].
- [84] P. Cheng, F. E. Serna, Z. Q. Yao, C. Chen, Z. F. Cui and C. D. Roberts, Phys. Rev. D **106**, 054031 (2022) [arXiv:2207.13811 [hep-ph]].
- [85] G. Eichmann and C. S. Fischer, Eur. Phys. J. A **48**, 9 (2012) [arXiv:1111.2614 [hep-ph]].
- [86] C. Chen, C. S. Fischer, C. D. Roberts and J. Segovia, Phys. Lett. B **815**, 136150 (2021) [arXiv:2011.14026 [hep-ph]].
- [87] C. Chen, C. S. Fischer, C. D. Roberts and J. Segovia, Phys. Rev. D **105**, 094022 (2022) [arXiv:2103.02054 [hep-ph]].
- [88] M. Kirchbach, D. O. Riska and K. Tsushima, Nucl. Phys. A **542**, 616 (1992).

- [89] S. Boffi, L. Y. Glozman, W. Klink, W. Plessas, M. Radici and R. F. Wagenbrunn, *Eur. Phys. J. A* **14**, 17 (2002) [arXiv:hep-ph/0108271 [hep-ph]].
- [90] D. Merten, U. Loring, K. Kretzschmar, B. Metsch and H. R. Petry, *Eur. Phys. J. A* **14**, 477 (2002) [arXiv:hep-ph/0204024 [hep-ph]].
- [91] D. Barquilla-Cano, A. J. Buchmann and E. Hernandez, *Nucl. Phys. A* **714**, 611 (2003) [arXiv:nucl-th/0204067 [nucl-th]].
- [92] B. Julia-Diaz, D. O. Riska and F. Coester, *Phys. Rev. C* **69**, 035212 (2004) [erratum: *Phys. Rev. C* **75**, 069902 (2007)] [arXiv:hep-ph/0312169 [hep-ph]].
- [93] K. Khosonthongkee, V. E. Lyubovitskij, T. Gutsche, A. Faessler, K. Pumsa-ard, S. Cheedket and Y. Yan, *J. Phys. G* **30**, 793 (2004) [arXiv:hep-ph/0403119 [hep-ph]].
- [94] B. Pasquini and S. Boffi, *Phys. Rev. D* **76**, 074011 (2007) [arXiv:0707.2897 [hep-ph]].
- [95] C. Adamuscin, E. Tomasi-Gustafsson, E. Santopinto and R. Bijker, *Phys. Rev. C* **78**, 035201 (2008) [arXiv:0706.3509 [nucl-th]].
- [96] X. Y. Liu, K. Khosonthongkee, A. Limphirat, P. Suebka and Y. Yan, *Phys. Rev. D* **91**, 034022 (2015) [arXiv:1406.7633 [hep-ph]].
- [97] H. Dahiya and M. Randhawa, *Phys. Rev. D* **90**, 074001 (2014) [arXiv:1409.4943 [hep-ph]].
- [98] I. Atayev and S. Mamedov, *Int. J. Theor. Phys.* **61**, 250 (2022) [arXiv:2205.14958 [hep-ph]].
- [99] C. A. Dominguez, M. Loewe, C. Villavicencio and R. Zamora, *Phys. Rev. D* **108**, 074024 (2023) [arXiv:2308.05663 [hep-ph]].
- [100] K. Noro, W. Bentz, I. C. Cloët and T. Kitabayashi, *Phys. Rev. C* **109**, 025205 (2024) [arXiv:2308.13179 [nucl-th]].
- [101] T. Cai *et al.* [MINERvA], *Nature* **614**, 7946, 48 (2023)
- [102] O. Hen, G. A. Miller, E. Piassetzky and L. B. Weinstein, *Rev. Mod. Phys.* **89**, 045002 (2017) [arXiv:1611.09748 [nucl-ex]].
- [103] M. R. Frank, B. K. Jennings and G. A. Miller, *Phys. Rev. C* **54**, 920 (1996) [nucl-th/9509030].
- [104] D. H. Lu, K. Tsushima, A. W. Thomas, A. G. Williams and K. Saito, *Phys. Rev. C* **60**, 068201 (1999) [nucl-th/9807074].
- [105] G. A. Miller, *Phys. Rev. C* **66**, 032201 (2002) [arXiv:nucl-th/0207007 [nucl-th]].
- [106] T. Horikawa and W. Bentz, *Nucl. Phys. A* **762**, 102 (2005) [nucl-th/0506021].
- [107] I. C. Cloët, G. A. Miller, E. Piassetzky and G. Ron, *Phys. Rev. Lett.* **103**, 082301 (2009) [arXiv:0903.1312 [nucl-th]].
- [108] W. R. B. de Araújo, J. P. B. C. de Melo and K. Tsushima, *Nucl. Phys. A* **970**, 325 (2018) [arXiv:1707.00168 [hep-ph]].
- [109] A. Vega and M. A. Martin Contreras, *Eur. Phys. J. A* **57**, 113 (2021) [arXiv:1812.00642 [hep-ph]].
- [110] F. Osterfeld, *Rev. Mod. Phys.* **64**, 491 (1992).
- [111] H. Singh, A. Kumar and H. Dahiya, *Eur. Phys. J. A* **54**, 120 (2018).
- [112] K. Saito, T. Miyatsu and M. K. Cheoun, *Phys. Rev. D* **110**, 113001 (2024) [arXiv:2409.14764 [hep-ph]].
- [113] M. R. Schindler and S. Scherer, *Eur. Phys. J. A* **32**, 429 (2007) [hep-ph/0608325].
- [114] R. L. Workman *et al.* [Particle Data Group], *PTEP* **2022**, 083C01 (2022).
- [115] K. Park *et al.* [CLAS Collaboration], *Phys. Rev. C* **85**, 035208 (2012) [arXiv:1201.0903 [nucl-ex]].
- [116] S. Choi *et al.*, *Phys. Rev. Lett.* **71**, 3927 (1993).
- [117] V. Bernard, H. W. Fearing, T. R. Hemmert and U. G. Meissner, *Nucl. Phys. A* **635**, 121 (1998) [erratum: *Nucl. Phys. A* **642**, 563 (1998)] [arXiv:hep-ph/9801297 [hep-ph]].
- [118] H. W. Hammer, D. Drechsel and U. G. Meissner, *Phys. Lett. B* **586**, 291 (2004) [arXiv:hep-ph/0310240 [hep-ph]].
- [119] U. G. Meissner, *AIP Conf. Proc.* **904**, 142 (2007) [arXiv:nucl-th/0701094 [nucl-th]].
- [120] F. Gross, *Phys. Rev.* **186**, 1448 (1969); A. Stadler, F. Gross and M. Frank, *Phys. Rev. C* **56**, 2396 (1997) [arXiv:nucl-th/9703043].
- [121] V. Pascalutsa, M. Vanderhaeghen and S. N. Yang, *Phys. Rept.* **437**, 125 (2007) [arXiv:hep-ph/0609004 [hep-ph]].
- [122] D. Ronchen, M. Doring, F. Huang, H. Haberzettl, J. Haidenbauer, C. Hanhart, S. Krewald, U. G. Meissner and K. Nakayama, *Eur. Phys. J. A* **49**, 44 (2013) [arXiv:1211.6998 [nucl-th]].
- [123] C. Alexandrou, G. Koutsou, H. Neff, J. W. Negele, W. Schroers and A. Tsapalis, *Phys. Rev. D* **77**, 085012 (2008) [arXiv:0710.4621 [hep-lat]].
- [124] M. L. Goldberger and S. B. Treiman, *Phys. Rev.* **110**, 1178 (1958).
- [125] M. Kirchbach and A. Wirzba, *Nucl. Phys. A* **616**, 648 (1997).
- [126] R. Petti, R. J. Hill and O. Tomalak, [arXiv:2309.02509 [hep-ph]].
- [127] N. Kaiser and W. Weise, [arXiv:2404.11292 [nucl-th]].
- [128] W. M. Alberico, S. M. Bilenky and C. Maieron, *Phys. Rept.* **358**, 227 (2002) [arXiv:hep-ph/0102269 [hep-ph]].
- [129] A. Meucci, C. Giusti and F. D. Pacati, *Nucl. Phys. A* **744**, 307 (2004) [arXiv:nucl-th/0405004 [nucl-th]].
- [130] L. A. Ahrens, S. H. Aronson, P. L. Connolly, B. G. Gibbard, M. J. Murtagh, S. J. Murtagh, S. Terada, D. H. White, J. L. Callas and D. Cutts, *et al.* *Phys. Rev. D* **35**, 785 (1987)
- [131] Y. Fukuda *et al.* [Super-Kamiokande], *Phys. Rev. Lett.* **82**, 2430-2434 (1999) [arXiv:hep-ex/9812011 [hep-ex]].
- [132] M. A. Acero *et al.* [NOvA], *Phys. Rev. D* **107**, 052011 (2023) [arXiv:2109.12220 [hep-ex]].
- [133] M. Hoferichter, J. Menéndez and A. Schwenk, *Phys. Rev. D* **102**, 074018 (2020) [arXiv:2007.08529 [hep-ph]].
- [134] J. M. Chen, Z. R. Liang and D. L. Yao, [arXiv:2403.17743 [hep-ph]].
- [135] A. A. Abud *et al.* [DUNE], *JCAP* **10**, 065 (2021) [arXiv:2107.09109 [hep-ex]].

Appendix B: Numerical results for the axial-vector form factor G_A

We present here the numerical results for the form factors G_A for all transitions between octet baryon members discussed in Secs. VA, VB and VC. For a more clear comparison of magnitudes and shapes, we present the results of equivalent functions in the same column.

In the cases where the final result G_A is negative, we represent the function $-G_A$, for an easier comparison with the other transitions.

In Fig. B1 we present the results for the $|\Delta I| = 1$ transitions, and in Figs. B2 and B3 we present the results for the $|\Delta S| = 1$ transitions.

The axial-vector form factors in the vacuum are on the right column [Sec. VA]. The contributions from the quark core are represented by the dashed lines, and the contributions from the meson cloud by the dashed-dotted lines. The final results correspond to the solid lines. On the left column we present the final results of G_A for the vacuum ($\rho = 0$) and medium (densities $\rho = 0.5\rho_0$ and $\rho = \rho_0$) [Sec. VB].

In Figs. B4 and B5 we represent the ratios $G_A^*(Q^2)/G_A(Q^2)$ on the right column, and the ratios $G_A^*(Q^2)/G_A^*(0)$ on the left panel, for the $|\Delta I| = 1$ and $|\Delta S| = 1$ cases, respectively [Sec. VC].

Concerning the $|\Delta I| = 1$ transitions (Figs. B1 and B4), we recall that the form factors $\Sigma^+ \rightarrow \Lambda$ and $\Sigma^- \rightarrow \Lambda$ differ by a sign, and that the form factors $\Sigma^- \rightarrow \Sigma^0$ and $\Sigma^0 \rightarrow \Sigma^+$ are equal.

As for the $|\Delta S| = 1$ transitions (Figs. B2, B3 and B5), the ratios for the transitions $\Sigma^- \rightarrow n$ and $\Sigma^0 \rightarrow p$ are the same. The same is true also for the $\Xi^0 \rightarrow \Sigma^+$ and $\Xi^- \rightarrow \Sigma^0$ transitions.

Appendix C: Numerical results for the induced pseudoscalar form factor G_P

We present here the numerical results for the form factors G_P for all transitions between octet baryon members discussed in Secs. VA, VB and VC. For a more clear comparison of magnitudes and shapes we present the results of equivalent functions in the same column.

As for the function G_A , in the cases where the final result G_P is negative, we represent the function $-G_P$.

In Fig. C1 we present the results for the $|\Delta I| = 1$ transitions and in Figs. C2 and C3 we present the results for the $|\Delta S| = 1$ transitions.

On the right column we present the induced pseudoscalar form factors in the vacuum [Sec. VA]. In the figures, we discriminate the result for the bare contribution, the combination of the bare and pseudoscalar meson pole contribution, and the sum of all the contributions (Bare + Pole + Meson Cloud). On the left column we present the final results for the vacuum ($\rho = 0$) and medium (densities $\rho = 0.5\rho_0$ and $\rho = \rho_0$) [Sec. VB].

In Figs. C4 and C5, we represent the ratios $G_P^*(Q^2)/G_P(Q^2)$ on the right column, and the ratio $G_P^*(Q^2)/G_P(Q_p^2)$ where $Q_p^2 = 0.012 \text{ GeV}^2$, on the left column, for the $|\Delta I| = 1$ and $|\Delta S| = 1$ cases, respectively [Sec. VC].

As in the case of the form factor G_A , there are some relations between the theoretical calculations associated with different channels. For the $|\Delta I| = 1$ transitions (Figs. C1 and C4), we recall that the form factors $\Sigma^+ \rightarrow \Lambda$ and $\Sigma^- \rightarrow \Lambda$ differ by a sign, and that the form factors $\Sigma^- \rightarrow \Sigma^0$ and $\Sigma^0 \rightarrow \Sigma^+$ are the same.

As for the $|\Delta S| = 1$ transitions (Figs. C2, C3 and C5), the ratios for the transitions $\Sigma^- \rightarrow n$ and $\Sigma^0 \rightarrow p$ are the same. The same property is also valid for the $\Xi^0 \rightarrow \Sigma^+$ and $\Xi^- \rightarrow \Sigma^0$ transitions.

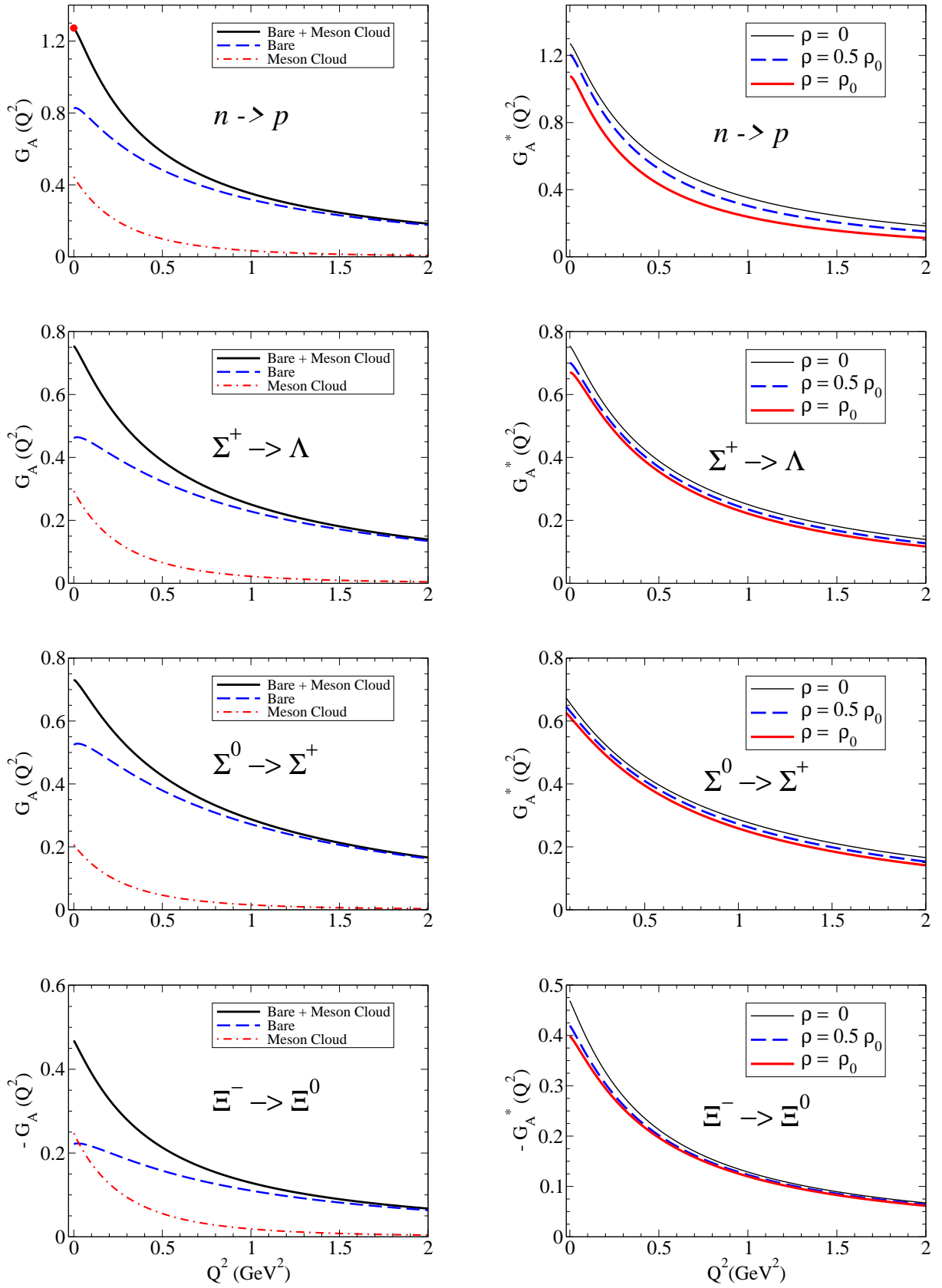


FIG. B1. Axial-vector form factor G_A for $|\Delta I| = 1$ transitions. **Left panel:** results in vacuum (bare, meson cloud and total). **Right panel:** total results for the medium $\rho = 0.5\rho_0$ and ρ_0 compared with vacuum ($\rho = 0$).

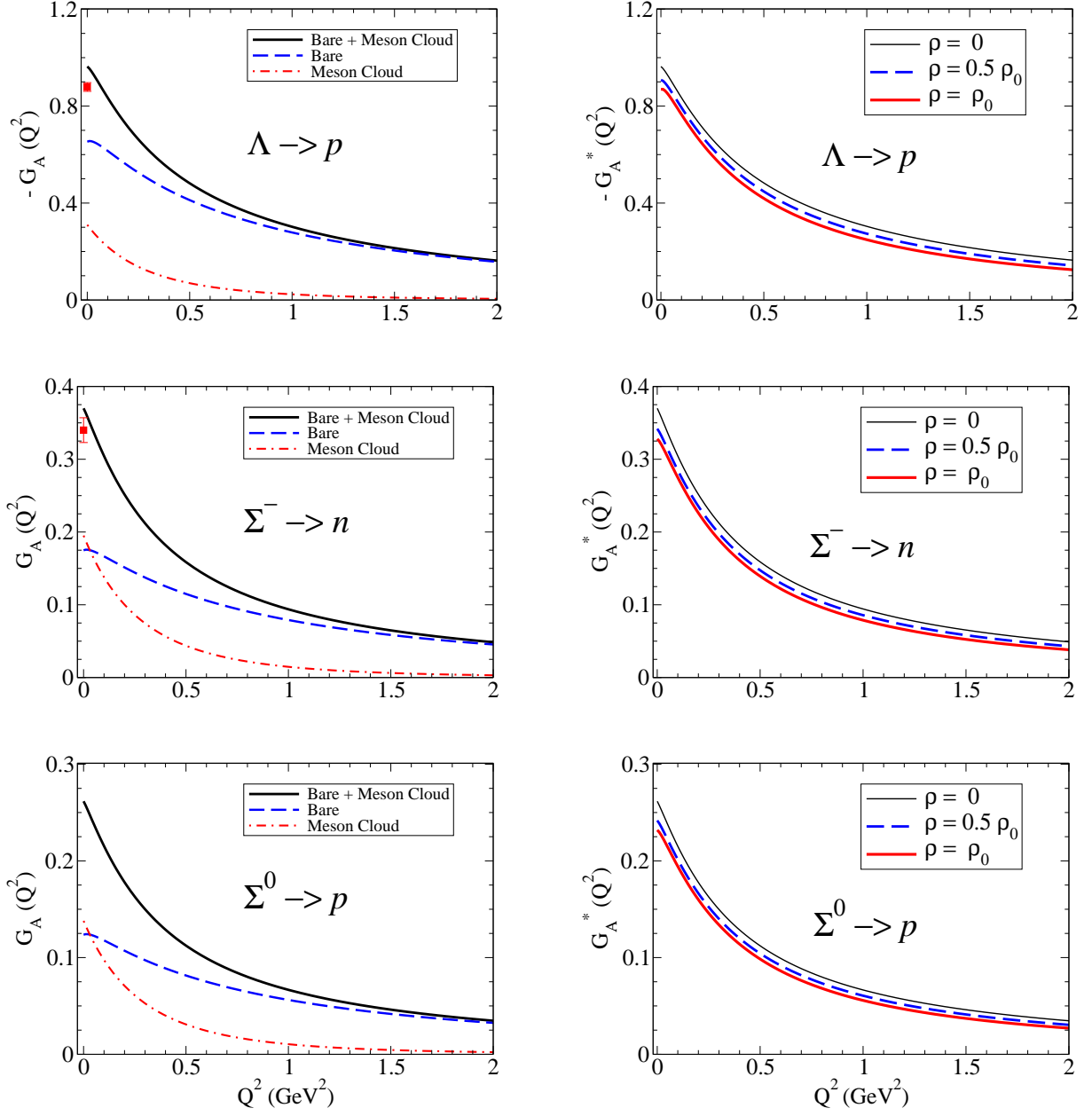


FIG. B2. Axial-vector form factor G_A for $|\Delta S| = 1$ transitions (part 1). **Left panel:** results in vacuum (bare, meson cloud and total). **Right panel:** total results for the medium $\rho = 0.5\rho_0$ and ρ_0 compared with vacuum ($\rho = 0$).

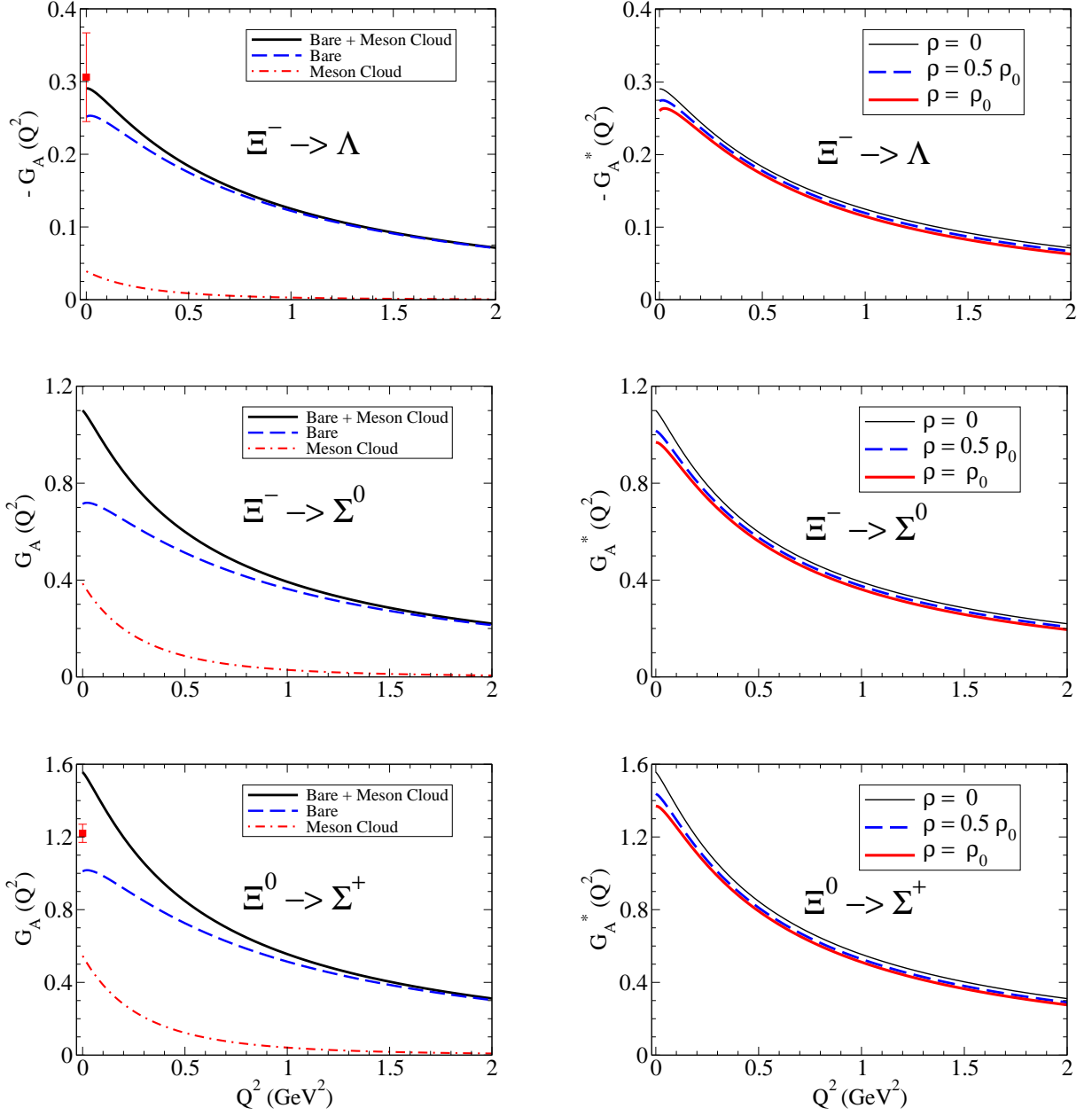


FIG. B3. Axial-vector form factor G_A for $|\Delta S| = 1$ transitions (part 2). **Left panel:** results in vacuum (bare, meson cloud and total). **Right panel:** total results for the medium $\rho = 0.5\rho_0$ and ρ_0 compared with vacuum ($\rho = 0$).

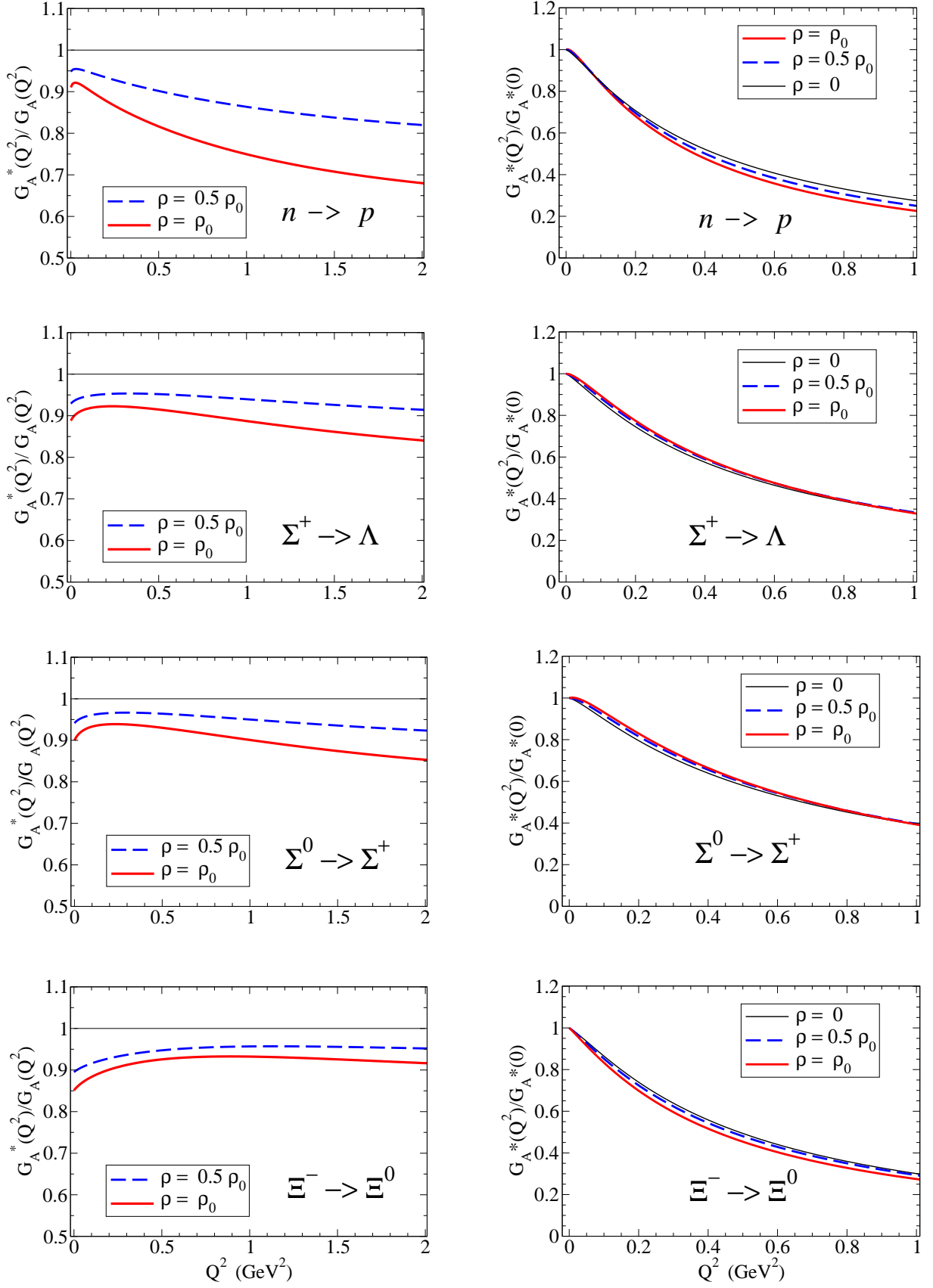


FIG. B4. Axial-vector form factor G_A for $|\Delta I| = 1$ transitions. Ratios G_A^*/G_A and $G_A^*(Q^2)/G_A^*(0)$.

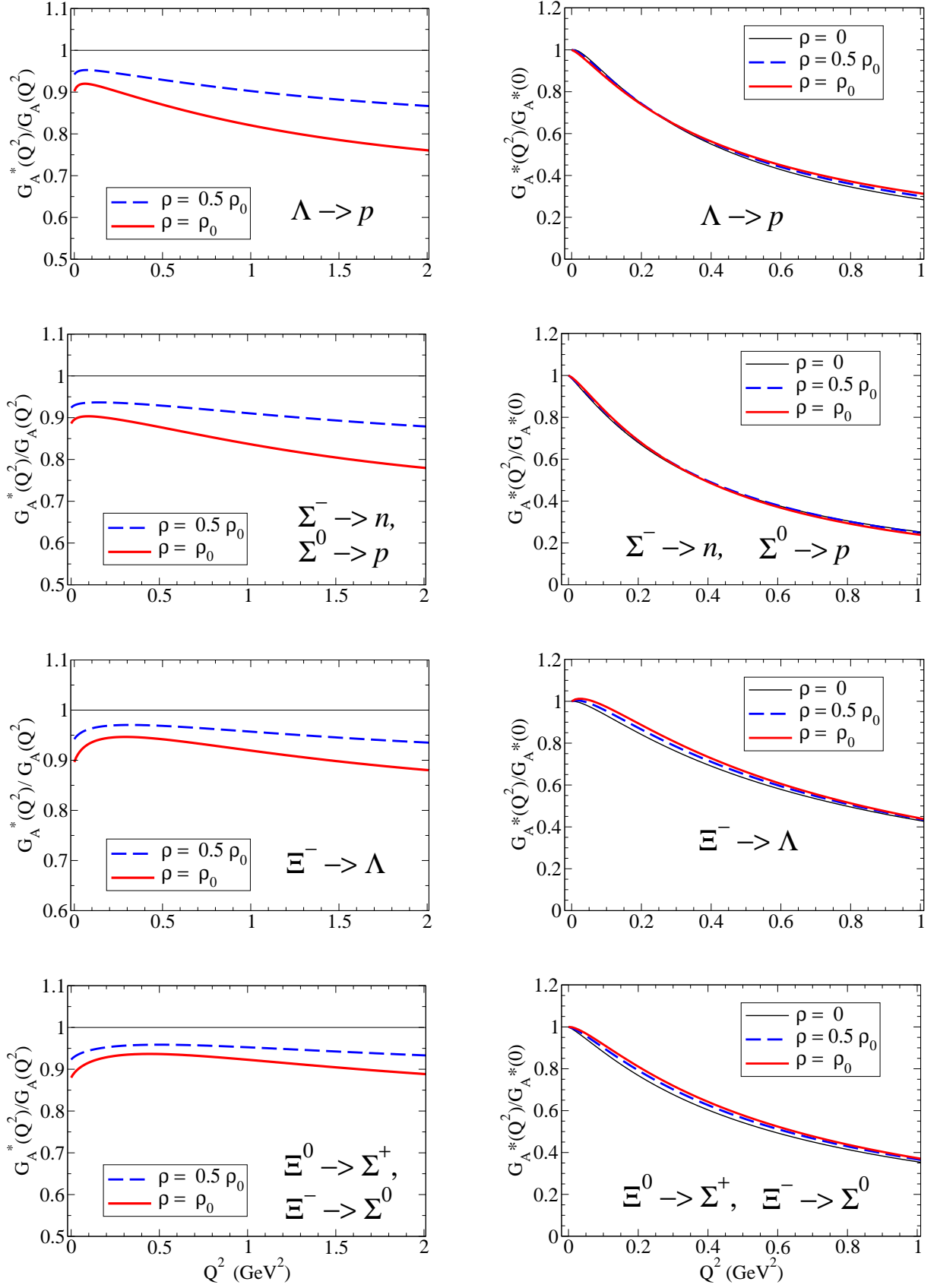


FIG. B5. Axial-vector form factor G_A for $|\Delta S| = 1$ transitions. Ratios G_A^*/G_A and $G_A^*(Q^2)/G_A^*(0)$. The ratios are the same for $\Xi^- \rightarrow \Sigma^0$ and $\Xi^0 \rightarrow \Sigma^+$. The ratios are the same for $\Sigma^- \rightarrow n$ and $\Sigma^0 \rightarrow p$.

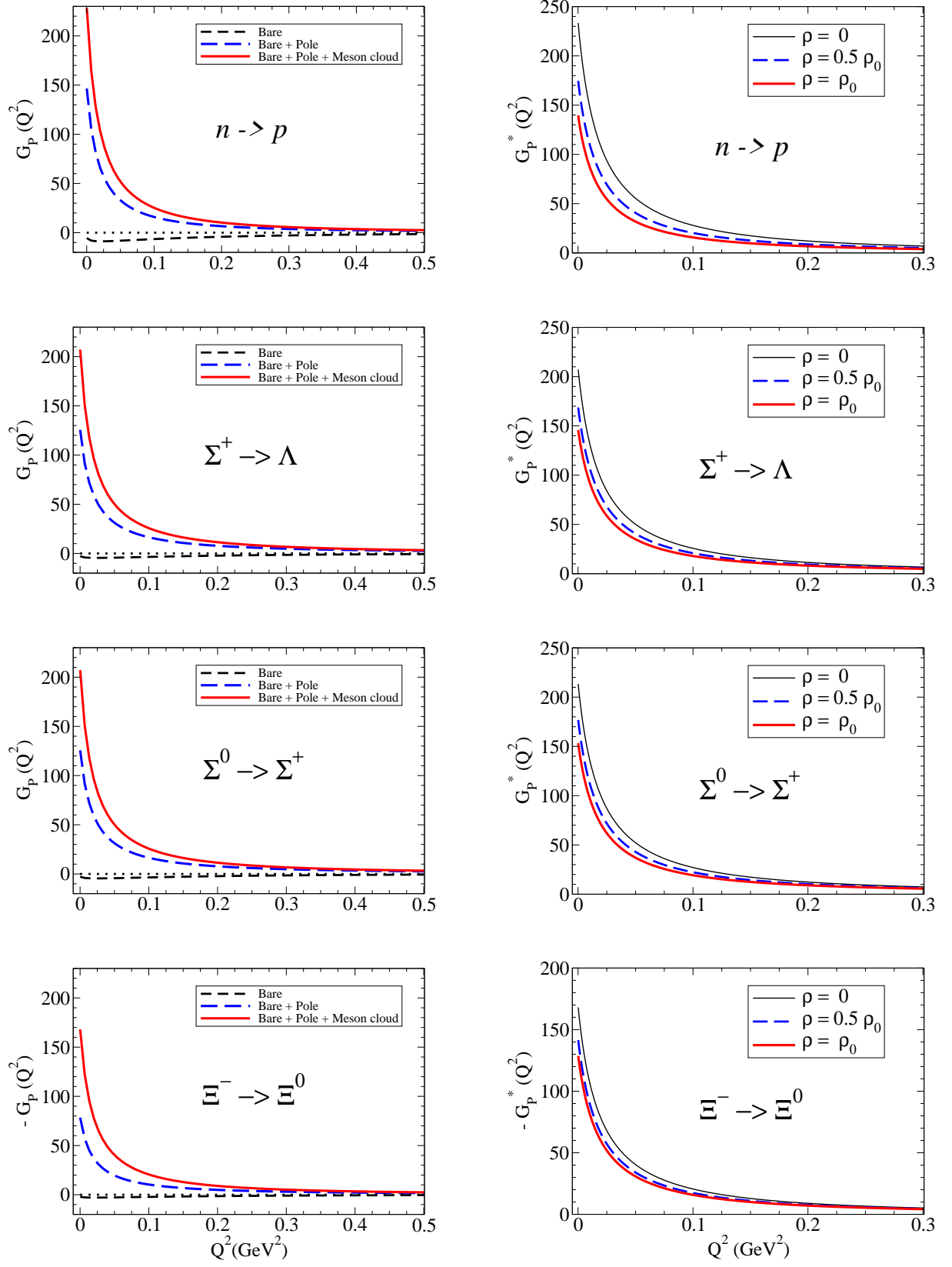


FIG. C1. Induced pseudoscalar form factor G_P for $|\Delta I| = 1$ transitions. **Left panel:** results for bare, bare plus meson cloud and total. **Right panel:** total results for the medium $\rho = 0.5\rho_0$ and ρ_0 compared with vacuum ($\rho = 0$).

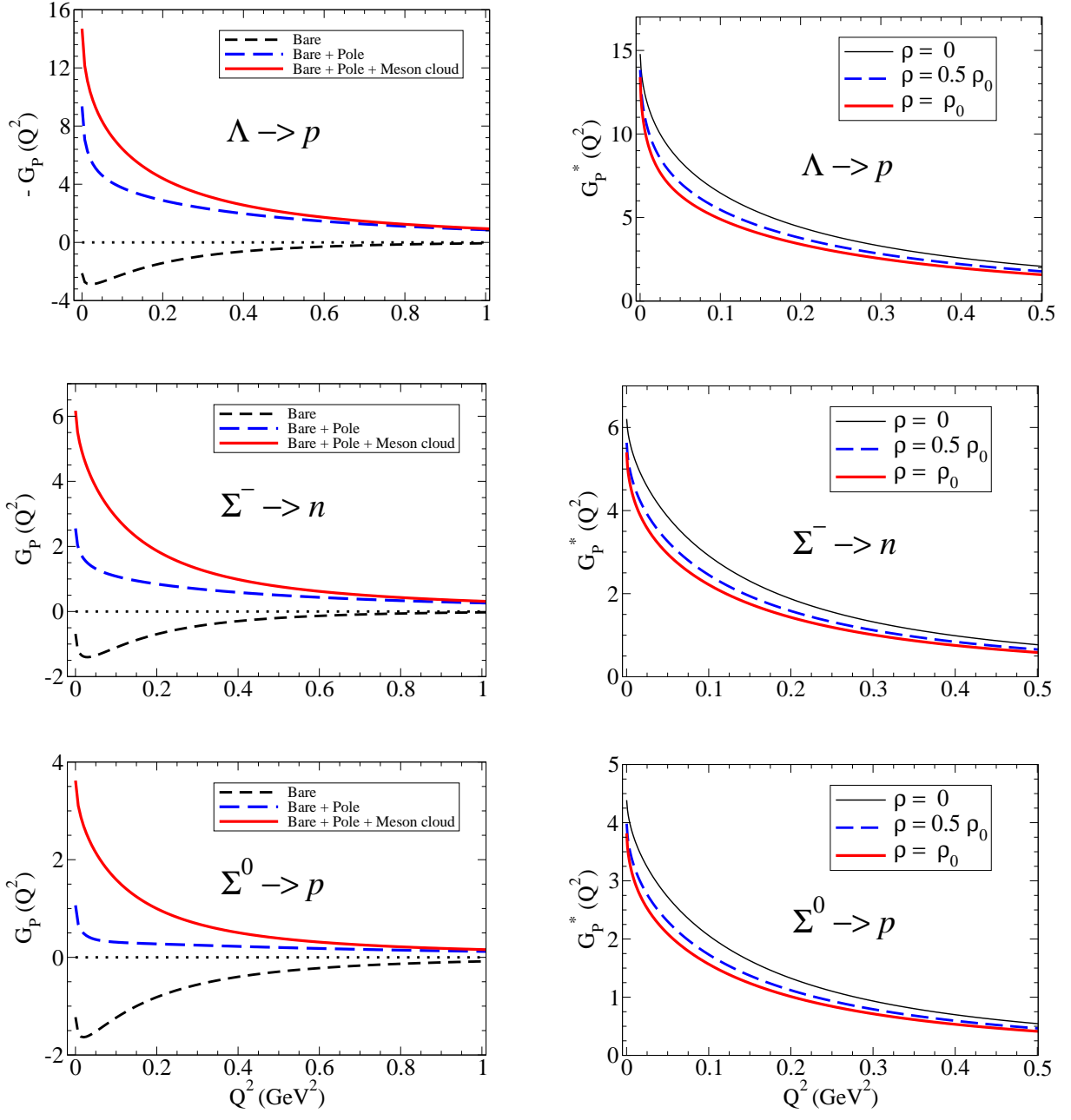


FIG. C2. Induced pseudoscalar form factor G_P for $|\Delta S| = 1$ transitions (part 1). **Left panel:** results for bare, bare plus meson cloud and total. **Right panel:** total results for the medium $\rho = 0.5\rho_0$ and ρ_0 compared with vacuum ($\rho = 0$).

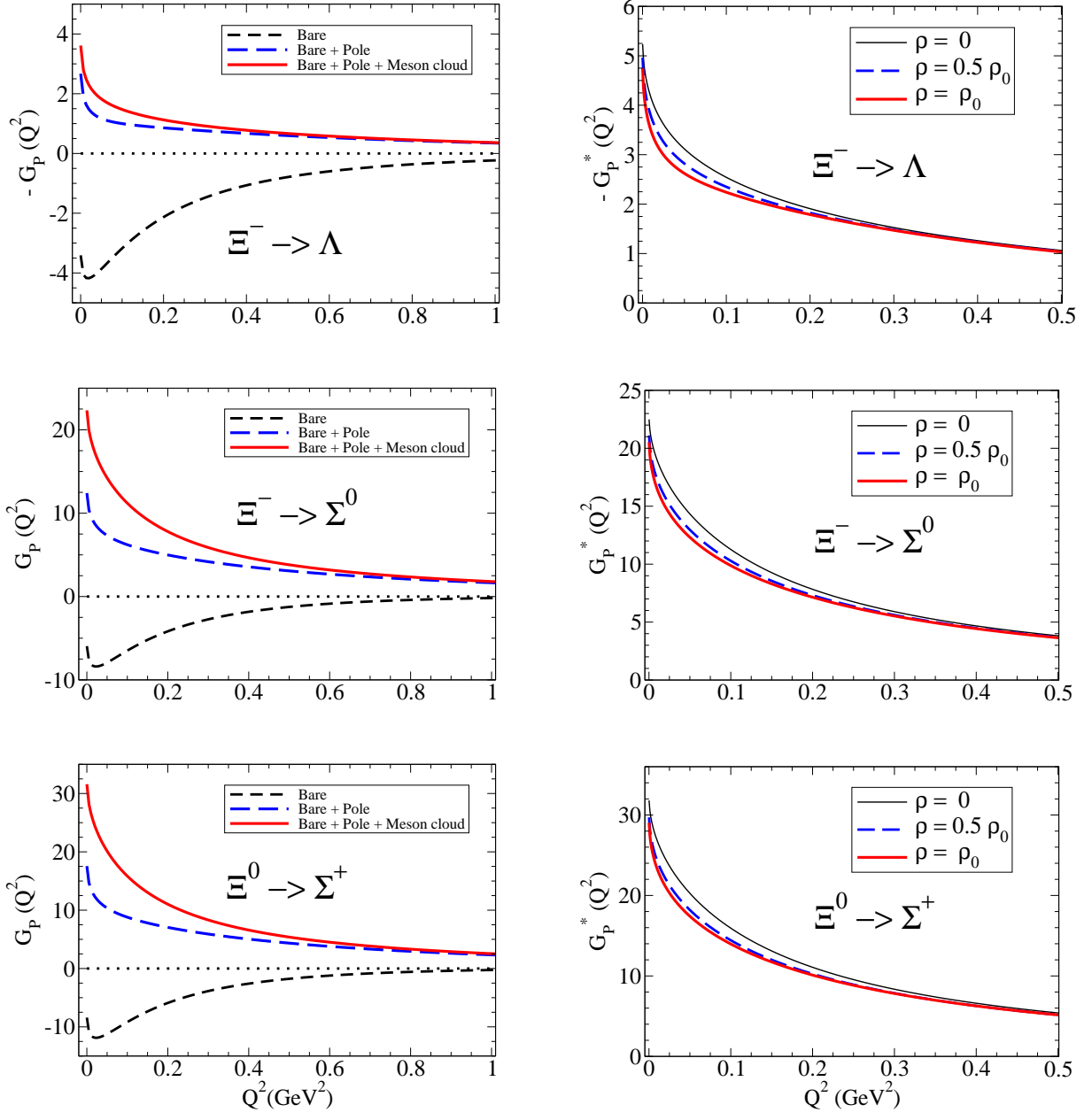


FIG. C3. Induced pseudoscalar form factor G_P for $|\Delta S| = 1$ transitions (part 2). **Left panel:** results for bare, bare plus meson cloud and total. **Right panel:** total results for the medium $\rho = 0.5\rho_0$ and ρ_0 compared with vacuum ($\rho = 0$).

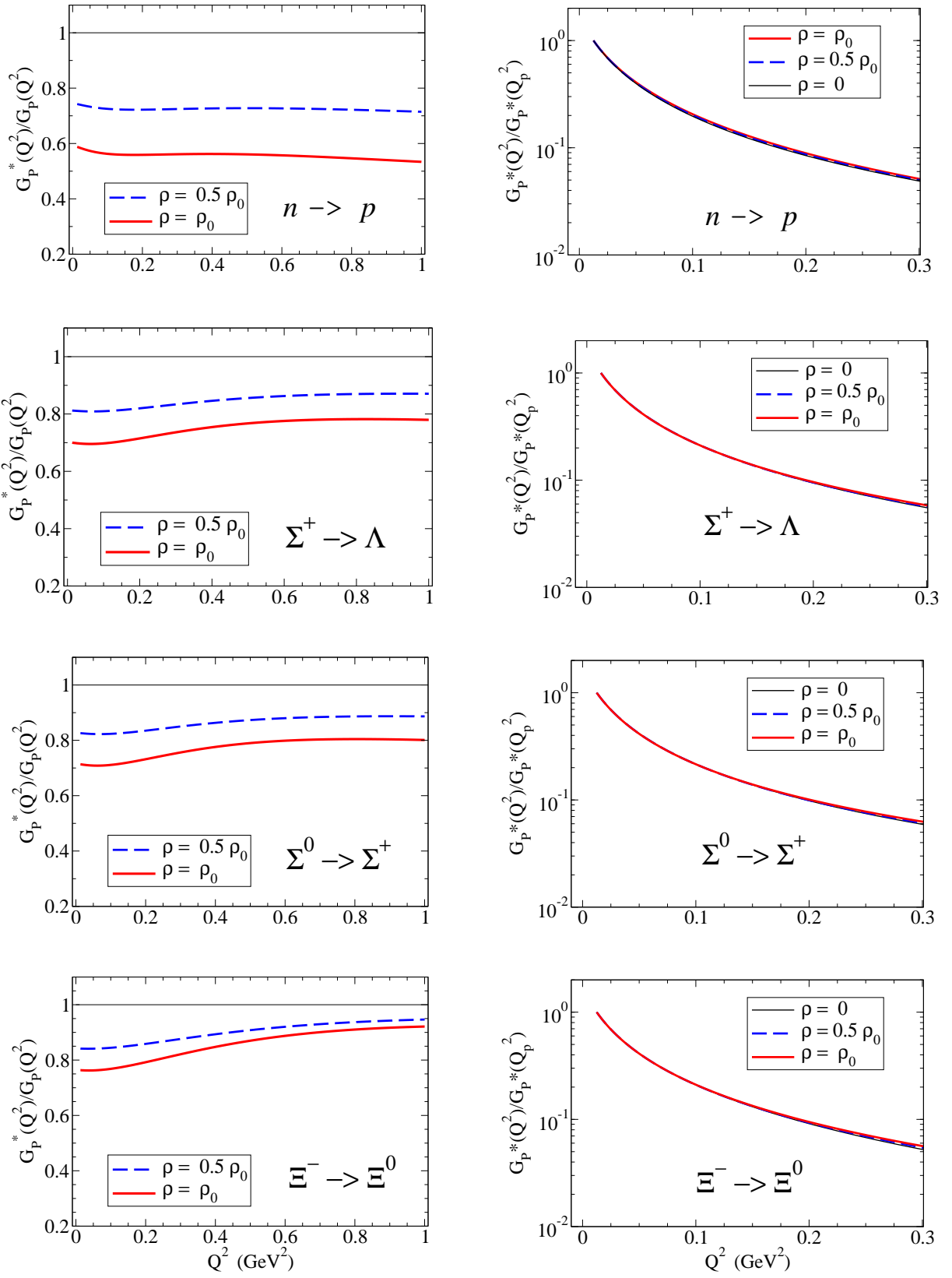


FIG. C4. Induced pseudoscalar form factor G_P for $|\Delta I| = 1$ transitions. Ratios G_P^*/G_P and $G_P^*(Q^2)/G_P^*(Q_p^2)$.

